Investigations of Diffusive Transport Processes in Sedimentary Rock

NWMO TR-2010-04 **June 2010**

Lisa Cavé, Tom Al, Yan Xiang and Diana Loomer

University of New Brunswick

nwmo

NUCLEAR WASTE MANAGEMENT ORGANIZATION

SOCIÉTÉ DE GESTION DES DÉCHETS NUCLÉAIRES

Nuclear Waste Management Organization
22 St. Clair Avenue East, 6th Floor
Toronto, Ontario
M4T 2S3
Canada

Tel: 416-934-9814
Web: www.nwmo.ca

Investigations of Diffusive Transport Processes in Sedimentary Rock

NWMO TR-2010-04

June 2010

Lisa Cavé, Tom Al, Yan Xiang and Diana Loomer
University of New Brunswick

ABSTRACT

Title: **Investigations of Diffusive Transport Processes in Sedimentary Rock**
Report No.: **NWMO TR-2010-04**
Author(s): Lisa Cavé, Tom Al, Yan Xiang and Diana Loomer
Company: University of New Brunswick
Date: June 2010

Abstract
Sedimentary rocks of low permeability and porosity are under investigation in Canada as potential host rocks for a deep geological repository for the long term containment of used nuclear fuel. One of the benefits of these rock types for this purpose is that they minimize, and in some cases may eliminate, advection. This results in extremely slow, diffusion-dominated transport of solutes in ground water. The overall objective of the research reported here was to develop methodologies and improve the knowledge of mechanisms controlling solute transport in diffusion-dominated sedimentary rock systems. This project focused on the quantification of diffusion and reaction processes, and rock pore-water characterization.

A study of rock diffusion properties across a sequence of Ordovician shale was conducted to investigate the scale-dependency of diffusive transport and the variations in diffusion properties with changes in lithology. Diffusion coefficients and diffusion-accessible porosity were measured on centimetre-scale samples from shale layers, and limestone and siltstone interbeds (hard beds), from across the Georgian Bay Formation, in the Michigan Basin. Diffusion measurements were made by radiographic and through-diffusion techniques using conservative aqueous tracers. Porosities and diffusion coefficients were found to be strongly dependent on the rock type, with higher porosities and diffusion coefficients measured for the shale than the hard beds. This information was combined with a very detailed geological log to determine the directional anisotropy in diffusion properties at the formation scale, identify a trend of slightly increasing diffusion coefficients with depth across the Georgian Bay Formation, and to develop a protocol for characterizing the variability in diffusive properties across a rock formation using the relationships between diffusion and physical and mineralogical properties of the rock.

A new radiography technique was also developed to quantify diffusion-reaction processes using a non-conservative tracer, cesium. The technique is based on the measurement of tracer concentration profiles as a function of time and was tested on samples of Queenston Formation shale. Reactive-transport modelling techniques were used to match experimental data and estimate mean cesium diffusion coefficients ($D_{p\,Cs} = 7.5 \times 10^{-11}$ m^2/s), cesium exchange selectivity coefficients (log $k_{Cs+/Na+} = 1.1$) and cation exchange capacity (CEC = 8.3 meq/100 g) for the intact samples. The estimated values for cesium are all slightly lower than measurements made by other techniques on argillaceous materials under consideration by national organizations for long-term radioactive waste management in Europe.

TABLE OF CONTENTS

LIST OF TABLES

Page

LIST OF FIGURES

Page

1. INTRODUCTION

1.1 OBJECTIVE

The overall objective of this research is to develop methodologies and improve the knowledge of mechanisms controlling solute transport in diffusion-dominated sedimentary rock systems. This project focused on the quantification of diffusion and reaction processes, and rock pore-water characterization in low-permeability sedimentary rocks.

Following the successful development of a new X-ray radiography technique for quantifying diffusion coefficients using a conservative iodide tracer (Cavé et al. 2009a, 2009b), several research questions were formulated, which the current project attempts to address:

- Can diffusion coefficient measurements on small sedimentary rock samples (< 2 cm path length) be used to assess the diffusion characteristics of the enclosing rocks at the larger, formation scale, such that they would be of benefit in supporting a safety case for a deep geological repository?
- Since many of the radionuclides of interest in radioactive waste do not display conservative transport behaviour, can the radiography method be expanded to investigate the reactive transport of non-conservative solutes in a sorption and diffusion-dominated system?

Two studies were initiated to investigate these issues. The first focussed on characterizing the diffusive properties and the physical, mineralogical and lithological properties of a series of representative Ordovician sedimentary rocks from the Georgian Bay Formation collected from deep boreholes. The intention was to quantify the porosity and diffusion coefficients for a series of samples across the thickness of a heterogeneous sedimentary formation to investigate whether diffusive properties could be related to lithology, and to use these relationships to scale up point measurements of diffusion coefficients to something that would be representative of the formation scale.

In the second study, the aim was to modify the existing method for the measurement of diffusion coefficients by X-ray radiography using iodide tracer, to provide a means of estimating ion-exchange parameters using a non-conservative tracer, cesium. The ability to employ numerical modelling tools to simulate the reactive transport of cesium by diffusion and ion exchange was key to the development of the new non-conservative tracer method.

1.2 STRUCTURE OF THE TECHNICAL REPORT

The main body of this report is divided into two major topics:

Investigations of diffusion and reaction processes in sedimentary rocks, including:

a) a study of variations in diffusion properties and their relationship to lithological changes across a sedimentary sequence (presented in Section 2); and

b) the development of a radiographic method for quantifying diffusion-reaction parameters for a non-conservative tracer in sedimentary rock (presented in Section 3).

Each of Sections 2 and 3 includes background information, a description of the materials and methods, results of the experimental work and a discussion of the outcome. Discussion of the results and conclusions of this research project are summarized in Section 4.

Additional data from the investigations can be found in the Appendices. In support of Section 2, photographs, solute diffusion profiles and through-diffusion data for the Georgian Bay Formation samples are presented in Appendix A. Appendix B provides a summary of the synthetic porewater and tracer solutions used in all laboratory experiments for measuring diffusion coefficients and porosity (Sections 2 and 3), and Appendix C gives an example of an input file used for reactive-transport calculations in Section 3.

2. VARIATIONS IN DIFFUSIVE PROPERTIES ACROSS A SEDIMENTARY SEQUENCE

A radiographic technique was developed to measure one-dimensional (1-D) iodide diffusion coefficients for sedimentary rock samples and the data were compared with results from through-diffusion experiments (Cavé et al. 2009a, b). These measurements were made on centimetre-scale samples of Ordovician shale and limestone from the Michigan Basin. Sample dimensions were approximately 1.1-cm diameter and 2-cm diffusion path length for radiography and 5- to 6-cm diameter and 1-cm diffusion path length for through-diffusion samples. Each diffusion coefficient determined by these techniques is effectively a bulk measurement for the entire sample and incorporates any heterogeneity in diffusive properties within the sample. When considering the diffusion properties of an entire rock formation, the small cm-scale samples are perhaps best considered as discrete point measurements within a continuum of diffusive properties.

During investigations of Ordovician shale and limestone, variations in 1-D diffusion coefficients were noted based on the lithology of the samples and the orientation of the sample with respect to the diffusive transport direction (Cavé et al. 2009a, b). Shale samples tended to have higher diffusion coefficients than limestone samples, and diffusion parallel to bedding was generally faster than diffusion normal to bedding, especially for shale. In attempting to understand rock diffusion properties at the formation scale, it is not practical to collect a continuous dataset by performing diffusion measurements at closely spaced intervals across hundreds of metres of core. However, it may be possible to define ranges of mineralogical and physical properties, including diffusion coefficients, that are characteristic of specific lithologic units such that detailed lithological logs from recovered core can provide a means of scaling up diffusion coefficient measurements.

The Georgian Bay Formation was considered a suitable source of sedimentary rock material to test this approach because of the localized heterogeneity and anisotropy caused by the occurrence of sandstone, siltstone and limestone “hard beds” that are interlayered with the shale. Samples collected from the Georgian Bay Formation were used to analyze relationships between lithology, physical properties and diffusion coefficients, and efforts have been made to scale up diffusive properties to the formation scale.

2.1 THE GEORGIAN BAY FORMATION

The Georgian Bay Formation in the Michigan Basin comprises blue-grey to green-grey shale with interbedded sandstone, siltstone and limestone layers termed “hard beds” (Guillet 1977, Armstrong and Carter 2010). The hard beds comprise 10 to 20 percent of the formation, and decrease in both abundance and thickness down the stratigraphic column. The hard beds are typically fossiliferous, with bryozoans, crinoids, pelecypods and brachiopods being the most common fossils (Armstrong and Carter 2006). The sandstone and siltstone are carbonate-rich, commonly cemented by calcite and also containing calcareous bioclastic material. The Georgian Bay Formation conformably overlies the Blue Mountain Formation and the gradational nature of the contact may make the two units difficult to distinguish. The Blue Mountain Formation consists of blue-grey to grey-brown shale with minor interbeds of sandstone and limestone. Hard beds are thinner and less abundant in the Blue Mountain Formation than in the Georgian Bay Formation (Armstrong and Carter 2006).

2.2 MATERIALS AND METHODS

2.2.1 Core Samples

Fresh rock core samples were collected from a deep cored borehole in the Michigan Basin. Thirteen samples representing shale and different forms of hard beds (Figure 1) were collected from the Georgian Bay Formation and two samples were collected from the underlying Blue Mountain Formation (Table 1, photographs in Appendix A). In the borehole, the Georgian Bay Formation was encountered from 518.5 to 609 m and the Blue Mountain Formation from 609 to 647 m below ground surface. The samples were selected by inspecting the core as it was retrieved from the drill hole and targeting a variety of shale, siltstone and limestone layers. Hard bed layers tended to remain intact on handling, but the shale layers are soft and break easily, often as a result of decompression when the core is brought to surface. This caused disking and grinding of the core below about 530 m and, as a result, many of the shale samples were collected in several pieces.

A photographic log of the core was collected by INTERA Engineering as soon as each core run (approximately 3 m length) was retrieved from the drill hole. Samples for porosity and diffusion testing were selected and photographed individually, then double-bagged; first in polyethylene bags flushed with nitrogen gas, then in polyethylene-lined aluminum foil bags; and vacuum sealed within 45 minutes of receiving the core. Sampling was conducted in June 2007 and the packed, preserved samples were shipped and received at UNB in mid-July 2007. Samples were held in refrigerated storage until they were opened in November 2007 for porosity and diffusion measurements.

Figure 1: Photographs of Drill Core Samples Showing Examples of Hard Beds (siltstone and fossiliferous limestone) and Homogeneous Shale Sections from the Georgian Bay Formation.

Table 1: Core Samples Used for Measurements of Porosity and Diffusion Properties

Sample ID*	Length (cm)	Formation	Description	Radio-graphy	Through-diffusion	ϕ_w
DGR2-535.08	15	Georgian Bay	**Hard Bed**: Graded grey calcareous sandstone layer (~10 cm) in grey-green shale	2 NB	-	2
DGR2-537.32	8	Georgian Bay	**Shale/Hard Bed**: Grey-green shale with siltstone	-	1 NB - I 1 NB - HTO	1
DGR2-539.69	12	Georgian Bay	**Shale**: Grey-green shale with thin interbedded calcareous sandstone layers (<1 cm)	1 PB	-	2
DGR2-544.05	17	Georgian Bay	**Hard Bed**: Laminated sandstone/siltstone	1 NB 1 PB	1 NB - I 1 PB - I	1
DGR2-549.63	26	Georgian Bay	**Shale/Hard Bed:** Dark grey-green shale with fossils	1 NB	-	2
DGR2-553.04	12.5	Georgian Bay	**Hard Bed:** Cemented fossiliferous unit (8 cm) in grey-green shale	1 NB	-	1
DGR2-561.90	21	Georgian Bay	**Hard Bed:** Laminated sandstone/siltstone layer (8 cm) with cross bedding	1 NB 1 PB	-	1
DGR2-568.47	16	Georgian Bay	**Hard Bed**: Cemented fossiliferous unit (13 cm)	1 NB	-	1
DGR2-575.36	13	Georgian Bay	**Shale/Hard Bed**: Siltstone in grey-green shale	1 NB	-	1
DGR2-583.18	20	Georgian Bay	**Shale:** Grey-green shale with calcareous material	1 NB	-	1
DGR2-593.53	26	Georgian Bay	**Shale:** Grey-green shale with sulfurous odour.	1 NB 1 PB	-	1
DGR2-597.25	20	Georgian Bay	**Shale:** Grey-green shale with carbonate nodules (<1 cm).	-	1 NB - I 1 NB - HTO	1
DGR2-604.44	12	Georgian Bay	**Shale/Hard Bed:** Grey-green shale with partially cemented carbonate fossils.	1 NB	-	1
DGR2-608.08	14	Georgian Bay	**Shale:** Grey-green shale with siltstone bed (3 cm)	-	Archived	-
DGR2-620.95	20	Blue Mountain	**Shale:** Homogeneous dark grey shale. Petroliferous and sulfurous odour.	1 NB	1 NB - I 1 NB - HTO	1

* The sample ID contains the core name and sample depth in metres below ground surface, measured to the centre of the core segment. NB = normal to bedding, PB = parallel to bedding, I = iodide tracer, HTO = tritium tracer, ϕ_w = number of water loss porosity samples.

2.2.2 Mineralogy and Physical Properties

Subsamples were collected from rims cut off around the diffusion samples and were sent to the Institute of Geological Sciences, University of Bern, Switzerland for mineralogical and physical measurements (Sections 2.2.2.1 to 2.2.2.6) to be made immediately adjacent to the diffusion test pieces.

2.2.2.1 Whole Rock Mineralogy

Whole rock mineralogy was determined by X-ray diffraction (XRD) using a PHILIPS PW3710 diffractometer. Rock material was milled in a ring mill to a fine powder, mounted on a sample holder, disorientated with a stamp, and scanned with Cu Kα radiation from 2° to 70° 2θ. Quantification of the quartz, feldspar and carbonate (calcite, dolomite/ankerite) content was performed utilizing the diffraction-peak intensity ratio of the mineral to that of an internal LiF standard. The relative error of such determinations is about ±5-10 %.

The standardization method used is valid for individual mineral contents up to about 50 wt%. In some cases the content of calcite or dolomite exceeds this value and the apparent concentrations obtained by XRD must be corrected. The correction uses the total inorganic carbon content measured by IR-spectroscopy (see Section 2.2.2.2) from which the carbonate mineral contents are calculated according to their stoichiometry and relative XRD peak intensity. The pyrite content was calculated from the total sulfur concentration measured by IR-spectrometry, assuming that no other S-bearing phases are present. Pyrite content would be overestimated in samples containing significant anhydrite or gypsum but this is not anticipated to be a problem in the Georgian Bay Formation. The total content of sheet silicates, mainly clay minerals, was calculated by the difference between 100% and the sum of all the other minerals.

2.2.2.2 Inorganic and Organic Carbon and Total Sulfur

The concentrations of total carbon and inorganic carbon and of total sulfur were determined with a CS-Mat 5500 element analyzer (Ströhlein GmbH & Co, Germany). In this technique, approximately 0.02 to 0.1 g of rock powder were heated to 1350 °C and 1550 °C in an O_2 or N_2 atmosphere respectively, to liberate all volatile components.

Total carbon and sulfur are measured by infrared (IR) spectrometry as CO_2 and SO_2 after oxidation in an O_2 atmosphere. Inorganic carbon (i.e. essentially CO_3 from carbonate minerals) is measured separately in a N_2 atmosphere. The gas is passed through a Mg perchlorate tube to remove water and then pumped through the CO_2 and SO_2 analyzers. The peaks of CO_2 and SO_2 in the carrier gas are measured by IR-spectrometry. Separate non-dispersive infrared (NDIR) absorbance analyzers are used for each of the two species. Organic carbon is calculated by difference from total carbon and inorganic carbon. The calibration is made with pure $CaCO_3$ for carbon and Ag_2SO_4 for sulfur. The detection limits are around 0.1 wt% for total sulfur, total carbon and inorganic carbon.

To avoid analytical problems induced by the Cl content of the samples, they had to be washed with water prior to analysis. This does not affect the results significantly because the solubility and the dissolution kinetics of the relevant minerals are low.

2.2.2.3 Specific Surface Area (BET)

Nitrogen adsorption isotherms were measured on crushed samples (grain size ≤ 2 mm) using a Coulter SA 3100 surface analyzer. Prior to the adsorption measurements, the samples were degassed in vacuum at 150°C for 30 min. The nitrogen adsorption isotherms were mostly measured at relative pressures (P/P_0) from 0 to 0.4, but measurements for some samples were conducted from P/P_0 = 0 to 1.0. Surface areas were calculated by the Brunauer-Emmett-Teller (BET) method (Brunauer et al. 1938). The BET method considers the determination of the amount of sorbing gas required to cover the external pore surfaces of a solid with a complete monolayer. Using the monolayer capacity (n_m), which is determined from the adsorption isotherms, and considering the area of 0.162 nm^2 occupied by a single molecule in the monolayer (A_m), the specific surface area S is calculated from:

$$S = n_m \cdot A_m \cdot N_A \qquad [1]$$

where N_A is Avagadro's number.

2.2.2.4 Grain Density

The grain density (ρ_g), was measured by kerosene-pycnometry in duplicate (modified after ASTM D854). The volume of the pycnometer was derived from the weight of the pycnometer filled with kerosene initially ($M_{k1+pycn}$). The density of kerosene (ρ_k = 0.78 g/cm^3 at 20°C) was checked using an aerometer. For the measurement, powdered rock material was dried at 105°C to constant weight. Approximately 15 g of the sample were transferred into the pycnometer, which was subsequently filled with kerosene while continuously removing the air by a vacuum pump. The rock sample volume was calculated as the difference between the volume of kerosene in the pycnometer with and without the rock material. The grain density was then obtained according to:

$$\rho_g = \frac{(M_{rock+pycn} - M_{pycn})}{M_{rock+pycn} - M_{pycn} + M_{k1+pycn} - M_{rock+k2+pycn}} \cdot \rho_k \qquad [2]$$

where $M_{rock+pycn}$ is the sum of the masses of the dry powdered rock sample and the pycnometer, M_{pycn} is the mass of the pycnometer, $M_{k1+pycn}$ is the mass of the pycnometer filled with kerosene up to the meniscus, and $M_{k2+pycn}$ is the mass of the pycnometer with the rock sample inside and filled with kerosene up to the meniscus.

The combined relative error on the grain density measurement is approximately:

$$\frac{\sigma_{\rho_g}}{\rho_g} \approx \sqrt{6}\,\frac{\sigma_M}{M_{rock}} + \frac{\sigma_{\rho_k}}{\rho_k} \approx \frac{\sigma_{\rho_k}}{\rho_k} \quad . \qquad [3]$$

where M_{rock} is the mass of the dry rock sample, The relative error on the grain density is dominated by the error in kerosene density and amounts to 1.3% using σ_M = 0.002 g, M_{rock} = 15 g, σ_k = 0.01 g/cm^3 and ρ_k = 0.78 g/cm^3.

The presence of salts precipitated from porewater results in measured grain densities that are lower than the real values (the density of halite is 2.165 g/cm^3). In the studied samples, this effect is likely to be small.

2.2.2.5 Bulk Dry Density

The bulk dry density ($\rho_{b,dry}$) was measured in duplicate using the water displacement method (Blum, 1997). The principle of the method is the calculation of bulk dry density from sample mass and volume making use of Archimedes' principle. Two separate, homogeneous rock samples of a volume of approximately 2 to 3 cm^3 were dried at 105°C to constant weight. The sample volume was determined by weighing the rock sample in air and during immersion in water (ρ_w = 1.00 g/cm^3 at 20 °C) using a density accessory kit (Mettler Toledo). In order to minimize the water intrusion into the pore space, the dried sample was coated with paraffin (ρ_p = 0.90 g/cm^3) prior to the immersion into water. Paraffin was melted in a vessel at ca. 45°C. The sample was dipped rapidly into the paraffin and then allowed to cool. Then the coated sample was weighed in air and during immersion into water. The bulk dry density was calculated according to:

$$\rho_{b,dry} = \frac{\rho_w \cdot \rho_p \cdot M_{rock}}{\rho_p \cdot (M_{rock+p} - M_{(rock+p)sub}) - \rho_w \cdot (M_{rock+p} - M_{rock})} \quad [4]$$

where M_{rock} is the mass of the dry rock sample, M_{rock+p} is the mass in air of the dry rock sample coated with paraffin and $M_{(rock+p)sub}$ is the mass of the dry rock sample coated with paraffin submerged in water.

The presence of salts precipitated from porewater results in measured bulk dry densities that are slightly higher than the real values. In these samples, the effect is generally small.

2.2.2.6 Physical Porosity

Physical porosity (ϕ) was calculated from densities according to:

$$\phi = 1 - (\rho_{b,dry}/\rho_g) \quad [5]$$

Where ρ_g is the grain density and $\rho_{b,dry}$ is the bulk dry density. No salinity correction was applied to the physical porosity.

2.2.2.7 Water Loss Porosity

Measurements of water loss porosity (ϕ_w) were made at the University of New Brunswick and were used for comparison with physical porosity (ϕ) and tracer-accessible porosity (ϕ_I or ϕ_{HTO}) determinations from the radiography and through-diffusion experiments. Gravimetric measurements of ϕ_w provide an independent measure of the bulk porosity of the sample. Experimental procedures for the water-loss method were modified from the water imbibition technique presented by Emerson (1990) and Vilks and Miller (2007) and are consistent with that of Blum (1997) in that the measurements are adjusted to account for the high salinity of the porewater. Water loss porosity measurements were made at the University of New Brunswick on preserved rock samples that were packaged in the field to retain porewater. The preserved core was unwrapped and an intact portion of about 50 to 100 g was cut for porosity measurements. Where possible, the porosity sample was collected adjacent to the rock slice used for diffusion sample preparation.

The porosity sample was fitted with a nylon thread loop to allow the rock to be weighed by suspension below the calibrated balance (Sartorius 2100). The sample was lowered into a beaker filled with synthetic porewater (SPW, Appendix B) and the saturated submerged mass (M_{sub}) was measured as soon as possible after cutting the preserved rock core. After this, the sample was removed from the brine, gently patted dry on the outside, suspended in air and the mass of the saturated sample (M_{sat}) was measured. Sequential measurements were taken at one minute intervals as the sample surface dried. The intersection point of two tangential lines on the drying curve (representing drying only on the surface and drying from the pores) was used to determine the mass in air where the sample is saturated, but dry on the surface (Vilks and Miller 2007).

Samples were then oven dried at 40°C and the mass in air measured weekly until a constant mass was obtained ($M_{dry\ 40}$). The temperature of the oven was increased to 105°C and the samples were dried further to obtain a constant mass ($M_{dry\ 105}$). Each time the oven-dried mass was measured, the samples were first allowed to cool for at least 15 minutes in a desiccator with silica gel to absorb atmospheric moisture. The low temperature oven-drying step (40°C) was intended to measure the mass of porewater lost, but prevent the removal of bound water on clay minerals or the dehydration of minerals such as gypsum. The samples were dried for 52 to 77 days at 40°C before a mass change of less than 0.05% was recorded. Samples were dried for a further 14 to 35 days at 105°C to reach constant mass. The measured values for M_{sat}, M_{sub} and M_{dry} were used to determine ϕ_w:

$$\phi_w = V_1/V_2 = ((M_{sat} - M_{dry})/((1 - x) \cdot \rho_{brine})) / ((M_{sat} - M_{sub})/\rho_{brine}) \quad [6]$$

where V_1 is the volume of pore fluid (volume of voids), V_2 is the Archimedes' bulk volume (total volume of rock + voids), M_{sat} is the mass of saturated sample measured in air, M_{dry} is the mass of oven-dried sample measured in air, M_{sub} is the mass of saturated suspended sample when submerged in solution, ρ_{brine} is the density of the SPW brine solution (ρ_{brine} = 1.224 g/mL at 25°C) and x is the mass fraction of salts in the pore fluid. It is assumed that the mass fraction, x, is similar in the natural porewater and the SPW. Separate water loss porosity values for 40°C and 105°C are reported.

The mass measurements were also used to obtain grain densities (ρ_g) and water content (WC, mass percent):

$$\rho_g = M_{rock} / (V_2 - V_1) = (M_{dry} - V_1 \cdot \rho_{brine} \cdot x) / (V_2 - V_1) \quad [7]$$

$$WC = ((M_{sat} - M_{dry}) / M_{dry}) \cdot 100 \ (\%) \quad [8]$$

2.2.3 Diffusion Properties by Radiography

2.2.3.1 Pore Diffusion Coefficients

Diffusion coefficients were measured using a modification of the radiographic technique developed at the University of New Brunswick (Cavé et al. 2009a, b). Diffusion measurements were made by monitoring the movement of iodide (I^-) through a sample of rock under static (no flow) conditions using X-ray radiography. All X-ray data were collected on a Skyscan 1072 Desktop MicroCT system using 89.8 kV source energy, 110.2 μA current and averaging 4 image frames, each collected over a 9968 ms acquisition time. A 1-mm aluminum filter is used to filter out low energy X-rays from the polychromatic source, and the images were flat-field corrected. Samples were run in two batches to allow for the expected differences in diffusion rates of high ($\phi_w > 0.03$) and low porosity ($\phi_w < 0.03$) samples.

Cylindrical rock samples (11 mm diameter, 15-20 mm height) were cut from the drill core using a diamond-tipped drill bit. The cylinder axis was orientated either parallel or normal to bedding. The circumference of the sample was brushed with a thin layer of silicone then enclosed in heat-shrink tubing (FP-301, 3M) with the tubing protruding ~5 mm above the top of the sample. A disc of felt fabric and an aluminum disc internal standard (11 mm diameter, 3 mm height) were positioned inside the protruding tubing. The internal standard has a threaded hole through the disc to allow access for solutions. The lower end of the sample was positioned in a Delrin® diffusion cell reservoir and secured with a rim of silicone (Figure 2). Aluminum wire alignment guides were attached along the side of each sample.

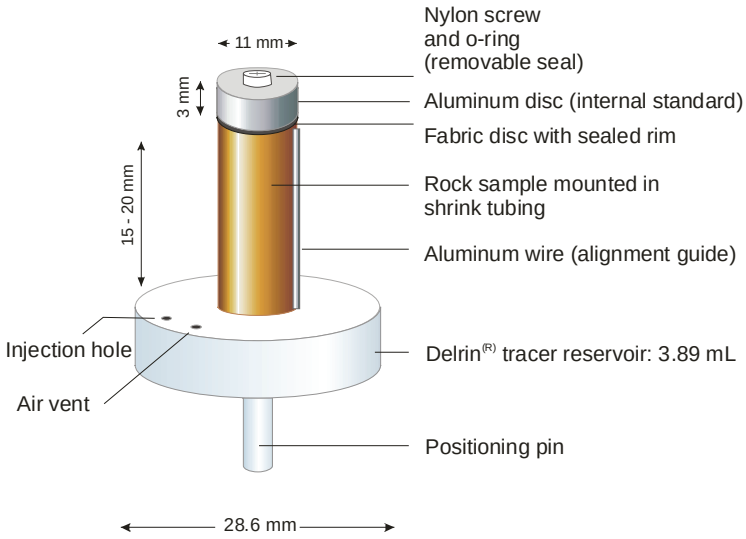

Figure 2: Diagram of the Diffusion Cell Used for Diffusion Experiments by X-Ray Radiography.

The sample was saturated with synthetic porewater (SPW, Appendix B) to replace pore fluid lost during sample preparation. This was done by filling the reservoir with SPW solution and injecting SPW through the hole in the Al disc. Solutions were refreshed weekly while allowing the sample to saturate for 5 weeks.

To initiate the diffusion tests, 15 to 20 mL of 1.0 M NaI tracer solution (Appendix B) were injected into the bottom of the reservoir, flushing out the SPW and using paper towel to wick away the displaced solution. The outside of the sample was rinsed with distilled water to remove any salt residue from overflow during filling, and gently blotted dry.

A reference radiograph (for background subtraction) was acquired immediately after tracer injection. For radiograph acquisition, the sample was positioned in the microCT sample chamber and the magnification, height and rotation adjusted so that the sample was completely in the field of view. Radiographs were acquired as 16 bit TIFF image files. A second reference image was acquired to allow for estimation of reproducibility errors by removing the sample, then replacing it in the chamber, before acquiring the second image.

Time series radiographs were collected over subsequent weeks using the same positioning and operating conditions as for the reference radiographs. Radiographs were collected at intervals of 2 to 3 days for high porosity samples and 3 to 4 days for low porosity samples until tracer break-through was observed at the top of the samples. Tracer solutions in the reservoirs were refreshed once or twice per week during the diffusion experiments and samples were stored at room temperature (22.5±0.5°C) in a closed container with an open dish of SPW to maintain constant humidity and prevent evaporative drying.

After tracer break-through, the samples were saturated with tracer solution by removing the screw fitting in the upper Al disc, inverting the sample and submerging the open end in a container of 1.0 M NaI tracer solution. Tracer was allowed to diffuse in from both ends until the sample was saturated with iodide solution. In order to monitor the saturation process, radiographs were acquired weekly to check on the progress of iodide through the rock. When no further change was observed, a final radiograph image of the iodide-saturated sample was acquired.

The image processing software, ImageJ, was used to analyze the radiograph data. The average greyscale intensity of the internal standard (Al disc) was determined and used to correct the image intensity of all time steps relative to the reference. Profiles of greyscale intensity (integrated across the width of the sample) versus length along the diffusion pathway were extracted and exported to a spreadsheet. Graphs of $\Delta\mu$ (change in X-ray attenuation) versus distance were then prepared for each time step from the greyscale profiles by taking the natural logarithm of the greyscale values and subtracting: ln (reference) – ln (time series). Plots of C/C_0 versus distance were prepared for each time step from the $\Delta\mu$ profiles by one of two alternatives:

a) using the iodide-saturated $\Delta\mu_{sat}$ profile to scale the pore iodide concentrations in the time series $\Delta\mu$ profiles, as described by Tidwell et al. (2000):

$$\left(\frac{C}{C_0}\right)_x = \frac{\ln\left(I_{ref}\right)_x - \ln\left(I_t\right)_x}{\ln\left(I_{ref}\right)_x - \ln\left(I_{sat}\right)_x} = \frac{\Delta\mu_x}{\left(\Delta\mu_{sat}\right)_x} \qquad [9]$$

where $(C/C_0)_x$ is the relative tracer concentration in the pores at distance x; I is the measured (transmitted) intensity at distance x; and $\Delta\mu$ is the change in X-ray absorption due to iodide at position x; with the subscripts t, ref and sat indicating the time series, reference and tracer-saturated radiograph images, respectively; or

b) using a linear calibration function to calculate relative tracer concentration (for samples where iodide-saturated image data are not available). Measurements of $\Delta\mu$ made using radiographs of standard iodide solutions in glass vials were used to determine the relationship:

$$\left(\frac{C}{C_0}\right)_x = \frac{\Delta\mu_x}{1.1799} \cdot \phi \qquad [10]$$

where C is the tracer concentration at distance x; C_0 is the tracer concentration in the reservoir; $\Delta\mu$ is the change in X-ray absorption due to iodide at position x; and ϕ the porosity. Concentration profiles were scaled by the bulk ϕ_w for each sample.

Solutions of Fick's Second Law were fitted by visual inspection to the C/C_0 versus distance plots to obtain the diffusion coefficient. For the appropriate initial and boundary conditions:

$$C_{(x,t)} = 0 \;\Big|_{x>0}^{t=0} \qquad C_{(x,t)} = C_0 \;\Big|_{x=0}^{t\geq 0} \qquad C_{(x,t)} = 0 \;\Big|_{x=\infty}^{t\geq 0}$$

the analytical solution is (Crank, 1975):

$$C(x,t) = C_0 \,\mathrm{erfc}\,\frac{x}{2\sqrt{D_p t}} \qquad [11]$$

where C is the concentration of tracer at a distance x from the diffusion boundary at time t since the start of diffusion; C_0 is the concentration of tracer at the influx boundary and erfc is the complimentary error function.

The porewater diffusion coefficient (D_p) was found by iterating until the analytical solution best matched the measured profiles. To obtain the effective diffusion coefficient (D_e), the value of D_p was multiplied by the porosity. Ideally, the tracer accessible porosity should be used to determined D_e, and ϕ_I was used when possible, but in cases where ϕ_I was not determined, D_e was calculated using ϕ_w. Based on differences between ϕ_I and ϕ_w (Table 7), this approach may overestimate D_e by 40 to 100%.

2.2.3.2 Iodide Accessible Porosity Profiles

Profiles of $\Delta\mu_{sat}$ were used to calculate iodide-accessible porosity. At each point (x) in the $\Delta\mu_{sat}$ profile, the value of $\Delta\mu$ gives a measure of the mass of iodide tracer in the rock pores, which can be calculated from the calibration function for standard iodide solutions. The ratio of the mass of iodide in the pores (assuming full saturation) to the known mass of iodide in the tracer solution (at 100% porosity) provides an estimate of the X-ray path length occupied by saturated pores at each point in the profile, i.e. the iodide-accessible porosity:

$$(\phi_I)_x = \frac{(m_{sat})_x}{m_0} = \frac{(\Delta\mu_{sat})_x}{1.1799} \qquad [12]$$

where $(\phi_I)_x$ is the iodide accessible porosity value at point x in the profile, $(m_{sat})_x$ is the calculated mass of iodide at the same point from the linear calibration function and m_0 is the mass (or

concentration) of iodide in the aqueous tracer solution. For the NaI tracer used in these experiments, m_0 = 1 and 1.1799 is the slope of the calibration curve measured for $\Delta\mu$ vs m_I using standard iodide solutions in an SPW matrix.

Most samples were typically fully saturated with tracer after about 30 days in contact with tracer solution from both ends, while some of the lower porosity (<3%) samples required longer periods up to 80 days. Four samples with very low porosity yielded poor radiographic data and ϕ_I was not determined.

2.2.4 Diffusion Properties by Through-Diffusion

Comparison measurements were made on a subset of the Georgian Bay Formation samples by a through-diffusion technique. Through-diffusion measurements are described by Choi and Oscarson (1996), Boving and Grathwohl (2001) van Loon et al. (2003a, 2003b) and many others.

The method used in these experiments involved cutting a cylindrical rock sample (25.2 mm diameter, 10 mm height) using a core drill and trimming the ends of the cylinder to 10 mm height using a diamond saw. The cylinder axis was oriented normal to the bedding plane. The sample was then mounted in a diffusion cell (Figure 3). The circumference of the cylindrical sample was coated with a thin layer of silicone and the sample positioned inside flexible vinyl tubing (25.4 mm ID, 3.3 mm wall thickness); a heat-shrink clamp (PowerGrip, McMaster-Carr); and 2 stainless steel gear clamps. Two stainless steel discs (100 μm average pore diameter, Mott Industrial, USA) and Delrin® plugs with ports that connect to the solution reservoirs were positioned against each end of the rock assembly. After assembling the cell, the heat-shrink clamp was activated by heating and the gear clamps tightened around the sample. Cells were checked for leakage or preferential pathways by applying fluid pressure to the ports on one side using a syringe filled with SPW and watching for leakage in the opposite reservoir. The cell was attached to the reservoirs and connected to a peristaltic pump (205U Watson Marlow or Ecoline VC-MS/CAB-6, Ismatec) via polyethylene tubing, ensuring that the direction of tracer flux was from bottom to top. The pump speed was adjusted to 20-30 mL/hr.

The sample was saturated with SPW (Appendix B) to replace pore fluid lost during sample preparation. This was done by circulating SPW solution in both reservoirs for approximately 3 weeks prior to the start of the diffusion phase.

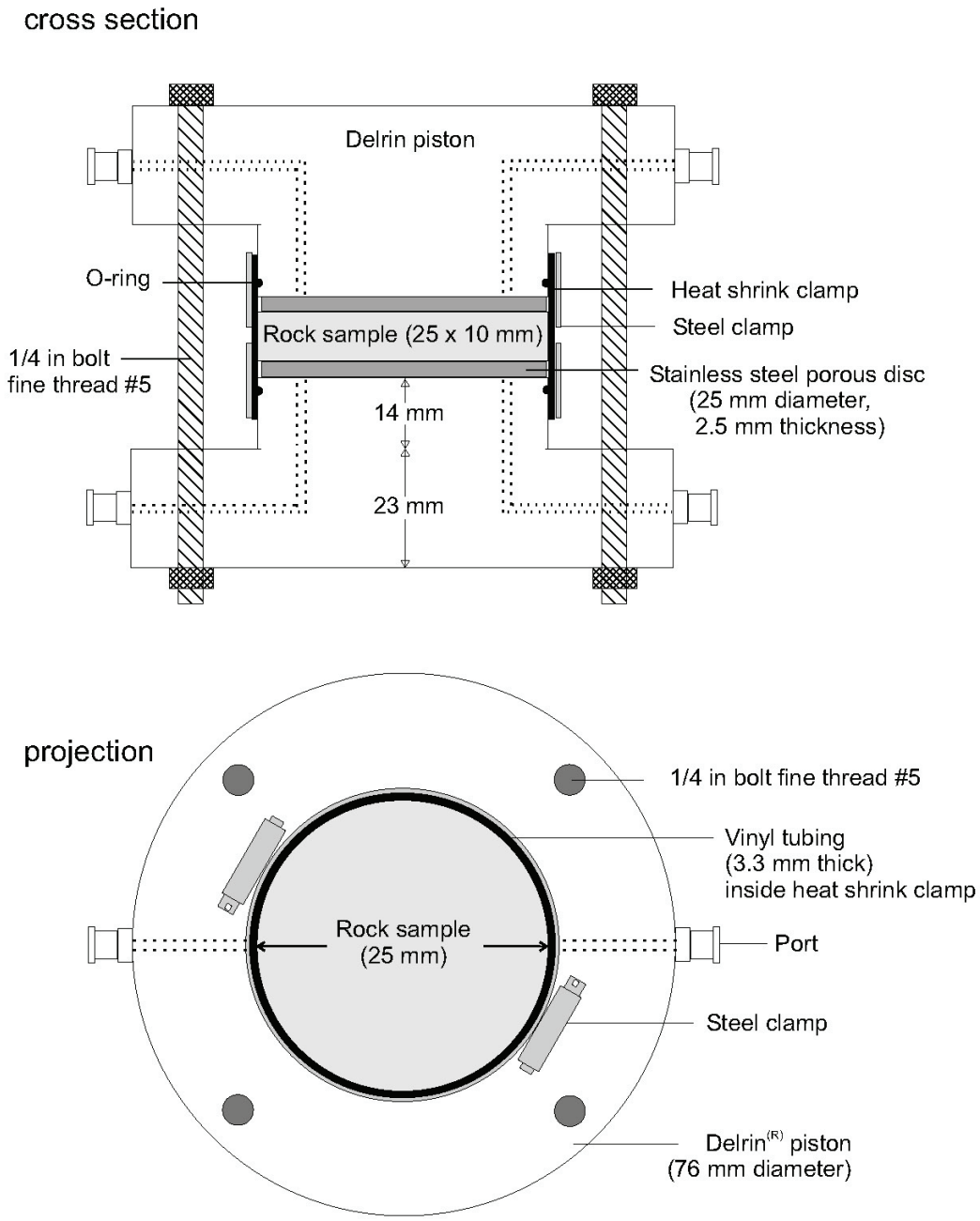

Figure 3: Diagrams of a Through-Diffusion Cell from Side (Top) and Projection of Half-Cell (Bottom).

Tritium diffusion experiments were initiated by replacing SPW in the high concentration reservoirs with HTO tracer solutions prepared in SPW matrix (5000 Bq/mL ^{3}H). A known volume of SPW was measured into the low concentration reservoir and the solutions were

circulated. Solutions in the low concentration reservoirs were collected for analysis at intervals of 3 to 4 days and replaced with fresh SPW solution of known volume. The concentration, and hence the flux of tritium that diffused through the sample was determined for each time increment using liquid scintillation counting (LS6000 series, Beckman; BCS scintillation cocktail, GE Healthcare). The cumulative mass of tritium that diffuses through the sample, Q_t (Bq), and the flux of the tracer (Bq/m^2/day) were calculated and plotted as a function of time for each sample. The effective diffusion coefficient (D_e) and diffusion-accessible porosity (ϕ_{HTO}) were then calculated from a solution of Fick's Second Law.

The through-diffusion experiments were designed so that the following initial and boundary conditions are fulfilled:

$$C_{(x,t)} = 0 \;\Big|_{x>0}^{t=0} \qquad C_{(x,t)} = C_0 \;\Big|_{x=0}^{t\geq 0} \qquad C_{(x,t)} = 0 \;\Big|_{x=L}^{t\geq 0}$$

and the analytical solution at steady-state may be simplified as (van Loon et al. 2003a):

$$Q_t = \frac{C_0 \cdot S \cdot D_e}{L} \cdot t - \frac{C_0 \cdot \alpha \cdot S \cdot L}{6} \qquad [13]$$

where C_0 is the concentration of the tracer present in the tracer reservoir (high concentration reservoir); L is the height of the cylindrical rock sample; S is the cross-sectional area of the rock sample; Q_t is the cummulative tracer mass that diffuses through the sample in time t; D_e is the effective diffusion coefficient and α is the rock capacity factor. In cases where the tracer is non reactive, α is equal to the diffusion-accessible porosity. The tracers used in this work, HTO and I^- are non reactive, therefore, α provides a measure of ϕ_{HTO} and ϕ_I.

The plot of flux versus time was used to find the time required for the diffusion process to achieve steady-state (constant flux). A linear regression analysis of Q_t versus time after steady-state was then performed and the values of D_e and ϕ_{HTO} were calculated from the slope and intercept, respectively, using equation [13]. To obtain D_p, the D_e value was divided by ϕ_{HTO}.

In preparation for the iodide tracer experiment, HTO was removed from the samples by circulating SPW through both reservoirs until no tritium activity was detected. Iodide diffusion experiments were then started by replacing SPW in the high concentration reservoir with NaI tracer solutions prepared in SPW matrix (1.0 M NaI). A known volume of SPW was measured into the low concentration reservoir and the solutions were circulated.

Solutions in the low concentration reservoirs were collected for analysis at intervals of 2 to 3 days and replaced with fresh SPW solution of known volume. The concentration, and hence the flux of tracer that diffused through the sample was determined for each time increment using an ion specific electrode (combination ISE, London Scientific Limited). The total accumulated tracer that diffuses through the sample, Q_t (mmol), and the flux of the tracer (mmol/m^2/day) were calculated and plotted as a function of time for each sample. The effective diffusion coefficient (D_e) and diffusion-accessible porosity (ϕ_I) were then calculated from a solution of Fick's Second Law as described for HTO (equation [13]).

All HTO diffusion cells were maintained in a fume hood at 20.5±0.5ºC, while the NaI cells were maintained in the open atmosphere in the laboratory at 23.5±0.5ºC.

2.3 RESULTS

2.3.1 Core Logs

Digital photographs of the entire drill core were obtained from Intera Engineering and used to log the occurrence and thickness of shale and hard bed layers through the Georgian Bay Formation. All individual layers thicker than 0.5 cm were measured, recorded and used to calculate the proportions of each lithological type (Table 2, Figure 4). Individual hard bed layers varied in thickness from 0.25 to 40 cm, interlayered with shale beds ranging in thickness from 0.5 cm to 2.3 m.

Table 2: Occurrence and Cumulative Thickness of Shale and Hard Bed Layers in Each Core Run through the Georgian Bay Formation.

Core run	Start depth (m)	Formation	No. of hard beds	Total shale thickness (%)	Total hard bed thickness (%)
23	517.85	Queenston	0	100.0	0.0
23	518.15	Georgian Bay	34	49.2	50.8
24	520.90	Georgian Bay	34	43.6	56.4
25	523.95	Georgian Bay	37	34.3	65.7
26	527.00	Georgian Bay	47	55.8	44.2
27	530.05	Georgian Bay	47	58.8	41.2
28	533.10	Georgian Bay	22	55.4	44.6
29	536.15	Georgian Bay	39	69.6	30.4
30	539.20	Georgian Bay	27	69.2	30.8
31	542.25	Georgian Bay	25	77.4	22.6
32	545.30	Georgian Bay	30	69.5	30.5
33	548.35	Georgian Bay	26	86.1	13.9
34	551.40	Georgian Bay	19	93.6	6.4
35	554.45	Georgian Bay	21	86.0	14.0
36	557.50	Georgian Bay	31	78.6	21.4
37	560.55	Georgian Bay	30	74.2	25.8
38	563.60	Georgian Bay	24	81.2	18.8
39	566.65	Georgian Bay	25	69.1	30.9
40	569.70	Georgian Bay	12	93.4	6.6
41	572.75	Georgian Bay	29	62.3	37.7
42	575.80	Georgian Bay	23	77.6	22.4
43	578.85	Georgian Bay	16	90.7	9.3
44	581.90	Georgian Bay	16	86.5	13.5
45	584.95	Georgian Bay	23	86.5	13.5
46	588.00	Georgian Bay	6	98.4	1.6
47	591.05	Georgian Bay	2	99.0	1.0
48	594.10	Georgian Bay	9	94.6	5.4

Core run	Start depth (m)	Formation	No. of hard beds	Total shale thickness (%)	Total hard bed thickness (%)
49	597.15	Georgian Bay	22	87.0	13.0
50	600.20	Georgian Bay	28	91.1	8.9
51	603.25	Georgian Bay	27	87.7	12.3
52	606.35	Georgian Bay	33	83.0	17.0
53	609.35	Blue Mountain	22	85.1	14.9
54	612.40	Blue Mountain	9	95.8	4.2
55	615.45	Blue Mountain	2	98.5	1.5
55	616.54	Blue Mountain	6	92.6	7.4
56	618.50	Blue Mountain	9	84.1	15.9
57	621.55	Blue Mountain	13	92.7	7.3
Total	**518 - 609**	**Georgian Bay**	**764**	**76**	**24**

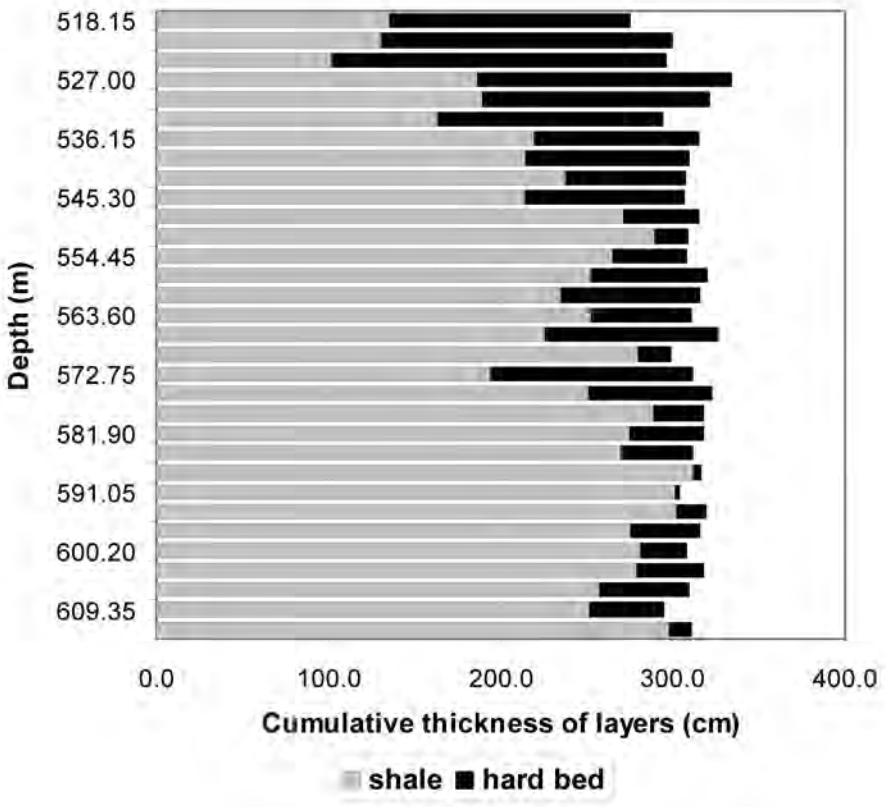

Figure 4: Summary of Relative Proportions of Shale and Hard Bed Layers through the Georgian Bay Formation (From Core Runs 23 – 54).

2.3.2 Mineralogy and Physical Properties

Mineralogical composition data for the Georgian Bay samples are reported in Table 3 and Table 4 and physical properties in Table 5.

2.3.2.1 Mineralogy

Table 3: Mineralogy Data (Weight %) for Samples from the Georgian Bay and Blue Mountain Formations

Sample ID	Rock type	Quartz	Plagioclase	K-Feldspar	Calcite	Dolomite/ ankerite	Pyrite[a]	Sum	Clay minerals[b]
DGR2_535.08_1	fine siltstone	18	<2	7	42	17	<0.2	85	15
DGR2_535.08_2	coarse siltstone	40	<2	8	7	18	<0.2	74	26
DGR2_537.32	siltstone/shale	25	<2	4	13	6	0.2	48	52
DGR2_539.69	grey shale	19	<2	2	4	4	0.4	29	71
DGR2_544.05	siltstone	43	<2	12	14	8	0.2	78	22
DGR2_549.63	grey shale	23	<2	4	8	4	0.2	40	60
DGR2_553.04	limestone	12	1	2	38	28	1.5	83	17
DGR2_561.90	siltstone	49	2	9	3	24	0.3	88	12
DGR2_568.47	limestone	6	<2	1	71	12	0.9	91	9
DGR2_575.36	siltstone/shale	31	2	8	7	13	0.5	61	39
DGR2_583.18	grey shale	22	1	3	4	4	1.0	36	64
DGR2_593.53	grey shale	19	1	2	6	8	2.2	38	62
DGR2_597.25	grey shale	22	1	2	7	7	1.4	41	59
DGR2_604.29	dolostone/shale	10	1	1	2	55	1.2	70	30
DGR2_620.95	grey shale	18	<2	2	11	1	2.4	34	66
Average for shale		20	<2	2	6	5	1.3	38	62
Average for hard beds		28	<2	7	29	18	0.5	83	17
Average for mixed lithologies		22	<2	4	7	20	0.7	57	43

[a] pyrite concentration calculated from total sulfur, assuming that pyrite is the only S-containing phase.

[b] XRD spectra show peaks for muscovite/illite and chlorite clay minerals in all samples and pyrite present in all samples except DGR2_544.05.

Table 4: Carbon and Sulfur Elemental Data for Samples from the Georgian Bay and Blue Mountain Formations

Sample ID	Rock type	C (organic) (wt%)	C (inorganic) (wt%)	Total S (wt%)
DGR2_535.08_1	fine siltstone	0.3	7.4	<0.1
DGR2_535.08_2	coarse siltstone	<0.1	3.1	<0.1
DGR2_537.32	siltstone/shale	<0.1	2.3	0.1
DGR2_539.69	grey shale	<0.1	0.9	0.2
DGR2_544.05	siltstone	<0.1	2.8	0.1
DGR2_549.63	grey shale	0.2	1.5	0.1
DGR2_553.04	limestone	0.5	8.2	0.8
DGR2_561.90	siltstone	0.1	3.5	0.2
DGR2_568.47	limestone	0.2	10.1	0.5
DGR2_575.36	siltstone/shale	<0.1	2.5	0.3
DGR2_583.18	grey shale	0.1	1.1	0.5
DGR2_593.53	grey shale	<0.1	1.8	1.2
DGR2_597.25	grey shale	0.2	1.8	0.7
DGR2_604.29	dolostone/shale	0.4	7.4	0.7
DGR2_620.95	grey shale	<0.1	1.4	1.3
Average for shale		0.1	1.4	0.8
Average for hard beds		0.2	5.8	0.3
Average for mixed lithologies		0.1	3.4	0.3

Table 5: Physical Properties for Samples from the Georgian Bay and Blue Mountain Formations

Sample ID	Rock type	BET surface area (m^2/g)	Bulk dry density[a] (g/cm^3)	Grain density[a] (g/cm^3)	Physical porosity[b] (-)
DGR2_535.08_1	fine siltstone	0.85	2.642	2.709	0.025
DGR2_535.08_2	coarse siltstone	1.80	2.684	2.689	0.002
DGR2_537.32	siltstone/shale	6.98	2.595	2.699	0.038
DGR2_539.69	grey shale	13.68	2.566	2.755	0.068
DGR2_544.05	siltstone	2.45	2.634	2.714	0.029
DGR2_549.63	grey shale	7.03	2.584	2.737	0.056
DGR2_553.04	limestone	2.35	2.741	2.818	0.027
DGR2_561.90	siltstone	1.64	2.662	2.704	0.015
DGR2_568.47	limestone	0.76	2.736	2.765	0.011
DGR2_575.36	siltstone/shale	4.17	2.603	2.718	0.043
DGR2_583.18	grey shale	13.75	2.563	2.747	0.067
DGR2_593.53	grey shale	11.89	2.579	2.706	0.047
DGR2_597.25	grey shale	8.15	2.587	2.752	0.060
DGR2_604.29	dolostone/shale	6.03	2.718	2.856	0.048
DGR2_620.95	grey shale	13.72	2.568	2.741	0.063
Average for shale		12.24	2.572	2.740	0.061
Average for hard beds		1.64	2.683	2.733	0.018
Average for mixed lithologies		6.05	2.625	2.752	0.046

[a] density measurements are an average of duplicate measurements.
[b] not corrected for salt content in the pores.

2.3.2.2 Water Loss Porosity

Results of the water loss porosity measurements are presented in Table 6.

Table 6: Water Loss Porosity, Grain Density and Water Content Measurements for Samples Dried at 40°C and 105°C

Sample ID	Rock type	Dried at 40°C Bulk porosity $\phi_{w,40}$ (-)	Dried at 40°C Grain density (g/cm^3)	Dried at 105°C Water content (wt%)	Dried at 105°C Bulk porosity $\phi_{w,105}$ (-)
DGR2_535.08_1	fine siltstone	0.018	2.69	0.74	0.022
DGR2_535.08_2	coarse siltstone	0.012	2.72	0.56	0.017
DGR2_537.32	siltstone/shale[a]	0.089	2.78	3.49	0.100
DGR2_539.69_1	grey shale	0.076	2.76	2.98	0.086
DGR2_539.69_2	grey shale	0.091	2.77	3.57	0.102
DGR2_544.05	siltstone	0.029	2.70	1.19	0.035
DGR2_549.63_1	grey shale[a]	0.080	2.76	3.21	0.092
DGR2_549.63_2	grey shale[a]	0.080	2.77	3.20	0.092
DGR2_553.04	limestone	0.014	2.77	0.59	0.018
DGR2_561.90	siltstone	0.016	2.72	0.67	0.020
DGR2_568.47	limestone	0.006	2.74	0.29	0.009
DGR2_575.36	siltstone/shale	0.046	2.73	1.79	0.053
DGR2_583.18	grey shale	0.087	2.77	3.37	0.097
DGR2_593.53	grey shale	0.083	2.79	3.17	0.092
DGR2_597.25	grey shale	0.082	2.76	3.17	0.091
DGR2_604.29	dolostone/shale	0.052	2.85	1.85	0.057
DGR2_620.95	grey shale	0.089	2.78	3.49	0.100
Shale average ± std. deviation		0.085 ± 0.005	2.77 ± 0.01	3.29 ± 0.22	0.095 ± 0.006
Hard beds average ± std. dev.		0.016 ± 0.008	2.72 ± 0.03	0.67 ± 0.30	0.020 ± 0.009
Mixed lith. average ± std. dev.		0.069 ± 0.019	2.78 ± 0.05	2.71 ± 0.82	0.079 ± 0.022

[a] Samples DGR2_537.32 and DGR2_549.63 contain mixed lithologies, but the portion used for water loss porosity measurements comprised only shale. Diffusion samples prepared from these two core sections have some hard bed material present.

After drying at 40°C, all samples lost additional mass on drying at 105°C, with the average mass loss for shales (0.267 ± 0.136 g) being about 3 times higher than the average additional mass loss for hard beds (0.158 ± 0.035 g). If all the mass lost is assumed to be structural water removed from either clay (illite) or gypsum, we can estimate the maximum amount (mass %) of each mineral present in the samples necessary to account for the additional loss of mass. For illite, these estimates are based on the assumption that H_2O may be lost from interlayer sites, and the mineral formula, $K_{0.6}(H_3O)_{0.4}Al_{1.3}Mg_{0.3}Fe^{2+}_{0.1}Si_{3.5}O_{10}(OH)_2 \cdot (H_2O)$, from http://webmineral.com/data/Illite.shtml. It should be noted that such estimates are not quantitative measurements of mineral content, but rather a means of testing whether loss of structural water by mineral dehydration is a realistic explanation for the additional loss of mass upon drying between 40 and 105°C.

Based on an estimated loss of 1.0 mol H_2O per mol illite, clay contents of 2.3% (for DGR2_568.47) to 9.1% (for DGR2_549.63_1) are required to account for the mass difference by dehydration of clays as a result of the temperature increase from 40 to 105°C. Measured clay mineral contents are greater than 9% in all samples (Table 3) indicating that there is sufficient structural water in clay to account for the observed mass loss. Alternatively, less than 2% gypsum content in the rocks could also account for the observed mass loss through dehydration of gypsum. These estimates suggest that the 40°C data could be representative of the porewater, while the 105°C data may over-estimate porosity by including a contribution from structural water in minerals when determining the porewater content of the saturated rock.

Because the differences between the 40°C and 105°C drying step could be accounted for by losses of mineral-bound water, rather than porewater, we have chosen to use the lower 40°C porosity data in the tables, graphs, calculations and discussion. The lower temperature data also provide better agreement with physical porosity for the lower porosity samples (Figure 5).

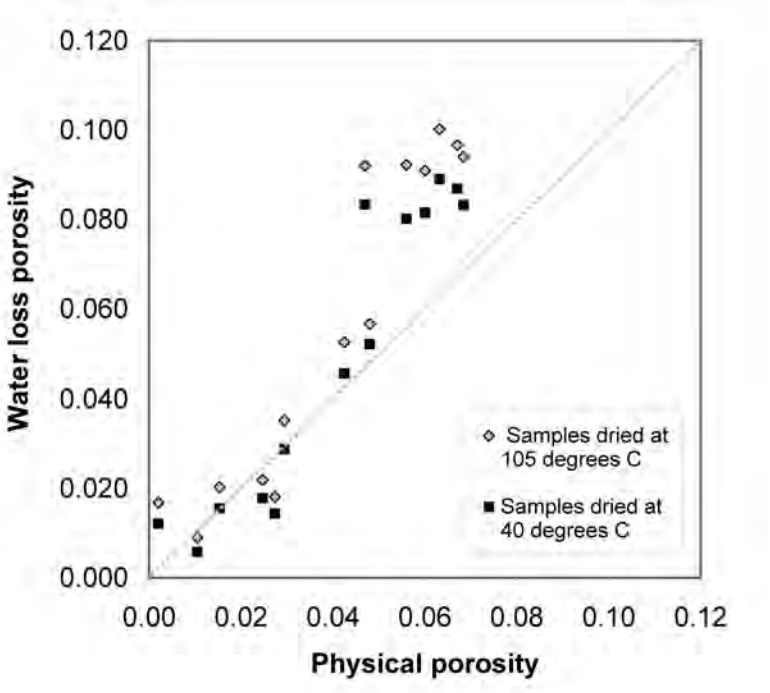

Figure 5: Comparison between Physical and Water Loss Porosity Measurements.

2.3.3 Diffusion Coefficients

2.3.3.1 Radiography Measurements

Results from the diffusion experiments are reported in Table 7 and the measured diffusion profiles are shown in Appendix A.

Table 7: Diffusion Coefficients and Mean Iodide Accessible Porosities by Radiography

Sample ID	$D_{p\,I}$ (m^2/s)	$D_{e\,I}$ (m^2/s)	Mean ϕ_I	$\phi_{w,40}$	$\phi_I/\phi_{w,40}$
Shale samples					
DGR2_539.69_PB	9.5×10^{-11}	5.8×10^{-12}	0.061	0.083	0.73
DGR2_583.18_NB	3.0×10^{-11}	1.8×10^{-12}	0.061	0.087	0.70
DGR2_593.53_NB	2.7×10^{-11}	1.1×10^{-12}	0.041	0.083	0.49
DGR2_593.53_PB	7.5×10^{-11}	3.6×10^{-12}	0.048	0.083	0.58
DGR2_620.95_NB	2.0×10^{-11}	9.1×10^{-13}	0.046	0.089	0.51
Hard bed samples					
DGR2_535.08_NB1[a]	2.0×10^{-12}	4.0×10^{-14}	- [a]	0.018	-
DGR2_535.08_NB2[a]	5.0×10^{-12}	6.0×10^{-14}	- [a]	0.012	-
DGR2_544.05_NB	6.0×10^{-12}	8.5×10^{-14}	0.014	0.029	0.49
DGR2_544.05_PB	1.2×10^{-11}	1.7×10^{-13}	0.014	0.029	0.50
DGR2_553.04_NB	9.5×10^{-12}	1.1×10^{-13}	0.011	0.014	0.80
DGR2_561.90_NB[a]	2.0×10^{-12}	3.0×10^{-14}	- [a]	0.016	-
DGR2_561.90_PB	1.0×10^{-11}	7.8×10^{-14}	0.008	0.016	0.50
DGR2_568.47_NB[a]	5.0×10^{-12}	3.0×10^{-14}	- [a]	0.006	-
Mixed lithologies					
DGR2_549.63_NB[b]	4.0×10^{-11}	7.2×10^{-13}	0.018	0.080	0.22[c]
DGR2_575.36_NB	3.3×10^{-11}	9.4×10^{-13}	0.029	0.046	0.63
DGR2_604.29_NB	3.5×10^{-11}	1.0×10^{-12}	0.029	0.052	0.55

[a] Samples below 3% bulk porosity give poor signal to noise ratio for radiographic measurements. These samples were not saturated with NaI, so no iodide accessible porosity measurements were made and C/C_0 profiles were determined from a calibrated approach. D_e was estimated from the product of $D_p \cdot \phi_w$ for these samples.

[b] DGR2_549.63 is affected by sample heterogeneity. The D_p value could only be fit for the first (72 hr) time series profile, all other time series were too noisy to attempt a fit.

[c] The $\phi_I/\phi_{w\,40}$ ratio is affected by the mixed lithology. The water loss porosity measurement was made on a portion of shale, while the diffusion sample contains some fossiliferous hard bed material.

Most samples were saturated with NaI tracer solution at the end of the experiment and D_p was determined by fitting the analytical solution to relative C/C_0 profiles and D_e calculated from the product of $D_p \cdot \phi_{I\ mean}$.

Figure 6 to Figure 8 present the profiles of iodide accessible porosity measured along the axis of the cylindrical samples. Both the shale and hard bed samples have relatively uniform porosity profiles, with average iodide-accessible porosities between 0.04 and 0.06 for shale, and 0.005 and 0.02 for hard beds. The profiles measured across the bedding direction (NB) display greater variability than those parallel to bedding (PB). Inflection points in the porosity profiles for the mixed lithology samples (Figure 8) indicate the position of changes in the rock type across the sample.

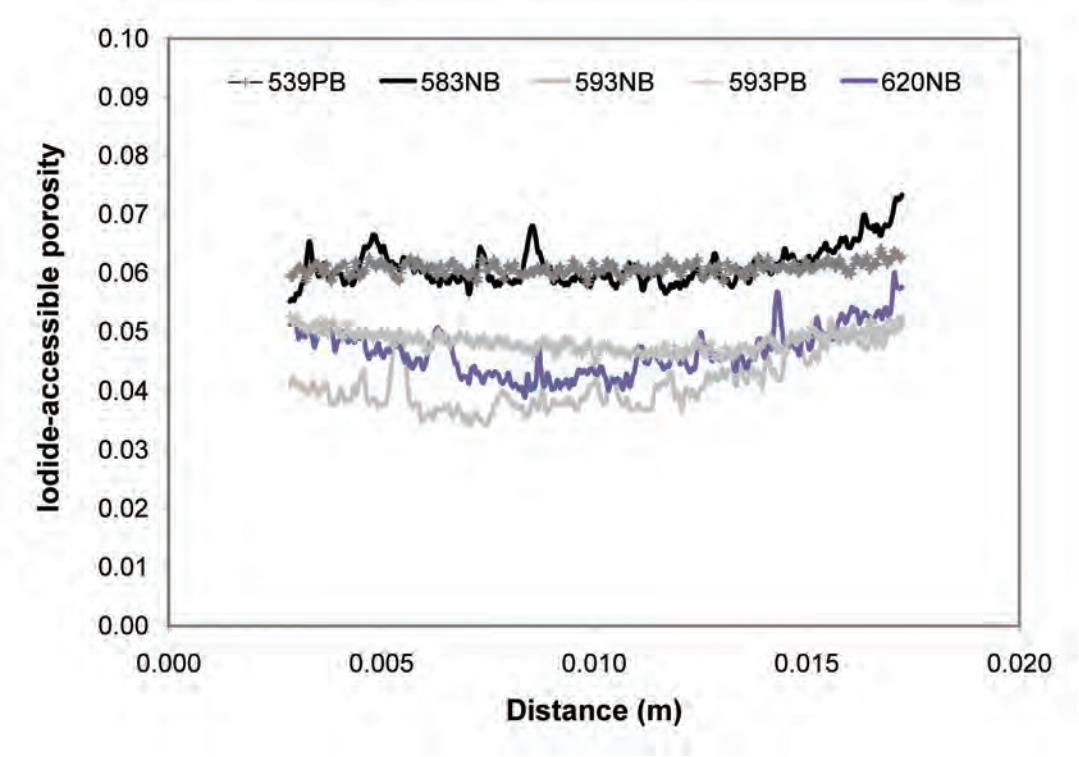

Figure 6: Iodide Accessible Porosity Profiles of Shale Samples.

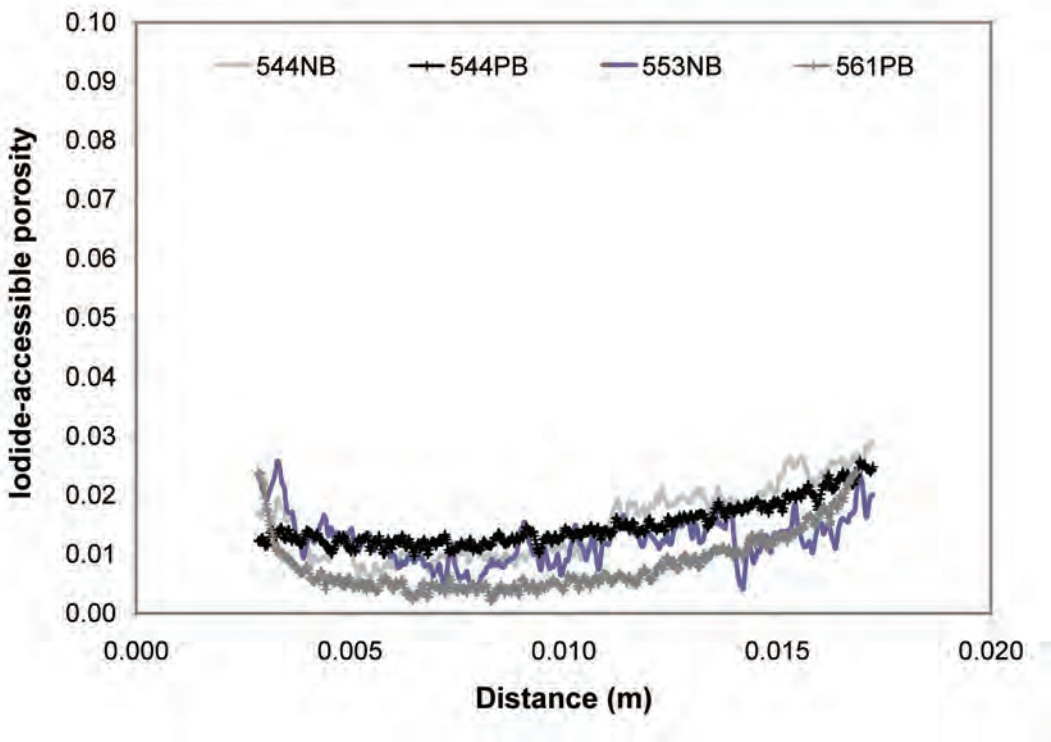

Figure 7: Iodide Accessible Porosity Profiles of Hard Bed Samples.

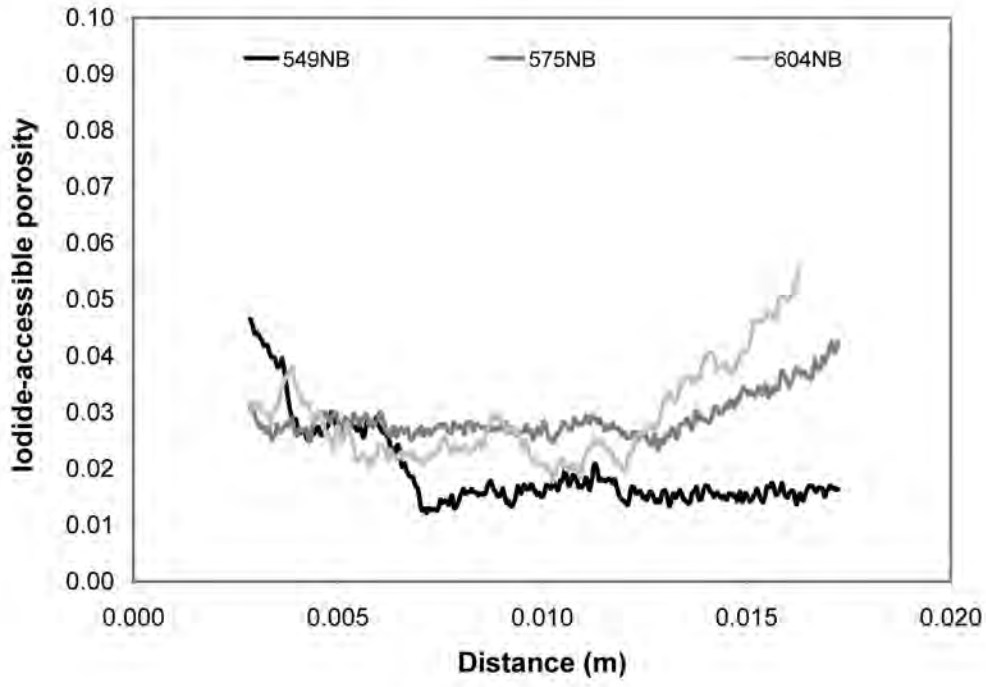

Figure 8: Iodide Accessible Porosity Profiles of Mixed Lithology Samples.

2.3.3.2 Through-Diffusion Measurements

A summary of the through-diffusion measurements appears in Table 8 and the experimental data are presented in graphical form in Appendix A.

Table 8: Diffusion Coefficients and Rock Capacity for Iodide and Tritium Measured by Through-Diffusion

Sample ID	$D_{e\,I}$ (m^2/s)	$D_{p\,I}$ (m^2/s)	α_I	$\phi_{w,40}$	$\alpha_I/\phi_{w,40}$
Shale					
DGR2_597.25_NB	2.2×10^{-12}	3.0×10^{-11}	0.075	0.082	0.92
DGR2_620.93_NB	8.5×10^{-13}	1.3×10^{-11}	0.067	0.089	0.75
Siltstone					
DGR2_544.05_NB	1.2×10^{-13}	5.9×10^{-12}	0.020	0.029	0.70
DGR2_544.05_PB	3.2×10^{-13}	1.2×10^{-11}	0.025	0.029	0.88
Siltstone/shale					
DGR2_537.32_NB	2.1×10^{-13}	9.8×10^{-12}	0.021	0.089	0.24[a]
Sample ID	**$D_{e\,HTO}$ (m^2/s)**	**$D_{p\,HTO}$ (m^2/s)**	**α_{HTO}**	**$\phi_{w,40}$**	**$\alpha_{HTO}/\phi_{w,40}$**
Shale					
DGR2_597.25_NB	4.6×10^{-12}	3.7×10^{-11}	0.124	0.082	1.52
DGR2_620.93_NB	2.4×10^{-12}	2.0×10^{-11}	0.118	0.089	1.32
Siltstone/shale					
DGR2_537.32_NB	4.3×10^{-13}	2.7×10^{-11}	0.016	0.089	0.18[a]

[a] $\alpha_I/\phi_{w,40}$ and $\alpha_{HTO}/\phi_{w\,40}$ for DGR2_537.32 are affected by sample heterogeneity. The porosity measurement was made on a portion of shale, while the diffusion sample contains mainly siltstone.

2.4 DISCUSSION

2.4.1 Comparison between Radiography and Through-Diffusion

Only three samples were run using both radiography and through-diffusion techniques (Table 9). This is a limited dataset and can not be considered statistically significant, but we observed that D_e values measured by radiography differed only slightly from those measured by through-diffusion, and α_I values determined by through-diffusion were greater than the average ϕ_I measurements from radiography.

Table 9: Comparison of Radiography and Through-Diffusion Results for Iodide

Sample ID	Radiography $D_{e\,I}$ (m^2/s)	Through-diffusion $D_{e\,I}$ (m^2/s)	Radiography ϕ_I	Through-diffusion α_I
DGR2_544.05_NB	8.5×10^{-14}	1.2×10^{-13}	0.014	0.020
DGR2_544.05_PB	1.7×10^{-13}	3.2×10^{-13}	0.014	0.025
DGR2_620.93_NB	9.1×10^{-13}	8.5×10^{-13}	0.046	0.067

Iodide-accessible porosity by both radiography and through-diffusion was about 3 times higher in DGR2_620.93_NB (Blue Mountain shale) than in either orientation (NB or PB) of DGR2_544.05 (Georgian Bay Fm siltstone). The Blue Mountain Formation shale D_e values were also higher than D_e for the Georgian Bay siltstone measured by either radiography or through-diffusion methods. Although the values measured by each technique are slightly different, the difference in all cases is less than a factor of 2 and there is generally good agreement in the trends observed for different rock types and sample orientation. This similarity between D_e values obtained by radiography and through diffusion is consistent with results of a method comparison reported by Cavé et al. (2009a).

2.4.2 Diffusion Anisotropy

To investigate possible anisotropy of diffusive properties, samples with the diffusion direction normal to bedding (NB) were paired with samples from the same core segment prepared with the diffusion direction parallel to the bedding (PB). Four such pairs were measured with radiography and one with through diffusion. The NB sample for one of the radiography pairs (DGR2_539.69) broke during sample preparation, so we have compared the results for DGR2_539.69PB with another shale NB sample, DGR2_583.18NB, which had the same measured iodide-accessible porosity (Table 10).

Table 10: Diffusion Coefficients and Iodide-accessible Porosities for Measurements Normal and Parallel to Bedding

Sample	Lithology	Iodide D_e (m^2/s)			ϕ_I or α_I		
		NB	PB	PB/NB	NB	PB	PB/NB
DGR2_544.05	siltstone	8.5×10^{-14}	1.7×10^{-13}	2.0	0.014	0.014	1
DGR2_544.05[TD]	siltstone	1.2×10^{-13}	3.2×10^{-13}	2.6	0.020	0.025	1.3
DGR2_561.90	siltstone	3.1×10^{-14}	7.8×10^{-14}	2.5	-	0.008	-
DGR2_593.53	shale	1.1×10^{-12}	3.6×10^{-12}	3.3	0.041	0.048	1.2
DGR2_539.69	shale	-	5.8×10^{-12}	3.2	-	0.061	1
DGR2_583.18	shale	1.8×10^{-12}	-		0.061	-	

[TD] = through diffusion sample.
– = no measurement available.

The number of samples for analysis of anisotropy is limited, but the results so far suggest that diffusion is faster in the direction parallel to bedding. Effective diffusion coefficients parallel to bedding for shale were more than 3 times higher than those measured normal to bedding, while siltstones had a slightly lower PB/NB ratio for the effective diffusion coefficients. Iodide accessible porosity measurements show very little difference in the average values with sample orientation, but measurements normal to bedding have greater heterogeneity in the porosity profiles than those made parallel to bedding (Figure 9).

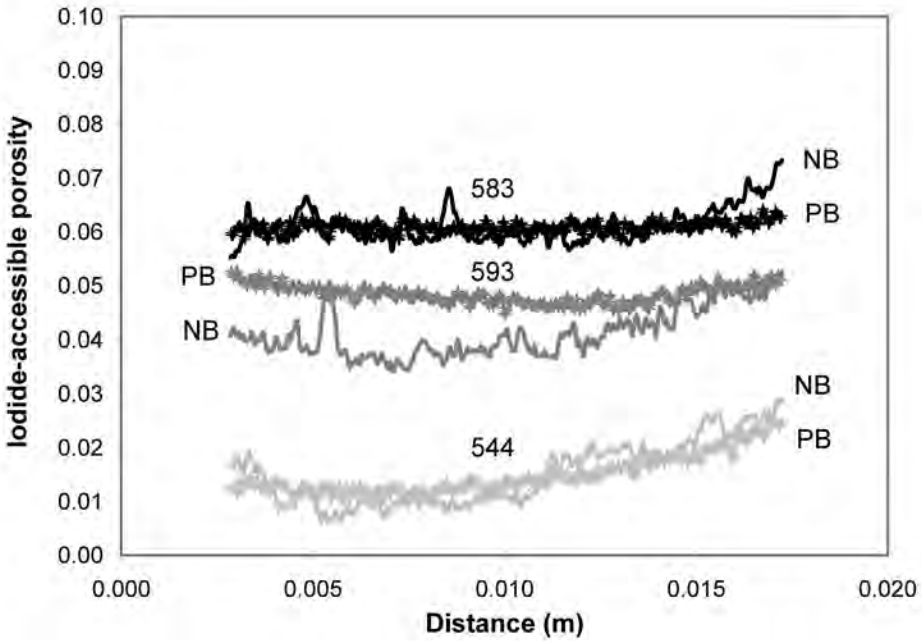

Figure 9: Iodide Accessible Porosity Profiles of Paired Radiography Samples with Diffusion Direction Normal (NB) and Parallel (PB) to Bedding.

2.4.3 Sample Heterogeneity and Diffusion Coefficients by Radiography

Fitting of an analytical solution to the C/C_0 diffusion profiles from radiography experiments is based on the assumption of a homogeneous porous medium. For the heterogeneous mixed lithology samples, the approach of using a single diffusion coefficient can only give an approximation of the diffusive coefficient of the sample. The measurement may be biased towards the rock material first encountered by the tracer, i.e. the lithology near the influx boundary, which would control the early time C/C_0 profiles. Among the heterogeneous samples, diffusion profile fitting was more successful for mixed lithology samples DGR2_575NB and DGR2_604NB (Figure 10, Figure 11), which display relatively flat porosity profiles near the influx boundary compared to DGR2_549NB which has a steep porosity gradient near the influx boundary. Only the 72 hour profile could be matched for sample DGR2_549NB because the C/C_0 profiles became too noisy for adequate profile matching at later times when the tracer encountered the lower porosity material in the upper part of the radiography sample (Figure 12).

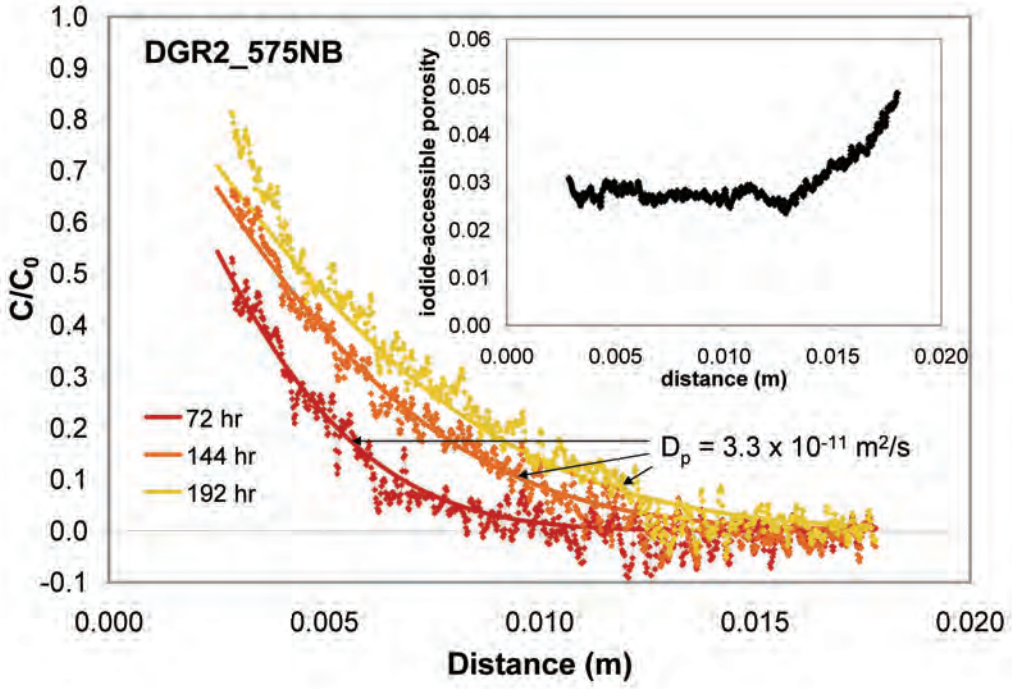

Figure 10: Fitting of an Analytical Solution to Time Series Profiles of C/C_0 for Mixed Siltstone/Shale Sample DGR2_575NB.

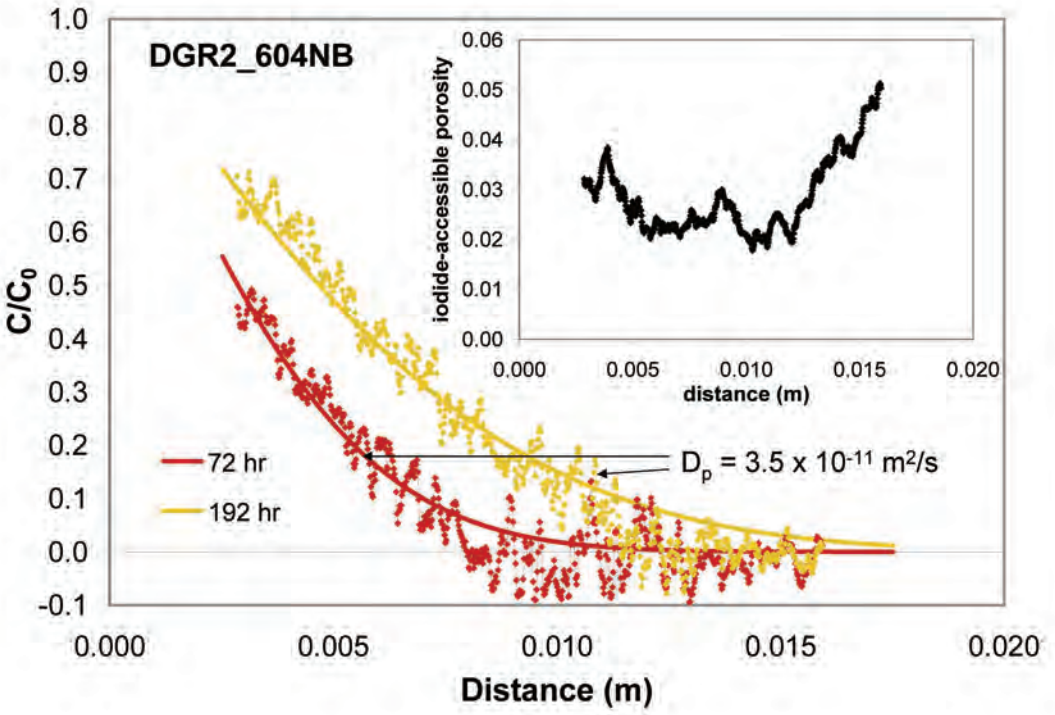

Figure 11: Fitting of an Analytical Solution to Time Series Profiles of C/C_0 for Mixed Dolostone/Shale Sample DGR2_604NB.

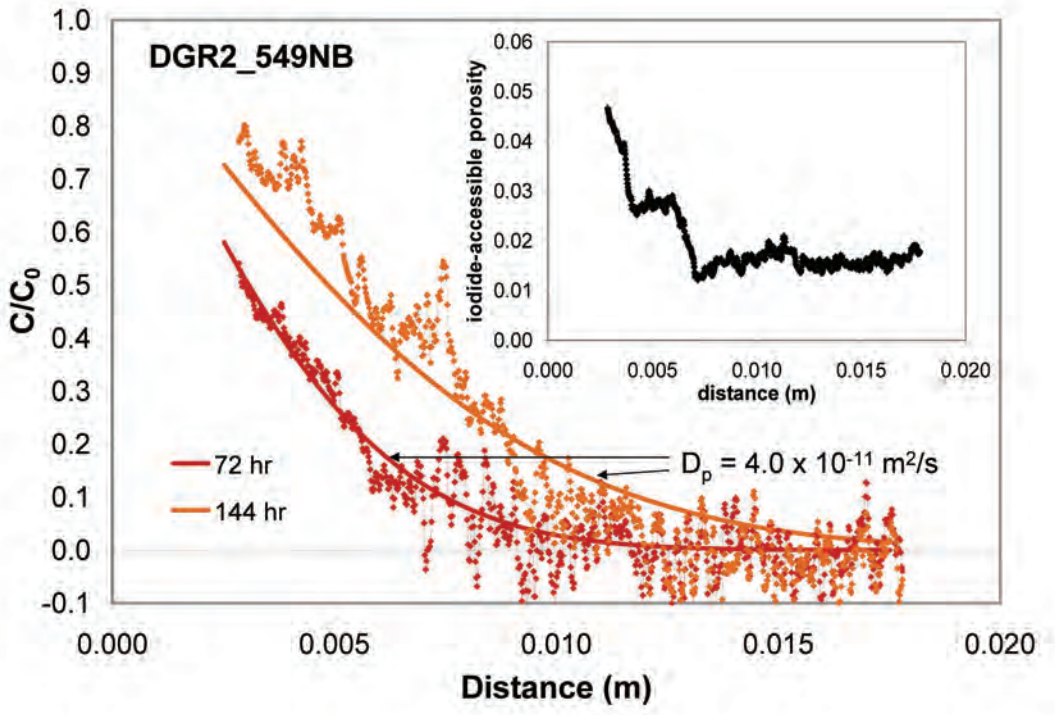

Figure 12: Attempted Fitting of an Analytical Solution to Time Series Profiles of C/C_0 for Mixed Shale/Limestone Sample DGR2_549NB. The fit of the analytical solution to the experimental data is poor at late time (144 hr).

2.4.4 Lithological Controls on Porosity and Diffusion Properties

Porosity is strongly dependent on the lithology of the samples. The values of ϕ_w for grey shale is four to five times greater than ϕ_w for limestone and siltstone samples (Figure 13). Over the 100 m depth range from which these samples were collected, the porosities for each rock type appear to be independent of sample depth, although it should be noted that porosity tests and diffusion experiments were conducted on core samples brought to surface and stored at atmospheric pressure, which would not reproduce the confining pressure of in situ conditions. Two samples (DGR2_575.36 and DGR2_604.29) contained a mixture of shale and siltstone or dolostone material and their intermediate ϕ_w values probably reflect contributions from both higher and lower porosity materials.

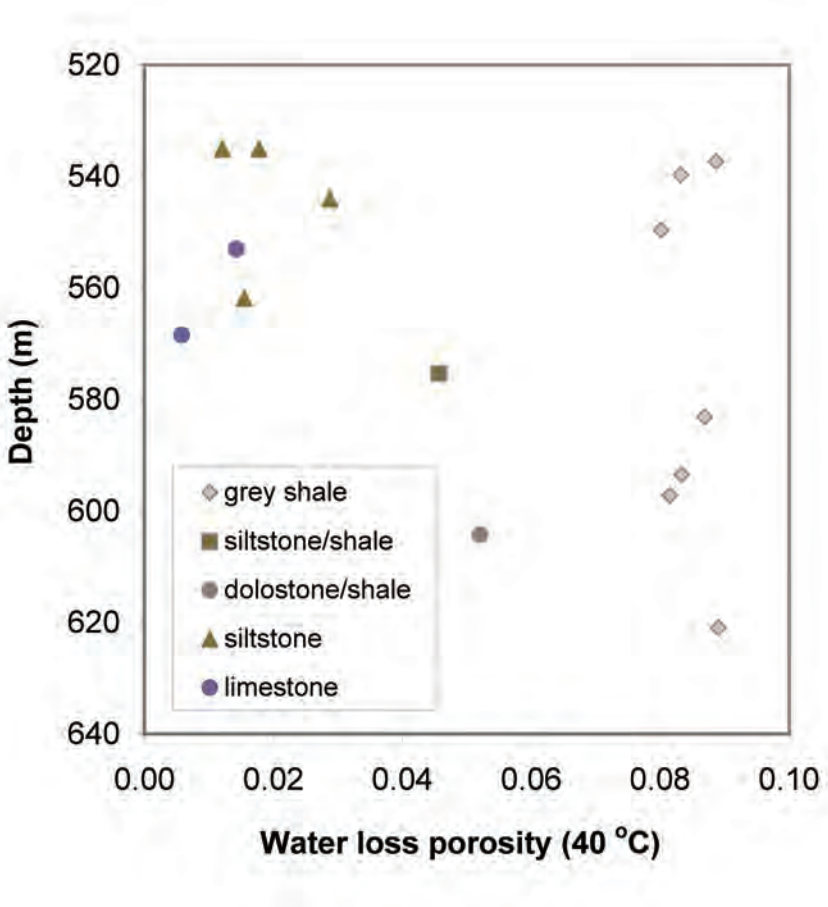

Figure 13: Water Loss Porosity as a Function of Lithology and Depth.

Another indicator of the lithological control on porosity is the good linear correlation between clay mineral content (weight %) and ϕ_w values (Figure 14). There is a weaker inverse relationship between porosity and carbonate mineral content (Figure 15).

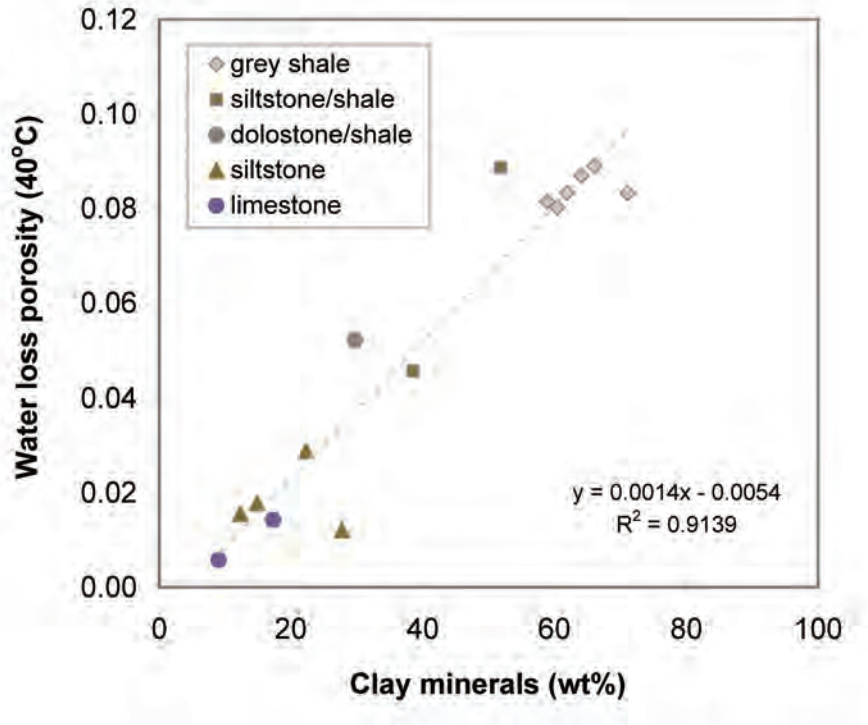

Figure 14: Relationship between Water Loss Porosity and Clay Content of Samples from the Georgian Bay Formation.

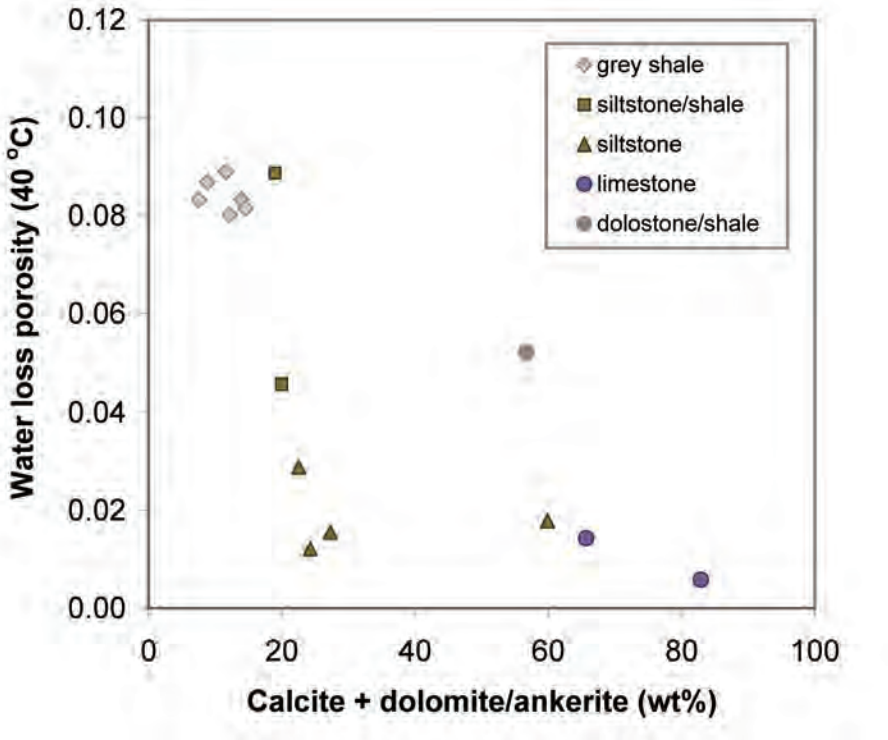

Figure 15: Inverse Relationship between Water Loss Porosity and Carbonate Content of Samples from the Georgian Bay Formation.

Similar correlations with lithology are also found using diffusion-accessible porosity measurements instead of water loss porosity, with higher iodide-accessible porosity values measured for shale than for hard beds (Figure 16). In all cases the iodide-accessible porosity (ϕ_I) measured in radiography and through-diffusion experiments is lower than the bulk water loss porosity (ϕ_w) measured on an adjacent sample from the same rock core segment. This suggests that a lower proportion of the total porosity is accessible to iodide, possibly due to anion-exclusion of the large iodide anion in small clay-filled pores. Two mixed-lithology samples have been circled in Figure 16, because the data for DGR2_537NB and DGR2_549NB should be treated with caution here. Diffusion-accessible porosities were measured on samples that appeared to be mainly siltstone, while water-loss porosity measurements were measured on adjacent shale material from the same core sample (see notes below Table 7 and Table 8).

A summary of the through-diffusion measurements appears in Table 8 and the experimental data are presented in graphical form in Appendix A.

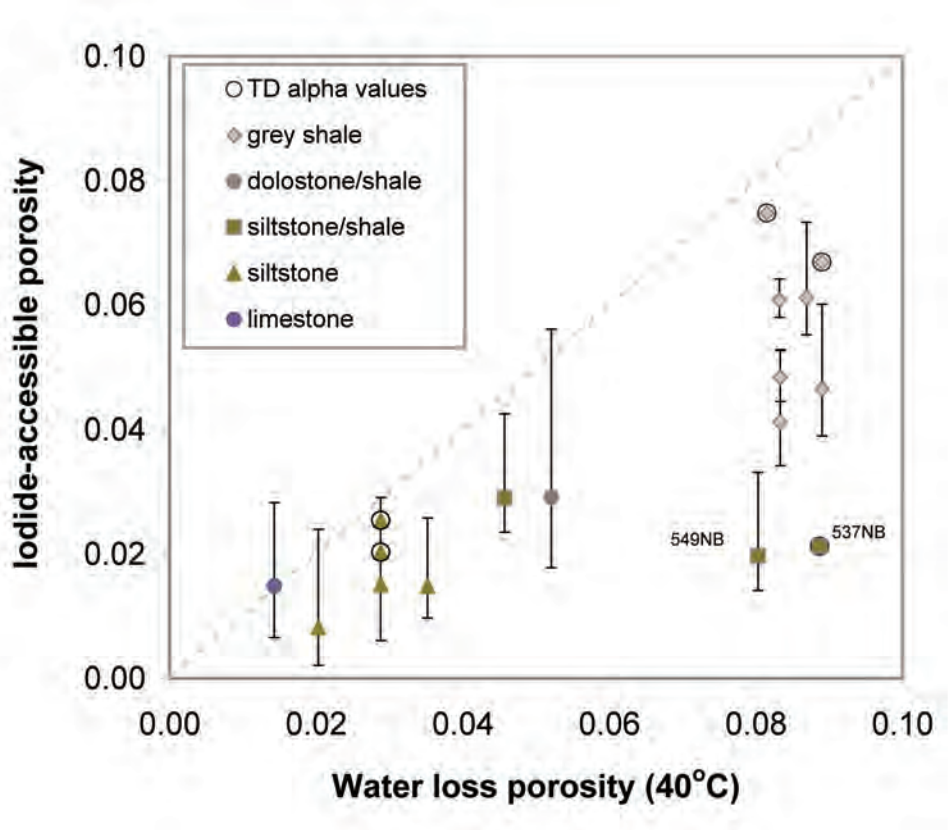

Figure 16: Comparison between Iodide-accessible Porosity Measurements in Diffusion Experiments measured using Radiography and Through Diffusion (TD) versus Bulk Water-loss Porosity Measurements for Georgian Bay Formation Samples. Solid Symbols indicate average ϕ_I measured using radiography with bars indicating the range of ϕ_I values measured along the length of the samples.

Lithology and sample orientation also have a strong control on D_e. Effective diffusion coefficients for the shale layers in the Georgian Bay Formation are up to an order of magnitude higher than the D_e values for hard bed interlayers, while mixed lithology samples yielded intermediate values. Effective diffusion coefficients appear to be correlated with clay mineral content (Figure 17), although given the dependence of D_e on porosity, the apparent correlation between D_e and clay content may simply reflect the strong correlation between clay content and porosity (Figure 14). There is an apparent negative correlation between D_e and carbonate-mineral content (Figure 18), which may also reflect an underlying control on D_e by porosity because samples with elevated carbonate-mineral content generally have low porosity (Figure 15).

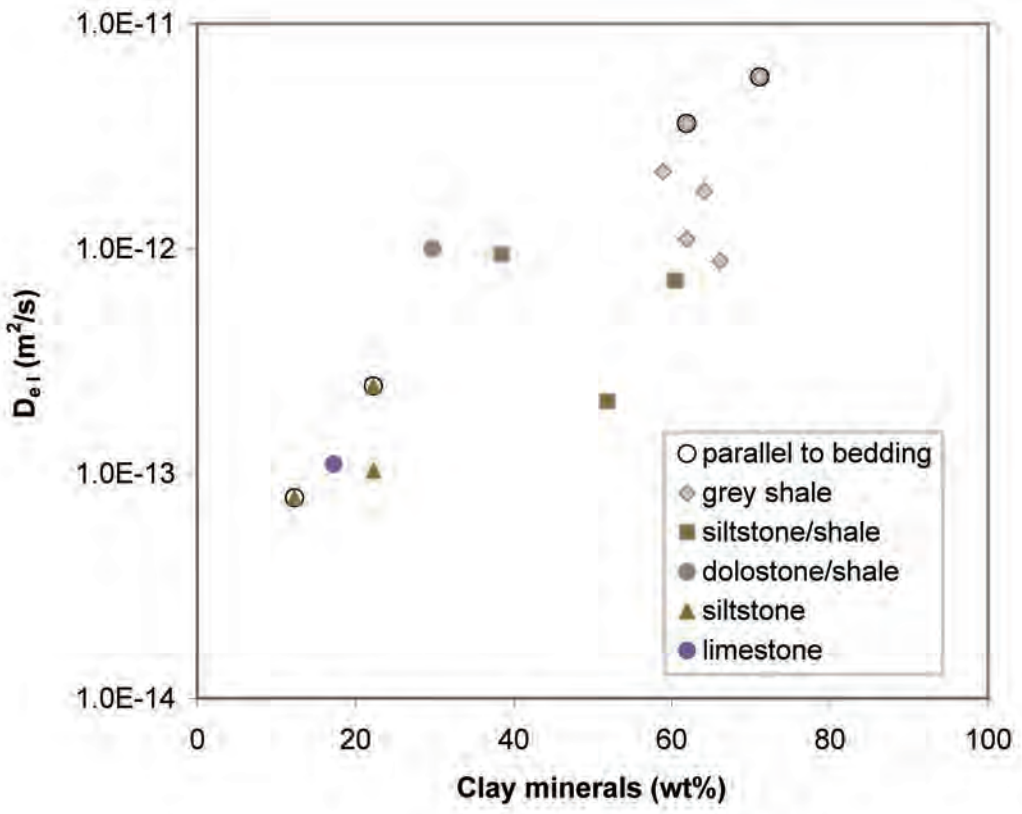

Figure 17: Iodide Effective Diffusion Coefficients as a Function of Clay Mineral Content and Lithology. Note That Circled Data Points Represent Samples That Were Measured Parallel to Bedding.

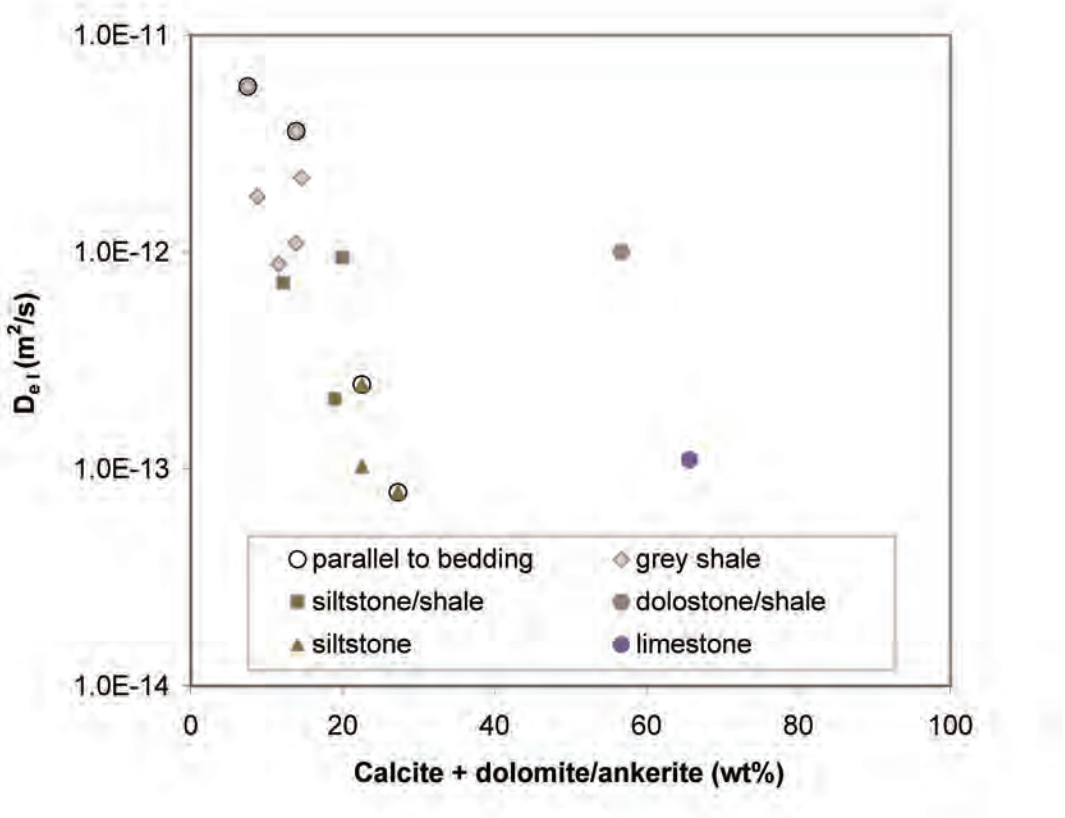

Figure 18: Iodide Effective Diffusion Coefficients as a Function of Carbonate Mineral Content and Lithology. Note That Circled Data Points Represent Samples That Were Measured Parallel to Bedding.

Relationships between diffusive properties and porosity have been described in the literature using Archie's Law (e.g. Boving and Grathwohl, 2001). The normalized diffusion coefficient (or diffusivity, D′) is related to the porosity by an empirical expression:

$$D_e/D_0 = D' = \phi^m \qquad [14]$$

where D_e is the effective diffusion coefficient; D_0 is the free-water diffusion coefficient for the solute; D′ is the diffusivity; ϕ is the total porosity; and m is an empirical Archie's law exponent.

For these samples, diffusivity was calculated by dividing D_e by a D_0 value for iodide of 2.045 x 10^{-9} m^2/s (Vanýsek 2006) and plotted against the bulk physical porosity (Figure 19). Through-diffusion and radiography data were combined in this analysis, taking a mean value for those samples where D_e was determined by both techniques.

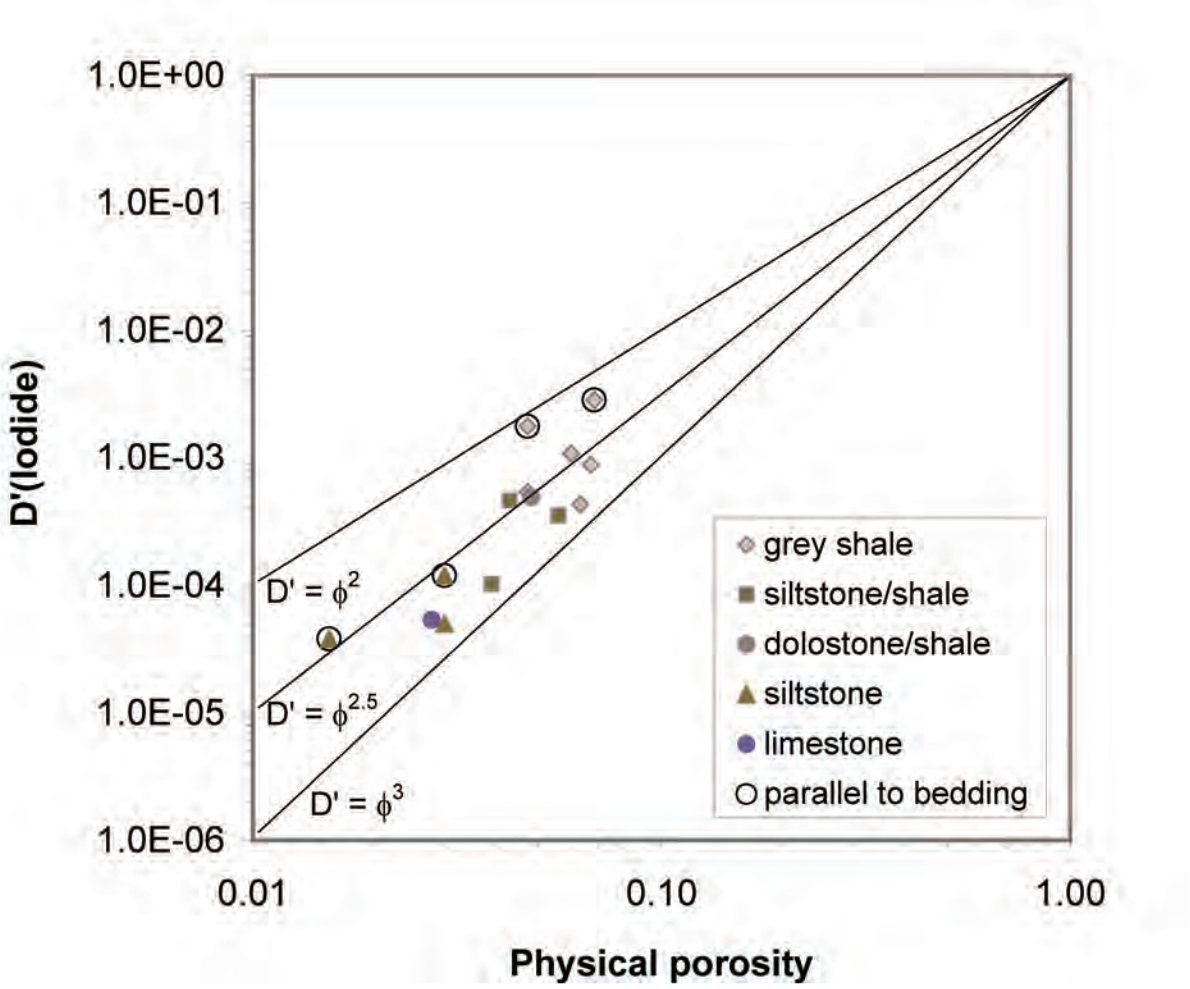

Figure 19: Calculated Diffusivities versus Measured Physical Porosities for Samples from the Georgian Bay and Blue Mountain Formation. Note That Circled Data Points Represent Samples That Were Measured Parallel to Bedding.

Archie's law with an exponent of 2 to 2.5 would best describe the diffusivity measurements made parallel to the bedding direction, while those normal to the bedding fall within a range of m = 2.5 to 3. Boving and Grathwohl (2001) fit their data for sandstone and limestone samples with typically higher porosities than these samples, using a value for m of 2.2.

2.4.5 Representative Values of Iodide Diffusion Coefficients for Shale and Hard Beds

Available iodide D_e data for the Georgian Bay Formation from Southern Ontario were combined in an attempt to find end-member values for shale and hard beds that could be used to estimate the formation scale diffusion properties. Samples in Table 11 were selected as being representative of either shale or hard beds and heterogeneous samples containing mixed

lithologies were excluded from the analysis. The data include both radiography and through-diffusion measurements.

Table 11: Summary of Iodide Diffusion Coefficient Data for Georgian Bay Shale and Hard Bed Samples

Sample	Description	D_p (m^2/s)	$\phi_{I\,av}$ or α_I	D_e m^2/s
DGR2_554NB	shale, NB, rad	2.3×10^{-11}	0.044	1.0×10^{-12}
DGR2_583NB	shale, NB, rad	3.0×10^{-11}	0.061	1.8×10^{-12}
DGR2_593NB	shale, NB, rad	2.7×10^{-11}	0.041	1.1×10^{-12}
DGR2_596NB	shale, NB, rad	3.5×10^{-11}	0.039	1.4×10^{-12}
DGR2_596NB	shale, NB, TD	1.8×10^{-11}	0.080	1.4×10^{-12}
DGR2_597NB	shale, NB, TD	3.0×10^{-11}	0.075	2.2×10^{-12}
DGR3_608NB	shale, NB, rad	1.2×10^{-11}	0.041	4.8×10^{-13}
DGR4_595NB	shale, NB, rad	1.4×10^{-11}	0.042	6.0×10^{-13}
Mean ± std.dev	**shale, NB**	**$2.4 \pm 0.8 \times 10^{-11}$**	**0.053 ± 0.017**	**$1.2 \pm 0.6 \times 10^{-12}$**
DGR2_539PB	shale, PB, rad	9.5×10^{-11}	0.061	5.8×10^{-12}
DGR2_593PB	shale, PB, rad	7.5×10^{-11}	0.048	3.6×10^{-12}
DGR2_596PB	shale, PB, rad	7.5×10^{-11}	0.067	5.0×10^{-12}
DGR3_608PB	shale, PB, rad	5.4×10^{-11}	0.043	2.3×10^{-12}
DGR4_595PB	shale, PB, rad	6.3×10^{-11}	0.045	2.8×10^{-12}
Mean ± std.dev	**shale, PB**	**$7.2 \pm 1.5 \times 10^{-11}$**	**0.053 ± 0.011**	**$3.9 \pm 1.5 \times 10^{-12}$**
DGR2_537NB	hard bed, NB, TD	9.8×10^{-12}	0.021	2.1×10^{-13}
DGR2_544NB	hard bed, NB, rad	6.0×10^{-12}	0.014	8.5×10^{-14}
DGR2_544NB	hard bed, NB, TD	5.9×10^{-12}	0.020	1.2×10^{-13}
DGR2_553NB	hard bed, NB, rad	9.5×10^{-12}	0.011	1.1×10^{-13}
Mean ± std.dev	**hard bed, NB**	**$7.8 \pm 2.1 \times 10^{-12}$**	**0.017 ± 0.005**	**$1.3 \pm 0.5 \times 10^{-13}$**
DGR2_544_PB	hard bed, PB, rad	1.2×10^{-11}	0.014	1.7×10^{-13}
DGR2_544_PB	hard bed, PB, TD	1.2×10^{-11}	0.025	3.2×10^{-13}
DGR2_561_PB	hard bed,PB, rad	1.0×10^{-11}	0.008	7.8×10^{-14}
Mean ± std.dev	**hard bed, PB**	**$1.1 \pm 0.1 \times 10^{-11}$**	**0.016 ± 0.009**	**$1.9 \pm 1.2 \times 10^{-13}$**

PB is parallel to bedding
NB is normal to bedding
TD = through-diffusion
rad = radiography

2.4.6 Scaling-Up Diffusion Measurements with Weighted Averages

Using mean values of iodide D_e measured normal to the bedding direction for shale (1.2×10^{-12}) and hard beds (1.3×10^{-13}) (Table 11), D_e values normal to bedding were estimated for each 3-metre core run through the Georgian Bay Formation in DGR2 using the harmonic mean weighted by the proportions of each rock type (Table 2). The results are presented as a depth profile of estimated D_e values for transport in the direction normal to bedding (Figure 20). Point

measurements of D_e from individual shale and hard bed samples are also shown for comparison. The slight increase in estimated D_e values with depth is a result of the decreasing frequency and thickness of hard bed layers in the lower parts of the Georgian Bay Formation. Similarly, estimates of D_e in the direction parallel to bedding were estimated for each 3-metre core run (Figure 21) using the arithmetic mean weighted by the proportions of each rock type (Table 2). The individual anisotropy ratios (PB:NB) for the 3 m core runs range from 3.5 to 8.7. A formation scale anisotropy ratio for D_e (PB:NB ratio) which accounts for all of the discrete hard bed and shale units was also estimated. This was done by calculating the formation arithmetic mean for D_e parallel to bedding and the formation harmonic mean for D_e normal to bedding, each weighted by the measured proportions of hard bed and shale (Table 2). A formation scale anisotropy ratio of 7.2 is obtained from the ratio of the arithmetic to the harmonic mean.

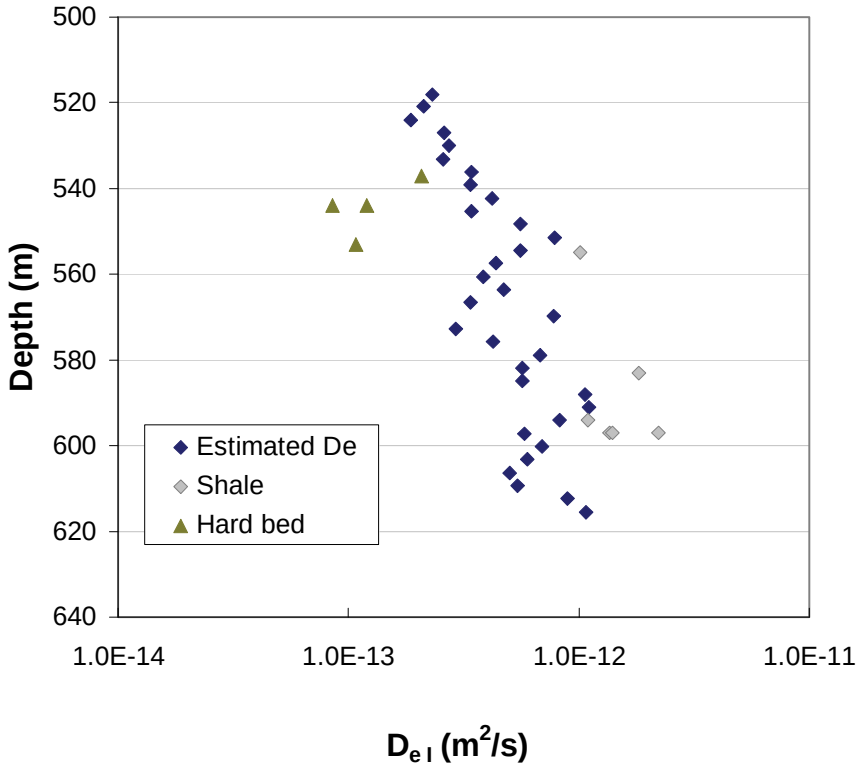

Figure 20: Weighted Harmonic Average of Iodide D_e Values Normal to Bedding (i.e. Vertical Diffusion) as a Function of Depth, Based on the Proportions of Shale and Hard Bed Material in each Core Run.

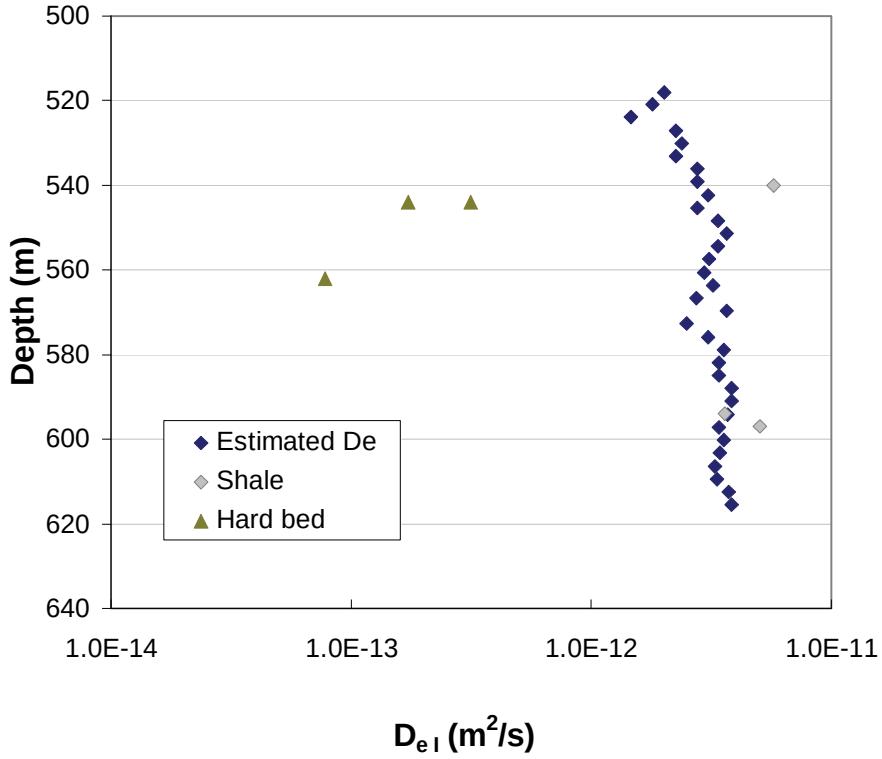

Figure 21: Weighted Arithmetic Average of Iodide D_e Values Parallel to Bedding (i.e. Horizontal Diffusion) as a Function of Depth, Based on the Proportions of Shale and Hard Bed Material in each Core Run.

2.5 CONCLUSIONS

This section describes the development of a protocol for characterizing the variability in diffusive properties across a sedimentary rock formation using the relationships between diffusion and physical and mineralogical properties of the rock. The heterogeneous interlayered shales and hard beds of the Ordovician Georgian Bay Formation were used as a demonstration case.

Diffusion coefficients and diffusion-accessible porosity were measured on fifteen samples representing shale layers, hard beds and mixed lithologies from across the Georgian Bay Formation in Southern Ontario. The measurements were made by radiographic and through-diffusion techniques using conservative tracer species. These were supported by characterization of the mineralogy (including clay mineral content), inorganic and organic carbon and total sulfur, water-loss porosity, physical porosity, bulk density, grain density and surface area of adjacent samples. Relationships were then sought between physical and mineralogical properties of the rocks and diffusive properties. A detailed log of the centimetre-scale changes in lithology across the entire Georgian Bay Formation was also prepared from a

photographic log of the core, encompassing nearly 800 discrete hard bed layers alternating with grey shale.

The Georgian Bay Formation, as represented in samples collected as part of this study, displays a high degree of lithological heterogeneity at the centimetre to metre scale. Shale intervals range in thickness from 0.5 to 230 cm, with thin hard bed interlayers of 0.25 to 40 cm. Over the depth interval from 518 to 616 m, shale makes up 77.5% and hard beds 22.5% of the total thickness. There is a general trend of decreasing thickness and occurrence of hard beds with depth through the formation. These variations in lithology are expected to affect the diffusive properties across the formation.

Porosity and D_e were found to be strongly dependent on sample lithology, with shale samples displaying higher porosities and diffusion coefficients than the hard beds. For the shale samples, the average physical porosity was 0.061, average ϕ_w was 0.085, average ϕ_I was 0.053. There was little distinction between the average values for physical porosity (0.018), ϕ_w (0.016) and ϕ_I (0.017) for the hard bed samples. Iodide D_e values measured normal to the bedding direction averaged 1.2×10^{-12} m^2/s for shale and 1.3×10^{-13} m^2/s for hard beds. Average D_e values for shale measured parallel to the bedding were approximately three times higher than those normal to bedding (3.9×10^{-12} m^2/s vs 1.2×10^{-12} m^2/s) while the ratio of D_e values measured parallel versus normal to bedding for hard beds was less than two (1.9×10^{-13} m^2/s vs 1.3×10^{-13} m^2/s). Samples of mixed lithology tend to show intermediate values for porosity and diffusion coefficients.

Average D_e values for shale and hard beds, and the detailed lithological logs, were combined to predict formation-scale trends in D_e versus depth for diffusion normal and parallel to bedding (Figures 20 and 21). In the case of diffusion normal or parallel to bedding, the trend is toward a slight increase in D_e versus depth because of the decreasing hard bed content with depth and the greater anisotropy in the diffusive properties of the shale compared to the hard bed layers.

3. QUANTIFICATION OF DIFFUSION-REACTION PROCESSES USING RADIATION IMAGING

So far the investigations of diffusive properties of low permeability rocks described in this report have been concerned with conservative tracers (iodide anion and tritiated water). In this section we describe an adaptation of the radiographic method that allows for investigations of diffusion and reaction using a non-conservative cationic tracer species in sedimentary rock materials. The method provides a means of quantifying cation exchange capacity in an intact rock sample.

3.1 DIFFUSION-SORPTION STUDIES WITH NON-CONSERVATIVE TRACERS

Non-conservative transport is of interest because many of the radionuclides present in used fuel may interact strongly with clay-based materials in engineered barriers (e.g. bentonite) and with host rocks that have appreciable sorption capacities (van Loon et al. 2005). Quantification of the retention of these solutes is, therefore, important in the safety assessment for a deep geologic repository.

In this section, we present a method for the quantification of diffusive transport properties using the non-conservative tracer cesium (Cs). The method is a modification of the radiographic technique that was developed for iodide diffusion measurements (Section 2.2.3). Time series measurements of changes in X-ray absorption are used to quantify the spatial distribution of Cs tracer mass during transport and reaction in low permeability, sedimentary rock. The resultant Cs relative concentration profiles are fitted using output from a reactive transport model that couples diffusion and ion exchange processes. The numerical model is used to find estimates for Cs diffusion coefficients ($D_{p\,Cs}$), ion-exchange selectivity coefficient for Cs relative to Na ($k_{Cs+/Na+}$) and cation exchange capacity (CEC) of the sample.

The occurrence and behaviour of Cs have made this one of the most widely studied elements in sorption experiments for radioactive waste disposal (e.g. Bradbury and Baeyens 2000; Melkior et al. 2005; Maes et al. 2008; Jakob et al. 2009). Cesium is a common radionuclide found in used nuclear fuel and radioactive ^{137}Cs (half-life = 30 years) has already been released to the environment from weapons testing and the Chernobyl accident (Bradbury and Baeyens 2000). Cesium is similar to potassium in being readily soluble and bioavailable. Its simple speciation (occurring predominantly as the monovalent cation Cs^+) and significant, reversible sorption make Cs a good tracer for diffusion-sorption experiments (Melkior et al. 2005). Cesium is also well suited for X-ray radiography detection because of its high atomic number and therefore strong X-ray absorption in comparison to the elements that make up the minerals in the bulk of a rock sample.

Other solute transport studies with Cs in low permeability materials have typically used through-diffusion experiments to determine apparent diffusion coefficients (D_a), but waiting for the experiment to reach steady state can be very time consuming with a strongly sorbing tracer (months to years). The radiography method allows diffusion-reaction data to be collected over a much shorter time frame (days to weeks) by measuring tracer profiles in the rock during the transient (non-steady state) portion of the experiment. This is similar to the Cs profiles obtained with an in-diffusion approach as used by Cormenzana et al. (2003) to measure apparent diffusion coefficients for Cs in compacted bentonite, with the exception that the radiographic method is non-destructive.

In some cases, D_a has been calculated from D_e values obtained with through-diffusion and conservative tracers such as HTO, and K_d values obtained from batch sorption experiments on crushed samples. However, that approach may under-predict diffusion of cations such as Cs^+ and Sr^{2+} (Bourg et al. 2003) and there is some debate as to whether results should be combined from intact (through-diffusion) and crushed (batch test) samples.

Crushed samples are also commonly used for measuring CEC, an empirical parameter that describes the total quantity of exchangeable cations (in milliequivalents of charge) available in a specified mass of rock or soil sample. Techniques for determining CEC use concentrated solutions of strongly exchangeable cations such as NH_4^+, Cs^+, Ca^{2+}, Sr^{2+} or Ba^{2+} or exchange complexes such as cobalt hexamine, silver thiourea or nickel ethylenediamine to displace all exchangeable cations from the exchange sites in batch experiments with disaggregated rock samples (Bradbury and Baeyens 2000). By using a concentrated Cs^+ tracer in the radiography diffusion-reaction experiments, cations on the exchange sites are exchanged for Cs^+, allowing for quantification of CEC on the intact rock samples.

3.2 MATERIALS AND METHODS

3.2.1 Core Sample

For initial testing of the modified radiographic method, a simple test case was sought which would be unlikely to suffer from artefacts due to very low porosity or sample heterogeneity. For this reason, a preserved, homogeneous, red shale sample with relatively uniform porosity and diffusive properties was selected from the Queenston Formation in a borehole drilled in Southern Ontario.

A photograph of the sample is presented in Figure 22 and a summary of the properties of Queenston Formation shale from related studies is given in Table 12. The samples were prepared by slicing a core segment of approximately 2 cm thickness from near the centre of the sample (Figure 22) and subcoring six minicores of 11 mm diameter from the core segment. All samples were orientated with the core axis normal to the bedding plane direction. Three of the minicores were used to determine the conservative transport (diffusion-only) properties of the rock using iodide tracer and the other three for non-conservative transport (diffusion and reaction) using Cs tracer. The material remaining in the segment after removing the minicores was divided in two and used for duplicate measurements of ϕ_w at 40°C, and a separate segment was cut from the large drill core for use in determining ϕ_w at 105 °C (Figure 22). All ϕ_w measurements were conducted with the method described in Section 2.2.2.7.

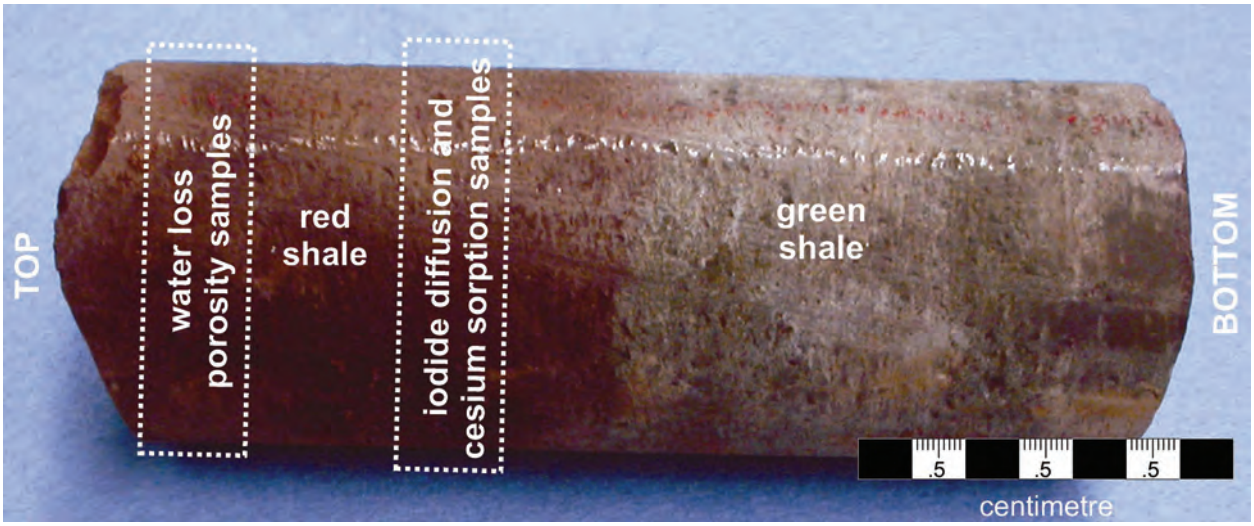

Figure 22: Photograph of Core Sample DGR3_468.02 Showing Locations of Red Shale Subsamples taken for Porosity and Diffusion-Reaction Measurements.

Table 12: Lithology and Physical Properties of Shale Samples from the Queenston Formation

Period	Formation	Sample ID	Rock type	n	Mean water loss porosity	Mean grain density
Ordovician	Queenston	DGR2_456.97	Red shale	4	9.04 ± 0.55	2.80
Ordovician	Queenston	DGR2_517.96	Red shale	3	7.80 ± 0.30	2.77
Ordovician	Queenston	DGR3_468.02	Red shale	2	10.93 ± 0.14 [a]	2.83
Ordovician	Queenston	DGR3_468.02P	Red shale	2	7.98 ± 0.05 [b]	2.76
Ordovician	Queenston	DGR4_516.89	Red shale	2	9.34 ± 0.29	2.80

Sample ID	**DGR2_456.97**	**DGR2_517.96**
Rock type	Red shale	Red shale
Quartz (wt%)	12	24
K-feldspar (wt%)	1	4
Calcite (wt%)	29	10
Dolomite/ankerite (wt%)	7	18
Sum (wt%)	49	56
Clay minerals (wt%)	51	43
Organic C (wt %)	0.3	<0.1
Other XRD peaks	Hematite, muscovite/illite, chlorite	Chlorite

Data from samples analyzed by University of New Brunswick and University of Bern.
[a] porosity measured on nearby subsamples (Figure 22) from the core sample (dried at 105°C).
[b] porosity measured on offcuts from the diffusion samples (dried at 40°C). This water loss porosity was used to calculate relative Cs concentration profiles in diffusion-reaction experiments.

3.2.2 Conservative Tracer Diffusion Properties by Radiography Using Iodide

Iodide D_p values and ϕ_I profiles were determined in triplicate on samples labelled DGR3_468A, DGR3_468B and DGR3_468C. The methods used to make these measurements are described in detail by Cavé et al. (2009a, b) and in Sections 2.2.3.1 and 2.2.3.2 of this report.

Two minor changes were made to the design of the diffusion cell for these measurements to improve the quality of the radiographic measurements:

- The aluminum internal standard cap was replaced by an impermeable ceramic cap which, unlike aluminum, was not subject to corrosion after prolonged contact with the brine solutions.
- Two wire alignment guides were positioned at 180° to each other along the sides of the samples and allowed to protrude slightly above the sample cap. These allowed for greater reproducibility in the rotational positioning of the sample between time series measurements.

3.2.3 Calibration of Cs X-Ray Absorption

Quantification of Cs concentrations in the rock samples was based on a calibrated relationship between Cs concentrations and change in X-ray absorption ($\Delta\mu$) measurements (Figure 23).

The calibration method involved preparing standard solutions of CsCl in synthetic porewater (SPW) matrix (Appendix B) at concentrations of 0.01, 0.02, 0.03, 0.05, 0.1 and 0.25 mol/L Cs. Glass vials with 11 mm internal diameter were used to collect 2 to 4 radiographs of each standard solution and a SPW reference solution (without Cs), using identical operating conditions to those used in experimental data collection.

The radiograph data were then analyzed using ImageJ processing software in a manner similar to that outlined in Section 2.2.3.1. The change in X-ray attenuation ($\Delta\mu$) versus distance was calculated for each standard solution from the greyscale profiles by taking the natural logarithm of the greyscale values and subtracting ln (SPW reference solution) – ln (CsCl standard solution). A mean value of $\Delta\mu$ was determined for each standard solution from the central portion of the $\Delta\mu$ versus distance profile where the profile is flat (e.g. 300 to 700 pixel range). A plot of mean $\Delta\mu$ versus Cs concentration was prepared (Figure 23) and the calibration curve fitted by linear regression. Duplicate standards and repeat radiographs were used to determine standard deviation and plot error bars for the $\Delta\mu$ values.

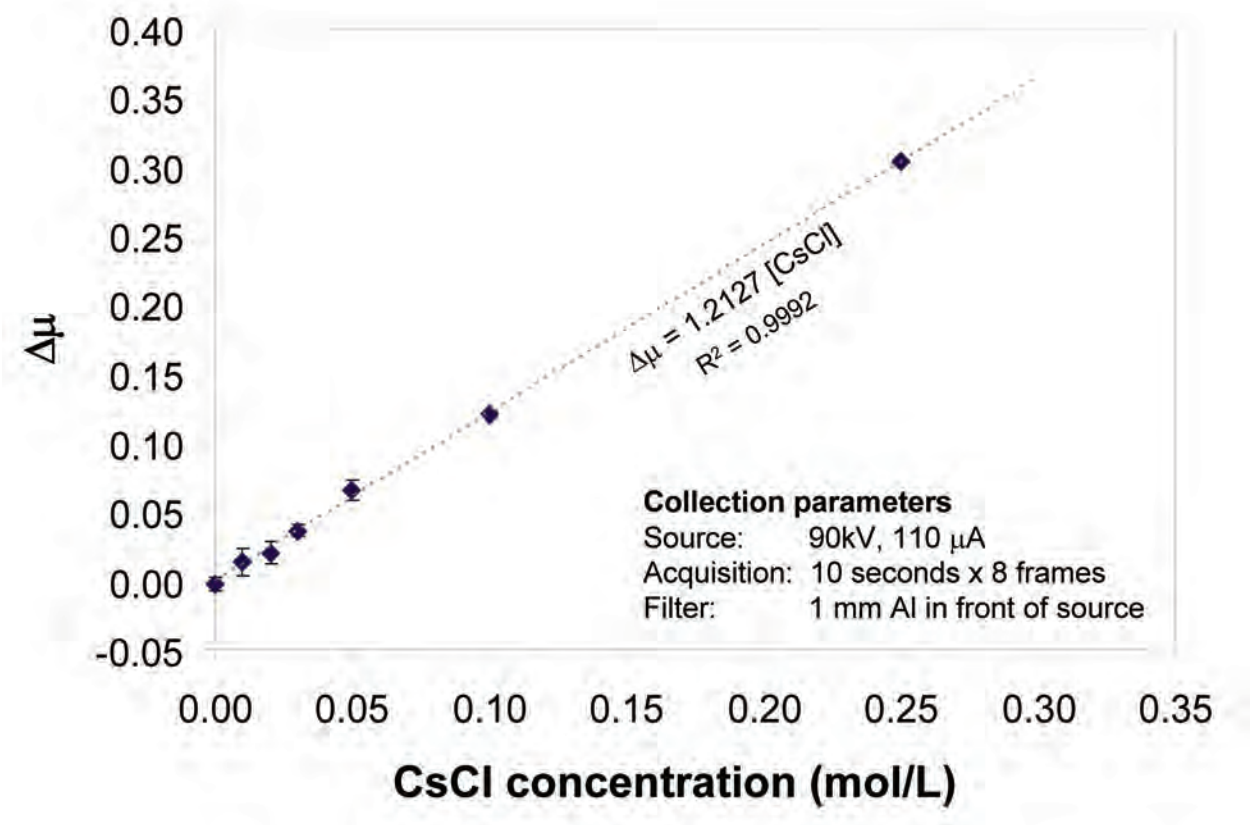

Figure 23: Calibration Curve Used to Determine Cs Concentrations from Radiographic Measurements of Δμ.

3.2.4 Non-Conservative Tracer Diffusion Properties by Radiography Using Cs

Diffusion-reaction measurements are made by monitoring the movement of Cs^+ through a sample of rock under hydrostatic conditions using X-ray radiography. All X-ray data were collected on a Skyscan 1072 Desktop MicroCT system using 90 keV source energy, 110 μA current and averaging 8 image frames, each of which was collected over a 10 s acquisition time. A 1-mm aluminum filter was used to filter out low energy X-rays from the polychromatic source and the images were flat-field corrected. Measurements were conducted at a temperature of 23°C.

In preparation for the experiments, the circumference of each sample was brushed with a thin layer of silicone then enclosed in heat-shrink tubing (3M FP-301) with the tubing protruding ~5 mm above the top of the sample. A disc of felt fabric and a non-porous ceramic disc standard (11 mm diameter, 3 mm height) were positioned inside the protruding tubing. The internal standard had a threaded hole through the disc to allow access for solutions. The lower ends of the samples were mounted in Delrin® diffusion cell reservoirs (Figure 2). Two aluminum wire alignment guides were attached at opposite sides along the side of each sample and cut to a length that protruded just beyond the cap. The samples were sealed around all joints with silicone.

Samples were saturated with synthetic porewater (SPW, Appendix B) to replace pore fluid lost during sample preparation. The reservoirs were filled with SPW solution and additional SPW injected through the hole in the ceramic disc. The reservoirs were sealed with electrical tape and a nylon screw and rubber o-ring were used to seal the hole in the cap. The solutions were refreshed weekly while allowing the sample to saturate for 7 weeks.

Diffusion-reaction tests were initiated by injecting 20 mL of 1.0 M CsCl tracer solution (Appendix B) slowly into the bottom of each reservoir, flushing out the SPW and using paper towel to wick away the displaced solution. The outside of the samples were rinsed with distilled water to remove any salt precipitated from overflow during filling, and gently blotted dry.

Reference radiographs (for background subtraction) were collected immediately after tracer addition to the reservoir. A sample was placed in the microCT sample chamber and the magnification, height and rotation adjusted so that the sample was completely in the field of view. Radiographs were collected as 16 bit TIFF image data files. Triplicate reference images were collected for each sample to check data reproducibility.

Time-series radiographs were collected using the same positioning and operating conditions as for the reference radiograph. Radiograph collection continued at intervals of 1 day, increasing to 3 days over the next 2 weeks. The tracer solutions were refreshed every 3 days. Samples were stored at room temperature (23°C) in a closed container with an open dish of SPW to maintain humidity and prevent evaporative drying.

ImageJ processing software was used to analyze the radiograph data. The average greyscale intensity of the internal standard (ceramic cap) was determined and used to correct the image intensity of all other time steps relative to the reference. Plots of $\Delta\mu$ versus distance were prepared from the greyscale profiles for each time step by log transforming the greyscale values and subtracting: ln (reference) – ln (time series).

The linear calibration function in Figure 23 was used to calculate relative tracer concentration from the $\Delta\mu$ profiles and prepare plots of C/C_0 versus distance for each time step. Measurements of $\Delta\mu$ were made using radiographs of standard Cs solutions in SPW matrix in glass vials (Section 3.2.3) and used to determine the relationship:

$$\left(\frac{C}{C_0}\right)_x = \frac{\Delta\mu_x}{1.2127} \cdot \phi \qquad [15]$$

where C is the accumulated tracer concentration at distance x; C_0 is the tracer concentration in the source reservoir; $\Delta\mu$ is the change in X-ray absorption due to Cs at position x; and ϕ is the porosity. Concentration profiles were scaled by the bulk ϕ_w determined at 40 °C for the shale offcut pieces from the diffusion samples.

3.2.5 Diffusion-Reaction Simulations

The geochemical code PHREEQC v 2.16.01 (Parkhurst and Appelo 1999) was used for analysis of the experimental Cs relative concentration profiles. Estimates of $D_{p\,Cs}$, $k_{Cs+/Na+}$ and CEC were obtained by iterative fitting of the simulated C/C_0 profiles to experimentally determined profiles. An example of the input files for the PHREEQC calculations is included in Appendix C.

For the simulations, the transport domain was divided into 40 cells along the length of a 2 cm sample. Each cell was initially filled with a synthetic porewater solution composition which was equilibrated with an exchange site density representing the cation exchange capacity of the sample. The transport phase was then initiated by introducing a 1M CsCl tracer solution composition and imposing a constant boundary condition at the influx cell and closed boundary condition at the end of the domain. Diffusion-only transport was specified for the transport calculations with ion-exchange equilibria occurring on the exchange sites in each cell. Eight-hour time steps over a two week duration were simulated in the transport calculations, to correspond with the time series data collected in the experiment. For each time-step the total concentration of Cs^{+}_{aq} in aqueous solution and the concentration of bound Cs-X on exchange sites for each of the 40 cells was written to an output file that was used to plot C/C_0 versus distance profiles for comparison with the experimental data.

Although the PHREEQC code can be used to simulate transport in porous media, the equilibrium calculations within the code are based on the aqueous phase, i.e. reactions occurring in the pore solution. Porosity is not considered explicitly so the transport calculations use a porewater diffusion coefficient (D_p) and the cation exchange site density is scaled to the total mass of porewater, rather than the volume or mass of the rock material.

3.3 RESULTS

3.3.1 Conservative Tracer: Iodide Diffusion and Diffusion-Accessible Porosity

The results from the iodide diffusion experiments are given in Figure 24 to Figure 26 and summarized in Table 13. The iodide D_p values for samples DGR3_468.02A and DGR3_468.02B display very good agreement, while the iodide D_p value for sample DGR3_468.02C was slightly lower. The reasons for the difference may be due to local heterogeneity.

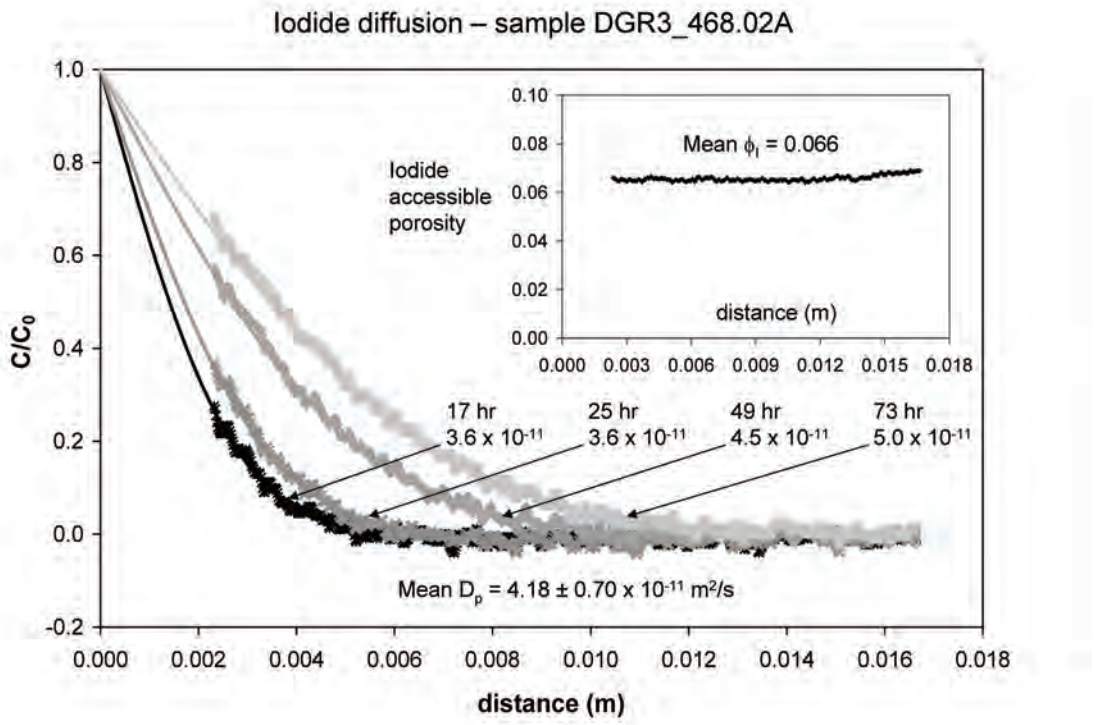

Figure 24: Diffusion Profiles, Fitted Analytical Solution, Diffusion Coefficients and Iodide-Accessible Porosity Profile for Queenston Shale Sample DGR3_468.02A.

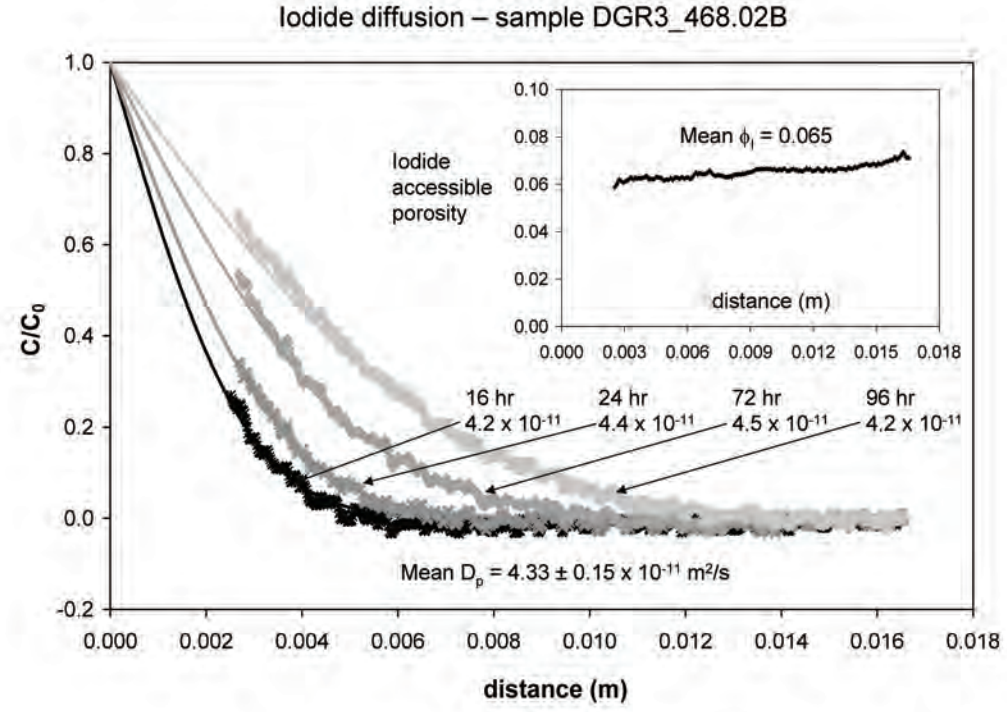

Figure 25: Diffusion Profiles, Fitted Analytical Solution, Diffusion Coefficients and Iodide-Accessible Porosity Profile for Queenston Shale Sample DGR3_468.02B

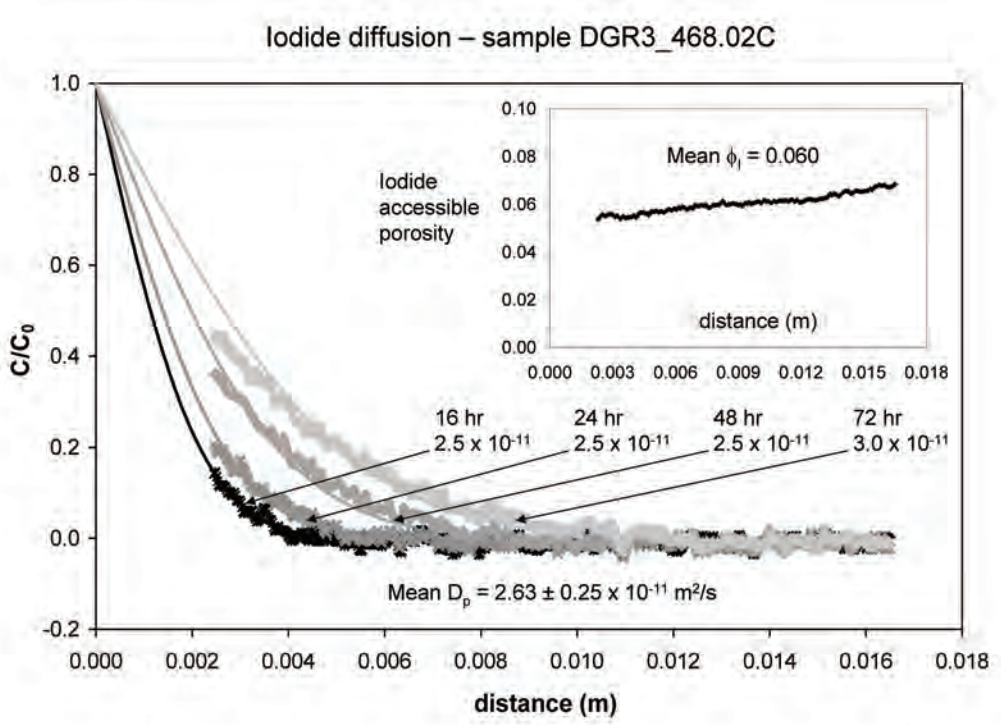

Figure 26: Diffusion Profiles, Fitted Analytical Solution, Diffusion Coefficients and Iodide-Accessible Porosity Profile for Queenston Shale Sample DGR3_468.02C.

Table 13: Summary of Iodide Diffusion Coefficients and Iodide-Accessible Porosity Measurements for Queenston Shale Samples

Sample	$D_{p\,I}$ (m^2/s)	$D_{e\,I}$ (m^2/s)	Mean ϕ_I	Orientation
DGR3_468.02A	4.2×10^{-11}	2.8×10^{-12}	0.066	Normal to bedding
DGR3_468.02B	4.3×10^{-11}	2.8×10^{-12}	0.065	Normal to bedding
DGR3_468.02C	2.6×10^{-11}	1.6×10^{-12}	0.060	Normal to bedding

3.3.2 Non-Conservative Tracer: Cs Diffusion-Reaction Profiles

The 1 M CsCl tracer solution proved very successful for radiography measurements because the strong X-ray absorbing properties of Cs and the accumulation of Cs mass on exchange sites gave a very good Δμ signal over background noise in the processed radiographs. Figure 27 gives an example of a set of time series Δμ images visualizing the transport of Cs through sample DGR3_468.02E.

The Δμ images presented in Figure 27 were prepared by subtracting log transformed greyscale intensity images for each time series from the corresponding log transformed Cs-free reference

image. The bright areas in the images indicate high Δμ values that represent high Cs mass diffusing in the pore fluid and accumulating on exchange sites near the influx boundary over time.

Using the image processing method described in Section 3.2.4, time series profiles of C/C_0 were calculated from Δμ profiles using the Cs calibration function and measured ϕ_w data (Table 12; Figure 28 to Figure 30).

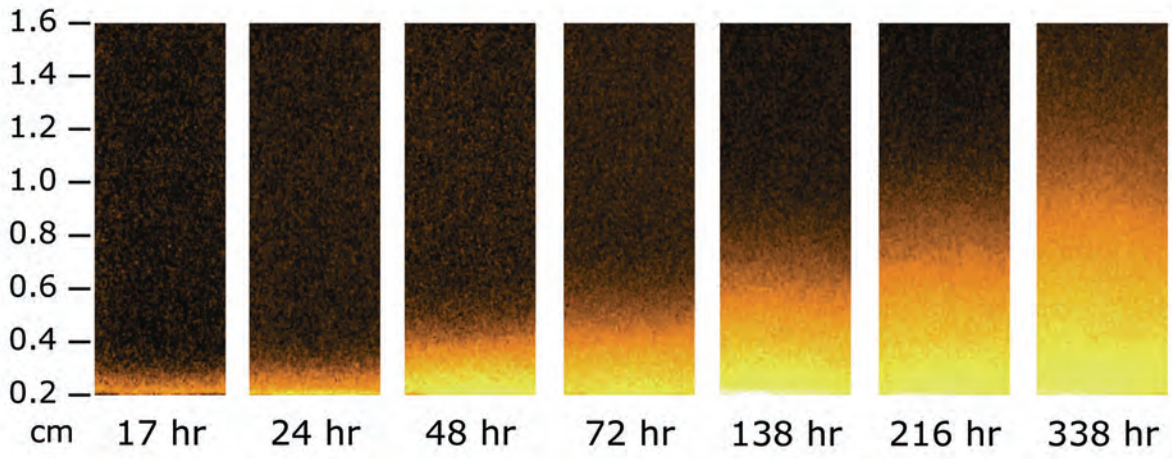

Figure 27: Time Series Δμ Images of Cs Transport in Sample DGR3_468.02E.

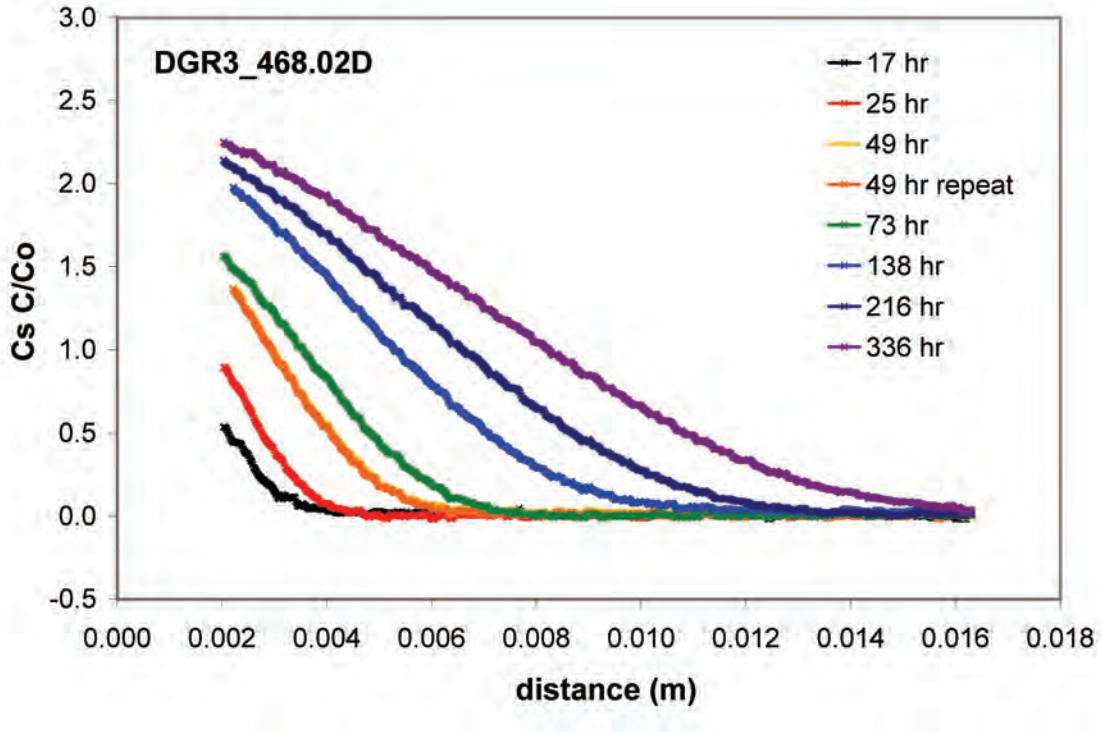

Figure 28: Time Series Profiles of Relative Cs Concentration Measured by Radiography for Sample DGR3_468.02D in the Diffusion-Reaction Experiment.

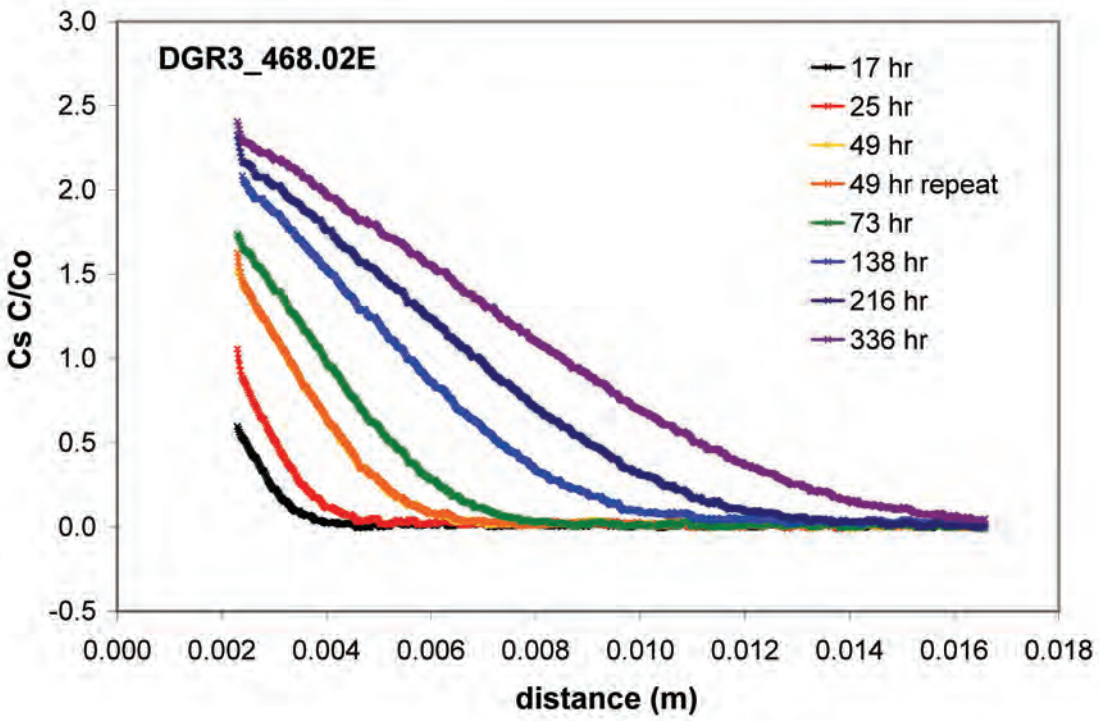

Figure 29: Time Series Profiles of Relative Cs Concentration Measured by Radiography for Sample DGR3_468.02E in the Diffusion-Reaction Experiment.

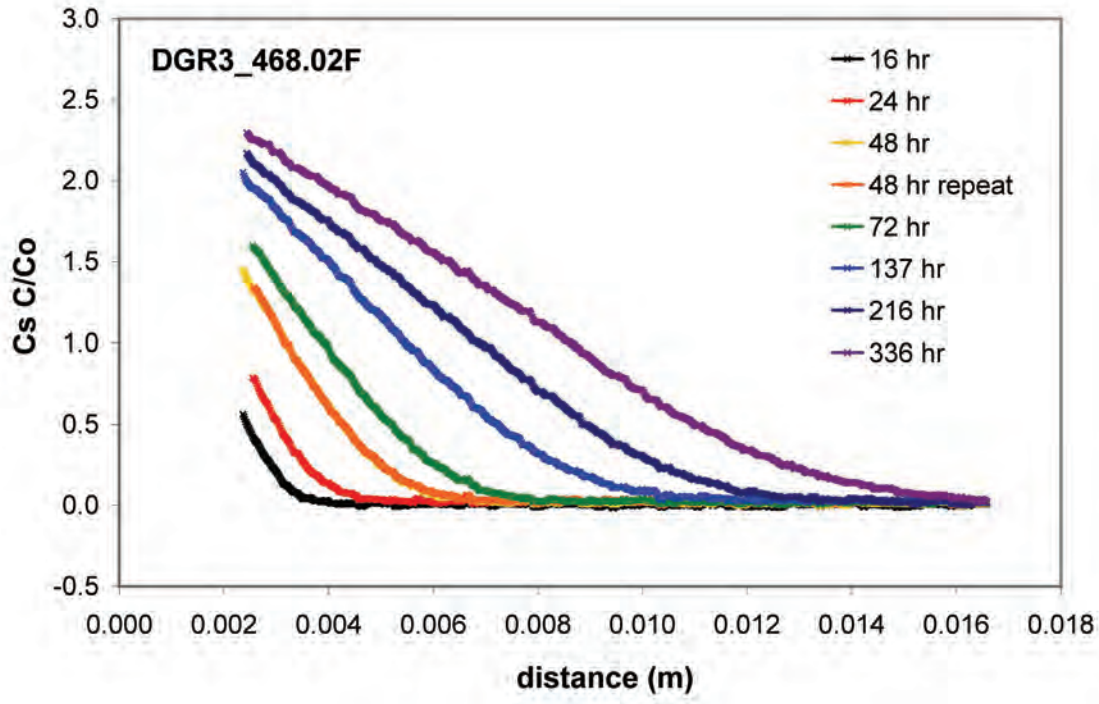

Figure 30: Time Series Profiles of Relative Cs Concentration Measured by Radiography for Sample DGR3_468.02F in the Diffusion-Reaction Experiment.

Because the radiography technique measures only the total change in X-ray absorption due to the mass of Cs in the X-ray path, the measured concentrations represent both the Cs^+ in the pore solution and the Cs-X bound on exchange sites. As a result, the concentration relative to the influx tracer solution concentration (C/C_0) exceeds 1.0 near the boundary as the pores become filled with Cs^+ tracer solution and additional Cs accumulates on the exchange sites.

3.3.3 Reactive Transport Calculations to Quantify Diffusion and Ion Exchange

Unlike the profiles generated in the iodide tracer experiment, it is not possible to fit the observed C/C_0 profiles for Cs using a diffusion-only model (Figure 31).

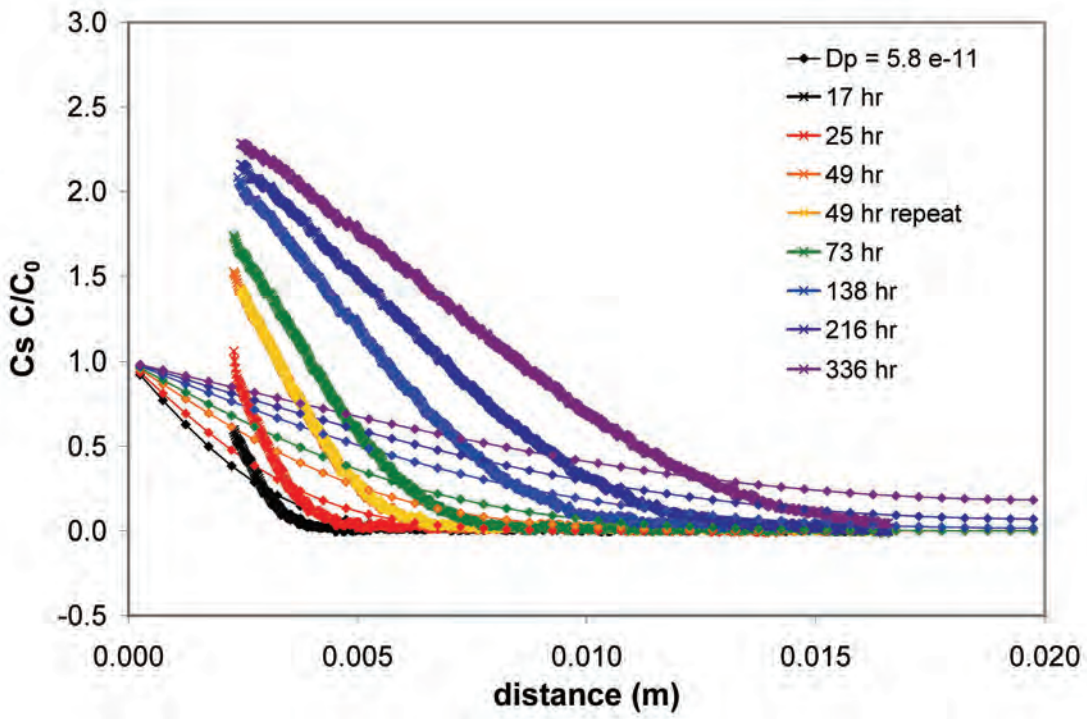

Figure 31: Observed Relative Concentration Profiles for DGR3_468E Cs C/C_0 Compared with a Diffusion-Only Model (thin lines).

The experimental data in the diffusion-reaction experiment can be reproduced using a coupled diffusion and cation exchange model involving Cs ion exchange on a single type of exchange site. The approach taken here is simpler than the Cs sorption models used in several other investigations with argillaceous material which employ either a two-site (e.g. Liu et al. 2004, Melkior et al. 2005) or more commonly, a three-site model to describe the uptake of Cs at lower concentrations (e.g. Bradbury and Baeyens 2000, Maes et al. 2008, van Loon et al. 2009).

Several PHREEQC simulations were conducted while testing the sensitivity to three parameters:

- the pore diffusion coefficient for Cs ($D_{p\,Cs}$)
- the density of cation exchange sites (CEC) and
- the selectivity coefficient for Cs^+ exchange with Na^+ (log $k_{Cs+/Na+}$)

and the fit between the simulated and experimental profiles. The profiles and input parameters obtained by fitting simulations to the observed data, are presented in Figure 32 to Figure 34 and Table 14.

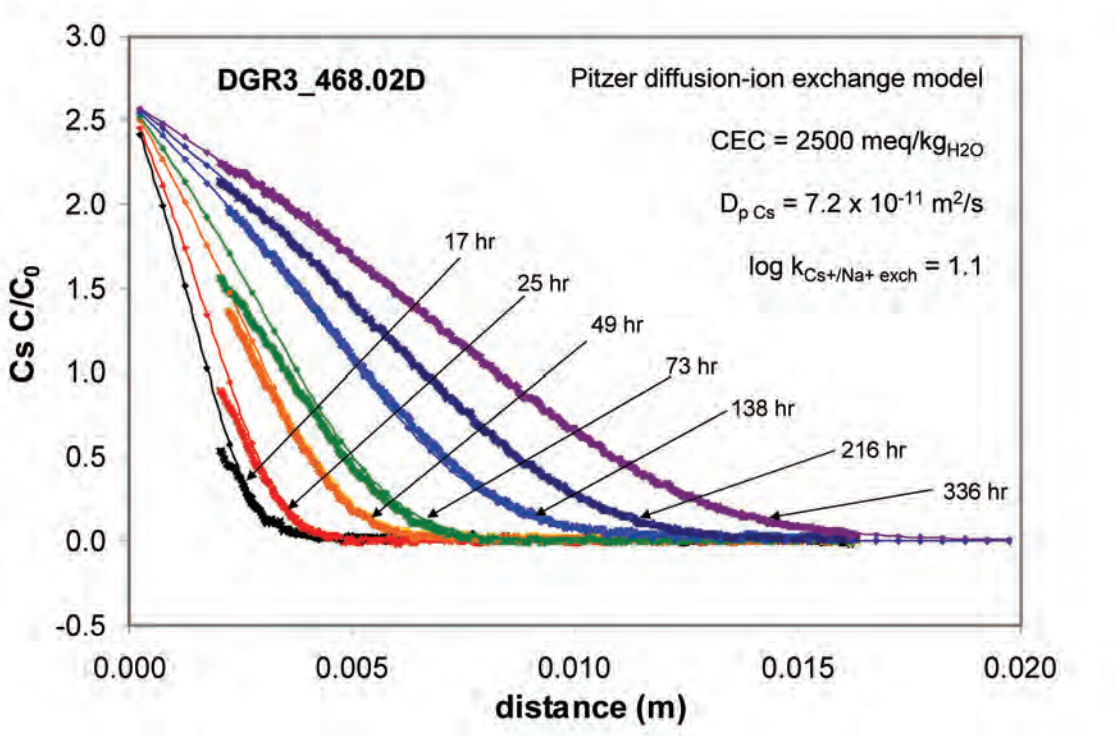

Figure 32: Relative Cs Concentration Profiles and Simulated Diffusion-Exchange Model Profiles (thin lines) for DGR3_468.02D.

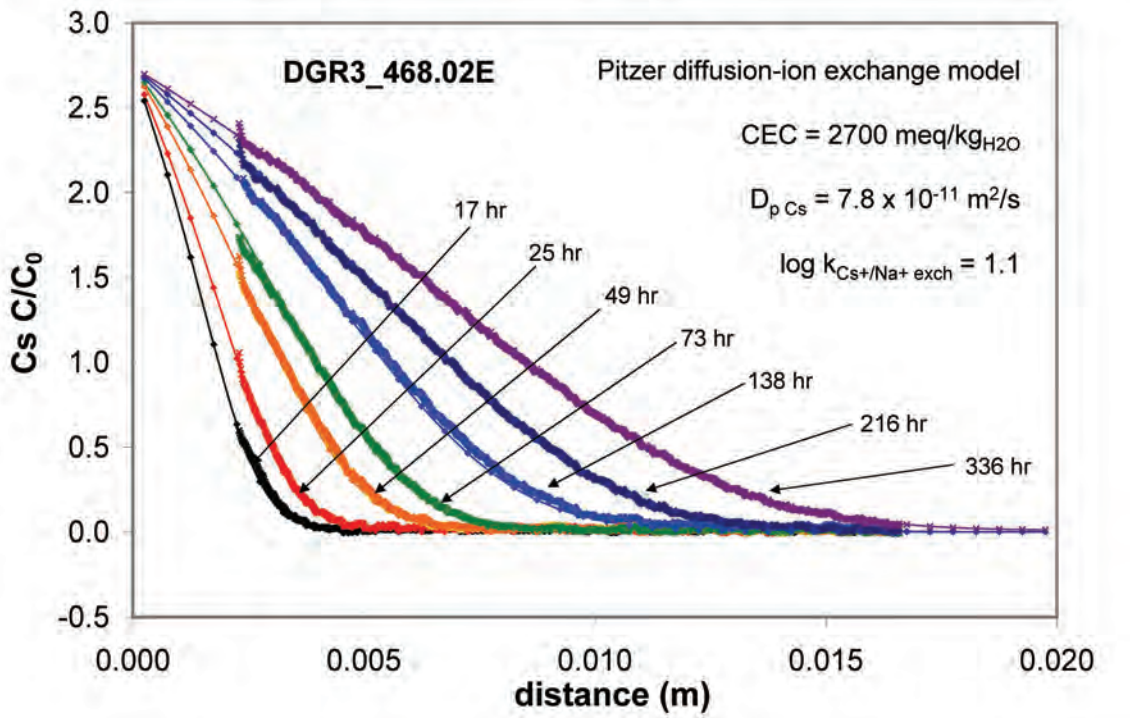

Figure 33: Relative Cs Concentration Profiles and Simulated Diffusion-Exchange Model Profiles (thin lines) for DGR3_468.02E.

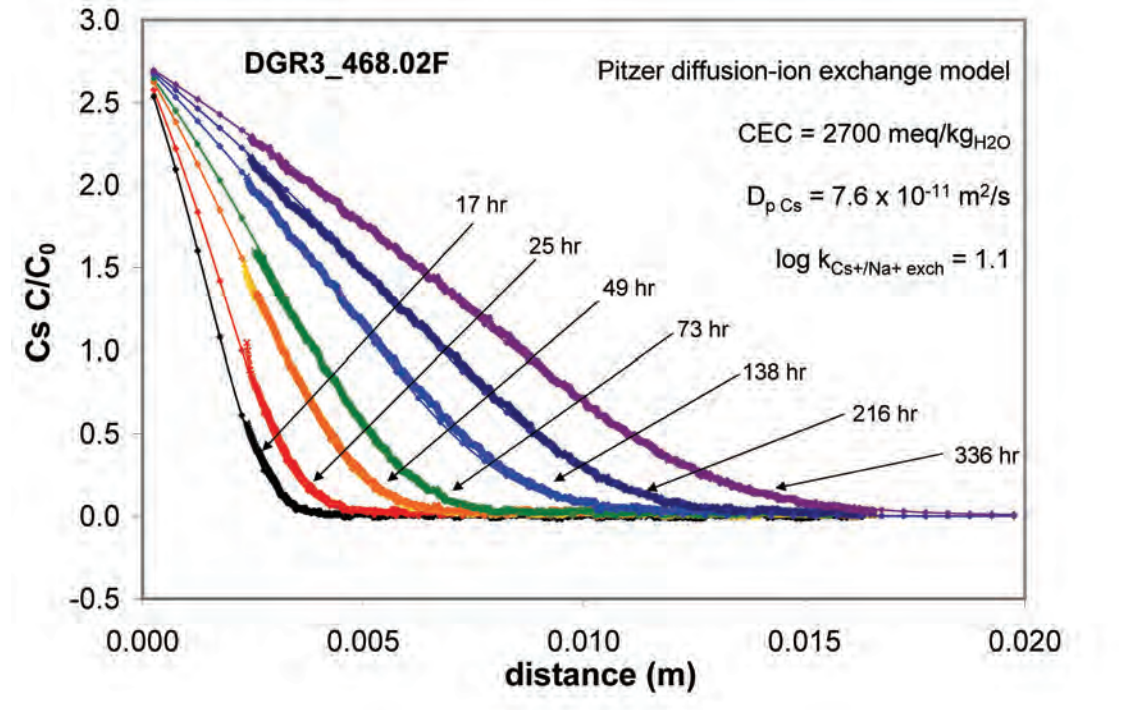

Figure 34: Relative Cs Concentration Profiles and Simulated Diffusion-Exchange Model Profiles (thin lines) for DGR3_468.02F.

Table 14: Values for $D_{p\ Cs}$, log $k_{Cs+/Na+}$ CEC Obtained from Radiography and Reaction-Transport Calculations for DGR3_468 Samples.

Sample	$D_{p\ Cs}$ (m^2/s)	log $k_{Cs+/Na+}$	CEC (meq/kg_{H2O})	CEC (meq/100g)
DGR3_468.02D	7.2×10^{-11}	1.1	2500	7.9
DGR3_468.02E	7.8×10^{-11}	1.1	2700	8.5
DGR3_468.02F	7.6×10^{-11}	1.1	2700	8.5
Average ± st.dev.	$7.5 \pm 0.2 \times 10^{-11}$	1.1	2633±94	8.3±0.3

Note: The PHREEQC model calculates CEC in units of $meq/kg_{H2O.}$ For ease of comparison these units have been converted to the more conventional units of meq/100g by normalizing to the mass of rock in contact with 1 kg of pore fluid. This conversion requires knowledge of the porosity and the bulk density.

The results in Table 14 show good agreement between the triplicate samples used in the experiments. Pore diffusion coefficients for Cs are slightly higher than for iodide measured in the DGR2_468.02 samples, but the overall transport rate for the non-conservative cation species Cs^+ is slower because of sorption effects.

It should be noted that the data in Table 14 are subject to uncertainties such as errors in the porosity measurement (which affects the C/C_0 calculated from the calibration curve) and the limitations of the PHREEQC model, particularly in the simulation of ion exchange (see Section 3.4.3).

3.4 DISCUSSION

3.4.1 Solute Activities in Brines

Because of the high salinity of the porewater, SPW, and the tracer solutions, non-ideal solute behaviour is expected and it becomes necessary to pay attention to the model used for determining the activities of aqueous species in PHREEQC. The standard Debye-Huckel expressions are useful below approximately 0.5 molal, but become inadequate at higher ionic strengths. For very high ionic strengths, the accepted approach is to use a specific ion interaction model (Pitzer 1973). This option is available in PHREEQC, but requires the addition of binary and ternary Pitzer coefficients for Cs which are not included in the Pitzer.dat database. Literature values for specific interaction parameters were added for these modelling simulations (Table 15). Coefficients based on measurements in the NaCl-CsCl system were favoured when selecting from a range of available literature values.

Table 15: Binary and Ternary Pitzer Coefficients for Cs Added to the Pitzer.dat Database Used for PHREEQC Calculations

Binary coefficients					
Ion-pair	**B_0**	**B_1**	**C_0**	**θ**	**Reference**
Cs^+ Cl^-	0.030	0.0558	0.00038		Pitzer and Mayorga 1973
Cs^+ SO_4^{2-}	0.0888	1.11075	0.00004		
Cs^+ OH^-	0.150	0.30	-0.00599803		
Cs^+ Na^+				-0.033	Pitzer and Kim 1974
Cs^+ K^+				0.0	
Cs^+ H^+				-0.044	
Ternary coefficients					
Ion group		**ψ**			**Reference**
Cs^+ Na^+ Cl^-		-0.003			Pitzer and Kim 1974
Cs^+ K^+ Cl^-		-0.0013			
Cs^+ H^+ Cl^-		-0.019			

3.4.2 Optimization of $D_{p\,Cs}$, log $k_{Cs+/Na+}$ and CEC using PHREEQC

PHREEQC simulations were used to estimate three different diffusion and sorption parameters which affect the transport of the Cs tracer cations: $D_{p\,Cs}$, log $k_{Cs+/Na+}$ and CEC. A sensitivity analysis was conducted by adjusting each parameter independently to test the effects on the shape of the diffusion-reaction profile. The results have been plotted in Figure 35 to Figure 37 using the fitting of the 48 hour time series data for DGR2_468.02E as an example.

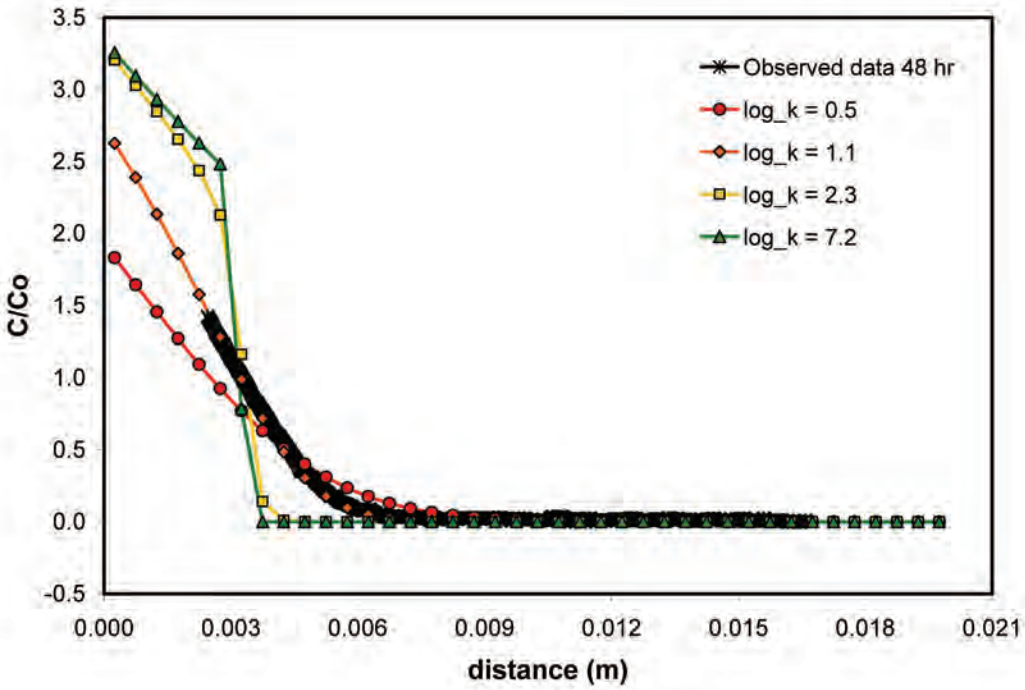

Figure 35: Effect of Varying Log $k_{Cs+/Na+}$ Selectivity Coefficient in the Diffusion-Cation Exchange Model.

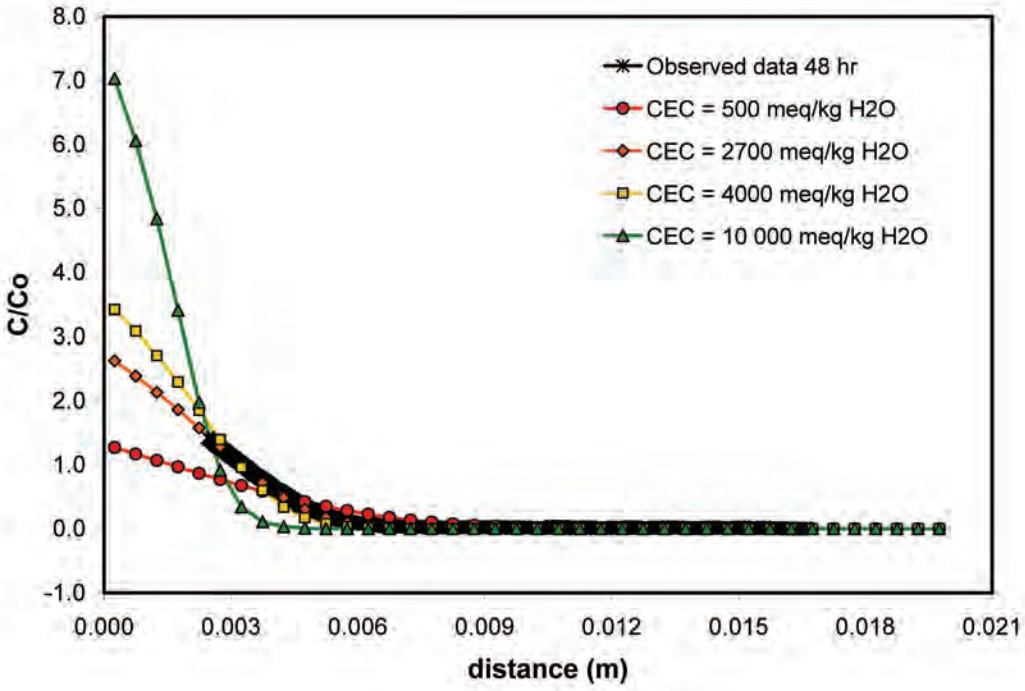

Figure 36: Effect of Varying Exchange Site Density (CEC) in the Diffusion-Cation Exchange Model.

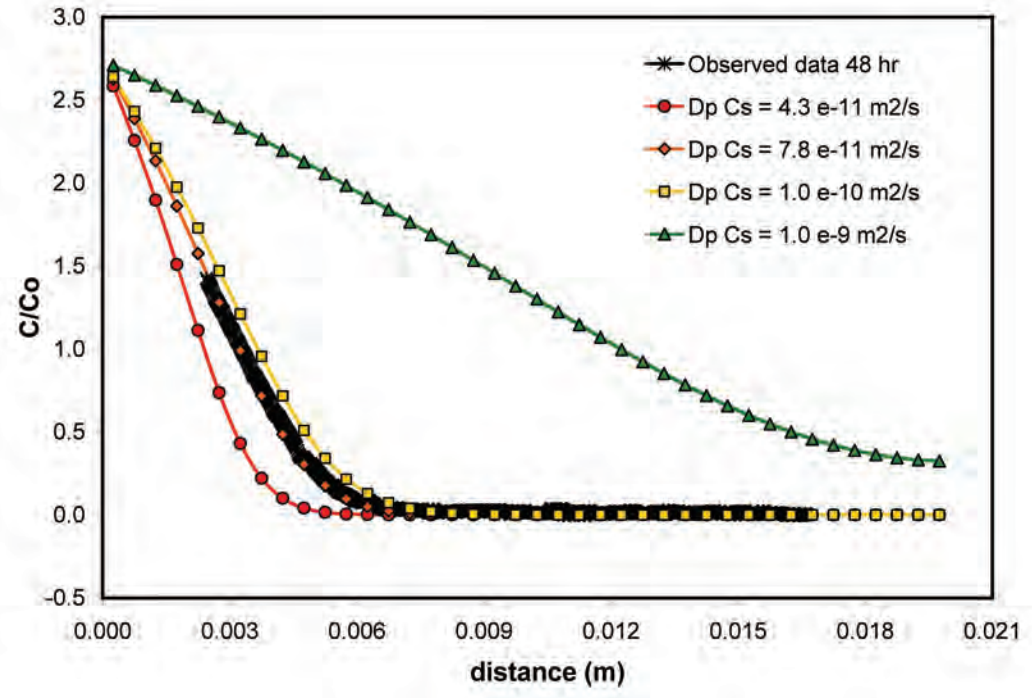

Figure 37: Effect of Varying $D_{p\,Cs}$ in the Diffusion-Cation Exchange Model.

Sodium is the dominant cation in the SPW and it is expected that most of the exchange sites at the start of the experiment will be occupied by Na^+. The selectivity of the Cs^+/Na^+ ion exchange reaction is therefore important in the model calculations. The log $k_{Cs+/Na+}$ value of 1.1 that provided the best fit to the experimental data is identical to that reported by Appelo and Postma (1996), but lower than the value of 1.6 used by Bradbury and Baeyens (2000) for planar sites which make up 80% of the reference illite exchange site capacity used in their three-site model. Other reported values for log $k_{Cs+/Na+}$ on a variety of exchange sites are higher (Table 16), but the higher values produce a steep slope on the advancing C/C_0 profiles, which was not observed in the experimental data.

Table 16: Comparison of Experimental and Literature Values for log $k_{Cs+/Na+}$

Model	Reference	Ionic strength (mol/kg)	C_0 Cs (mol/L)	Site type	Log $k_{Cs+/Na+}$
2-site Hanford sediments	Liu et al. 2004	5	$1x10^{-10}$ to 0.1	Site I Site II	7.2 2.3
2-site Bure mudrock	Melkior et al. 2005	0.05	$1x10^{-9}$ to 0.01	Weak Strong	4.6 (Cs^+/Ca^{2+})
3-site Reference illite CEC = 0.2 eq/kg	Bradbury and Baeyens 2000	Low ≤ 0.1	$1x10^{-10}$ to $1x10^{-3}$	FES (0.25% of CEC) Type II (20% of CEC) Planar (80% of CEC)	7.0 3.6 1.6
Soil exchange coefficient Cs^+/Na^+	Appelo and Postma 1996, p.160	Not specified	Not specified	X	1.097
1-site Queenston shale	This study	8.3	1.0	X	1.1

Initial CEC estimates for the model calculations were made using the empirical formula for soils (Breeuwsma et al. 1986):

$$CEC\ (meq/100\ g) = 0.7 \cdot (\%\ clay) + 3.5 \cdot (\%C) \quad [16]$$

using the composition of red Queenston Formation shale DGR2_456.97 reported in Table 12 to give a cation exchange capacity of 37 meq/100 g or 10 500 meq/kg $_{porewater}$. This estimate appears to vastly overestimate the exchange site density for intact shale samples and much lower CEC values were needed to fit the observed data. Cation exchange capacity values for other argillaceous formations (Table 17) of similar clay content which are under consideration for radioactive waste disposal are generally higher than the value reported in this study. The literature CEC values were typically determined on crushed rock material and may overestimate the value for intact rock, although there is evidence at least for the Opalinus clay that the Cs sorption behaviour in crushed and intact rock samples is similar, suggesting that all the exchange sites are available in the intact material (van Loon et al. 2009).

Table 17: Comparison of Literature Values for CEC of Argillaceous Materials

Material	Clay content (wt %)	CEC (meq/kg)	Reference
Opalinus clay	54 – 66	10 - 11	Mazurek et al 2008
Bure mudrock	24 – 50	14 - 21	Melkior et al 2005
Boom clay	30 – 60	~ 25	Maes et al 2008
Queenston shale	40 – 50	8.3	This study

A comparison of the $D_{p\,Cs}$ values obtained in this study with other diffusion coefficients reported in the literature indicates that the $D_{p\,Cs}$ values derived for the Queenston shale are at least 2 orders of magnitude lower than others reported from European argillaceous sediments (Table 18). This magnitude of difference is consistent with variations in diffusion coefficients for conservative tracers (I^- and HTO) reported for the Queenston Shale (Cavé et al. 2009a) and European argillaceous sediments (Mazurek et al. 2009).

The $D_{p\,I}$ values obtained in this study for Queenston shale samples (2.6×10^{-11} to 4.2×10^{-11} m^2/s) are about a factor of two lower than the $D_{p\,Cs}$ values. Relatively low diffusion coefficients are commonly observed for iodide, and diffusion coefficients for iodide have been found to be up to an order of magnitude lower than for tritiated water (HTO) in argillaceous materials (van Loon et al., 2003a; García-Gutiérrez et al., 2004; Vilks and Miller, 2007; Cavé et al. 2009a) due to anion exclusion effects of the large, negatively-charged iodide.

Table 18: Comparison of Experimental and Literature Values for $D_{p\,Cs}$ in Argillaceous Materials

Material	ϕ	$D_{e\,Cs}$ (m^2/s)	$D_{p\,Cs}$ (m^2/s)	$D_{a\,Cs}$ (m^2/s)	Reference
Opalinus clay	0.16[a]	$1.8\text{x}10^{-10}$	$1.1\text{x}10^{-9}$ [f]		Jakob et al 2009
Bure mudrock	0.14[b]	$2.3\text{-}2.7\text{x}10^{-10}$	$1.6\text{-}1.9\text{x}10^{-9}$ [f]		Melkior et al 2005
Boom clay	0.37[c]		3.8×10^{-9} [g]	$1.6\text{-}1.9\text{x}10^{-13}$	Maes et al 2008
FEBEX bentonite		$0.3\text{-}1.0\text{x}10^{-10}$		$0.9\text{-}3.3\text{x}10^{-13}$	Cormenzana et al 2003
Queenston shale	0.08[d]	$5.7\text{-}6.2\text{x}10^{-12}$ [e]	$7.2\text{-}7.8\text{x}10^{-11}$		This study

[a] reference value for Mont Terri from Mazurek et al. 2008
[b] total porosity measured by Hg intrusion (ϕ)
[c] HTO-accessible porosity from through-diffusion (ϕ_{HTO})
[d] water loss porosity ϕ_w from offcut sample DGR3_468.02P, dried at 40°C (Table 12)
[e] calculated using $D_e = D_p \cdot \phi_w$
[f] calculated from $D_p = D_e/\phi$
[g] fitted using PHREEQC and Bradbury-Baeyens model assuming all exchange sites available.

3.4.3 Uncertainties and Sources of Error

3.4.3.1 Sensitivity to Porosity Measurements

It is not possible to measure the Cs accessible porosity in a manner similar to the determination of the iodide accessible porosity (see Section 2.2.3.1) because the slow transport of the non-conservative tracer limits the possibility of saturating the radiography sample with Cs tracer solution, and because the Cs mass in the sample resides both in the pore fluid and on the exchange sites. Instead, the quantification of Cs concentrations relies on the calibration curve, with the fundamental measurements of Cs mass scaled by the porosity to provide the pore solution concentrations. Consequently, small differences in porosity could lead to large differences in the calculated C/C_0 values. Porosity is also used as a scaling parameter when converting between D_p and D_e. When using porosity measurements for these purposes it is important to recognize that there are different types of porosity measurements that can be

made on a sample (Pearson 1999), including bulk measurements and solute specific porosities, thus it is prudent to evaluate the sensitivity of the results to variations in the measured porosity.

For the diffusion-reaction experiment, we do not have a measurement for a Cs-accessible porosity, so the assumption is made that there are no ion exclusion effects and 100% of the water loss porosity is accessible to Cs^+. Other studies have applied the accessible porosity for tritiated water, ϕ_{HTO} to the Cs^+ cation (e.g. Maes et al. 2008).

As an indication of the magnitude of the sensitivity to porosity, the diffusion-reaction test data were also analyzed using a lower sample porosity of 6.6% (which corresponds to the mean iodide-accessible porosity, ϕ_I for the samples). In this case, the observed profiles can be fit with a diffusion-exchange transport model using mean values of:

- $\log k_{Cs+/Na+} = 1.1$;
- CEC = 3367 ± 94 meq/kg_{H2O} = 14.6 ± 0.4 meq/100g; and
- $D_{p\ Cs} = 9.2 \pm 0.3 \times 10^{-11}$ m^2/s

This suggests that the lower porosity does not affect the exchange coefficient obtained from the model, but the use of lower porosity values requires that higher CEC and $D_{p\ Cs}$ values are necessary to obtain a fit between the model and the experimental data.

3.4.3.2 Limitations of PHREEQC for Ion-Exchange Calculations

It is possible that the choice of numerical model, particularly the method used to determine activity of species on the exchange sites, may have some influence on the parameter estimation. The ion-exchange module in PHREEQC uses the Gaines-Thomas approach to specifying activities of the species attached to the exchange sites (Gaines and Thomas, 1953; Parkhurst and Appelo 1999). Using this model, the thermodynamic activity of an exchange species is equal to the moles of sites occupied by the exchange species divided by the total number of exchange sites (equivalent fraction). The effect on the parameter estimation of using a different model has not been evaluated in this study.

3.5 CONCLUSIONS

An X-ray radiography method for determination of diffusion coefficients has been modified to allow for the estimation of diffusion-reaction parameters for the non-conservative solute, Cs. Cesium tracer diffusion and sorption on cation exchange sites can be monitored in intact rock samples using radiographs to plot time series profiles of Cs relative concentration (C/C_0) as a function of transport distance during diffusion-reaction experiments. Cesium was found to be a very good tracer for these experiments, both because of its simple speciation and sorption behaviour and because of the sensitivity of X-ray attenuation measurements to Cs concentration.

The method was tested on red shale samples from the Ordovician Queenston Formation obtained from preserved drill core. Tracer experiments with 1M CsCl in a matrix of synthetic porewater (composed to mimic the natural porewater brines) produced smooth profiles of C/C_0 versus distance from the influx reservoir. High concentrations of Cs near the influx boundary arise from the combined effects of diffusion and sorption on exchange sites, and provide a

high-contrast X-ray absorption signal ($\Delta\mu$) for the Cs tracer. In future, lower Cs concentrations might be attempted to be consistent with Cs ion-exchange experiments reported in the literature.

We used a numerical model that couples diffusion and ion-exchange to simulate the time series profiles and fit diffusion-reaction parameters. Working with concentrated brine solutions required the use of Pitzer ion interaction coefficients in the model. The simulations were run iteratively to fit the simulated Cs C/C_0 profiles to the experimental data from all time steps. During these iterations, three parameters were estimated and adjusted to improve the fit: $D_{p\ Cs}$, log $k_{Cs+/Na+}$ and CEC. These data should not be considered as final measurements for the Queenston shale sample, but rather as a demonstration of how a combined radiography-transport modelling approach could be used to quantify the diffusion and sorption parameters.

Using radiography measurements and the numerical modelling approach, mean estimates for $D_{p\ Cs} = 7.5 \times 10^{-11}$ m/s, log $k_{Cs+/Na+} = 1.1$ and CEC = 8.3 meq/100 g were obtained from three samples of Queenston shale. The values for $D_{p\ Cs}$ and CEC are sensitive to the value of porosity used in the calculations, with a change of –1.4% in porosity resulting in an increase of 23% in the estimate for D_p and an increase of 76% for CEC.

4. GENERAL CONCLUSIONS ON METHODS FOR INVESTIGATING DIFFUSIVE TRANSPORT IN SEDIMENTARY ROCKS

This technical report prepared for the Nuclear Waste Management Organization documents the activities and outcomes of two research studies undertaken at the University of New Brunswick from 2007 to 2009. The overall objective of this research is to develop methodologies and improve the knowledge of mechanisms controlling solute transport in diffusion-dominated sedimentary rock systems. Such rocks are under consideration in Canada as potential host- and barrier rocks for a deep geological repository for the long-term management of used nuclear fuel.

Investigation of variability in diffusive properties and controlling lithological factors across heterogeneous rock formations

The first study developed protocols for investigating relationships between diffusive properties and lithology, and for scaling discrete cm-scale measurements to the formation scale. The interlayered grey shale and hard beds (siltstone, limestone and dolostone) of the Ordovician Georgian Bay Formation were used as a test case. The methods included characterization of physical and mineralogical properties such as diffusion coefficients, porosity and clay content in a sequence of rock samples, and an analysis of the relationships between diffusion coefficients and the other physical properties. The results were then combined with a very detailed log of the lithology across the entire formation, using a harmonic averaging approach, to estimate larger scale trends in diffusion behaviour.

Some of the key findings of the investigation were:

- The Georgian Bay Formation, as sampled in this study, displays a high degree of heterogeneity in lithology at the centimetre to metre scale.

The core retrieved from the borehole in the Michigan Basin was characterized by nearly 800 discrete hard bed layers alternating with shale. Hard beds decrease in occurrence and thickness with depth.

- Porosity and diffusion properties are strongly dependent on sample lithology.

Shale samples have higher porosity and porewater diffusion coefficients than hard bed samples. Porosity and diffusion coefficients display a positive correlation with total clay mineral content and a weak negative correlation with carbonate mineral content. Samples of mixed lithology tend to show intermediate values for porosity and diffusion properties.

- The observed relationships between lithology and diffusion coefficients and the distribution of lithologies (shale and hard beds) lead to a predicted trend of slightly increasing diffusion coefficients with depth across the Georgian Bay Formation.

The trend is more pronounced for diffusion measurements parallel to bedding because of the increasing proportion of shale with depth and the greater anisotropy in the diffusive properties of the shale compared with the hard bed layers.

Development of a modified radiography technique for estimation of diffusive properties and cation exchange capacity of intact rock samples using a non-conservative tracer

The second study expanded on the radiography technique for determination of diffusion coefficients by using a non-conservative tracer, Cs, to quantify diffusion-reaction processes. Samples of homogeneous red shale from the Ordovician Queenston Formation were used to develop and demonstrate the technique.

The radiography technique is based on the time series measurement of tracer concentration profiles during a diffusion-reaction experiment before steady-state conditions are reached. Measurements are made by X-ray radiography, and quantification is based on the sensitivity of X-ray attenuation to the presence of an X-ray absorbing tracer species inside the rock sample. Cesium proved a good choice of tracer species because of its simple speciation and sorption behaviour and its strong X-ray absorption properties.

Reactive-transport modelling techniques were used to match observed C/C_0 profiles for Cs to simulated diffusion-ion exchange models and to quantify:

- Cs pore diffusion-coefficients ($D_{p\ Cs}$);
- Cs-Na exchange selectivity coefficients (log $k_{Cs+/Na+}$); and
- cation exchange capacity (CEC) for the intact rock sample.

Pitzer ion interaction coefficients were included in the model because of the very high solute concentrations and ionic strength of the pore waters in these rocks.

Using the radiography measurements normal to bedding (in triplicate) and the numerical modeling approach, estimates of mean values:

- $D_{p\,Cs} = 7.5 \times 10^{-11}$ m^2/s;
- log $k_{Cs+/Na+} = 1.1$; and
- CEC = 8.3 meq/100 g

were obtained from the Queenston Formation shale. These data should not be considered as final measurements for the Queenston shale sample, but rather as a demonstration of how a combined radiography-transport modelling approach could be used to quantify the diffusion and sorption parameters.

The values for $D_{p\,Cs}$ and CEC are sensitive to the value of porosity used in the calculations, with a change of –1.4% in porosity resulting in an increase of 23% in the estimate for D_p and an increase of 76% for CEC.

Despite the slower solute transport of Cs due to ion exchange, $D_{p\,Cs}$ values are almost twice those obtained for the conservative tracer iodide on adjacent samples ($D_{p\,I} = 2.6 \times 10^{-11}$ to 4.3×10^{-11} m^2/s; Table 13). This difference may be explained by the influence of anion exclusion which tends to decrease D_p values for anions. Values of CEC determined for intact samples of Queenston shale (8 meq/100g) are slightly lower than CEC for argillaceous rocks from European studies (10 to 25 meq/100g), many of which were measured on crushed rock samples.

ACKNOWLEDGEMENTS

We would like to acknowledge with thanks the contributions of Sean Stirling (INTERA) who provided the complete set of core photographs for the Georgian Bay formation and Shubhi Singh who patiently measured the thickness of the hard beds and shale to compile the detailed core log.

REFERENCES

Appelo, C.A.J. and D. Postma. 1996. Geochemistry, groundwater and pollution. A.A. Balkema, Rotterdam, 536 pp.

Armstrong, D.K. and Carter, T.R. 2010. The subsurface stratigraphy of Southern Ontario; Ontario Geological Survey, Special Volume 7, 301p.

ASTM Standard D854, 2010, “Standard Test Methods for Specific Gravity of Soil Solids by Water Pycnometer" ASTM International, West Conshohocken, PA, 2003, DOI: 10.1520/D0854-10, www.astm.org.

Blum, P. 1997. Physical properties handbook: a guide to the shipboard measurement of physical properties of deep-sea cores. Ocean Drilling Program, Technical Note 26.

Bourg, I.C., A.C.M. Bourg and G. Sposito. 2003. Modeling diffusion and adsorption in compacted bentonite: a critical review. Journal of Contaminant Hydrology: 61, 293-302.

Boving, T.B. and P. Grathwohl. 2001. Tracer diffusion coefficients in sedimentary rocks: correlation to porosity and hydraulic conductivity. Journal of Contaminant Hydrology: 53, 85-100.

Bradbury, M.H. and B. Baeyens. 2000. A generalized sorption model for the concentration dependent uptake of caesium by argillaceous rocks. Journal of Contaminant Hydrology: 42, 141-163.

Breeuwsma, A., J.H.M Wösten, J.J. Vleeshouwer, A.M. Van Slobbe and J. Bouma. 1986. Derivation of land qualities to assess environmental problems from soil surveys. Soil Science Society of America Journal: 50, 186-190.

Brunauer, S., P.H. Emmett and E. Teller. 1938. Adsorption of gases in multimolecular layers. Journal of the American Chemical Society: 60, 309-319.

Cavé, L., T. Al, Y. Xiang, Y. and P. Vilks. 2009a. A technique for estimating one-dimensional diffusion coefficients in low permeability sedimentary rock using X-ray radiography: Comparison with through-diffusion measurements. Journal of Contaminant Hydrology: 103, 1-12.

Cavé, L., T. A. Al, and Y. Xiang. 2009b. X-ray Radiography Techniques for Measuring Diffusive Properties of Sedimentary Rocks. Prepared by the University of New Brunswick for Nuclear Waste Management Organization. Nuclear Waste Management Organization Technical Report No. NWMO-TR-2009-03. Toronto, Ontario.

Choi, J.-W. and D.W. Oscarson. 1996. Diffusive transport through compacted Na- and Ca-bentonite. Journal of Contaminant Hydrology: 22, 189-202.

Cormenzana, J.L, M. García-Gutiérrez, T. Missana and Á. Junghanns. 2003. Simultaneous estimation of effective and apparent diffusion coefficients in compacted bentonite. Journal of Contaminant Hydrology: 61, 63-72.

Crank, J. 1975. The Mathematics of Diffusion, 2nd edition. Clarendon Press, 414 pp.

Emerson, D.W. 1990. Notes on mass properties of rocks – density, porosity, permeability. Exploration Geophysics, 21, 209-216.

Gaines, G.L., and Thomas, H.C., 1953, Adsorption studies on clay minerals. II. A formulation of the thermodynamics of exchange adsorption: Journal of Chemical Physics, v. 21, p. 714-718.

García-Gutiérrez, M., Cormenzana, J.L., Missana, T., Mingarro, M., 2004. Diffusion coefficients and accessible porosity for HTO and 36Cl in compacted FEBEX bentonite. Appl. Clay Sci. 26, 65–73.

Guillet, G.R. 1977. Clay and shale deposits of Ontario. Ontario Geological Survey, Mineral Deposits Circular MDC 15.

Jakob, A., W. Pfingsten and L. Van Loon. 2009. Effects of sorption competition on cesium diffusion through compacted argillaceous rock. Geochimica et Cosmochimica Acta: 73, 2441-2456.

Liu, C., J.M Zachara and S.C. Smith. 2004. A cation exchange model to describe Cs^+ sorption at high ionic strength in the subsurface sediments at Hanford site, USA. Journal of Contaminant Hydrology: 68, 217-238.

Maes, N., S. Salah, D. Jacques, M. Aertsens, M. Van Gompel, P. De Cannière and N. Velitchkova. 2008. Retention of Cs in Boom Clay: Comparison of data from batch sorption and diffusion experiments on intact clay cores. Physics and Chemistry of the Earth: 33, S149-S155.

Mazurek, M., A. Gautschi, P. Marschall, G. Vigneron, P. Lebon and J. Delay. 2008. Transferability of geoscientific information from various sources (study sites, underground rock laboratories, natural analogues) to support safety cases for radioactive waste repositories in argillaceous formations. Physics and Chemistry of the Earth: 33, S95-S105.

Mazurek, M., P. Alt-Epping, A. Bath, T. Gimmi and H.N. Waber 2009. Natural Tracer Profiles Across Argillaceous Formations: The CLAYTRAC Project. OECD/NEA No. 6253, 361 pgs.

Melkior, T., S. Yahiaoui, S. Motellier, D. Thoby and E. Tevissen. 2005. Cesium sorption and diffusion in Bure mudrock samples. Applied Clay Science: 29, 172-186.

Parkhurst, D.L. and C.A.J. Appelo. 1999. User's Guide to PHREEQC (Version 2) – A Computer Program for Speciation, Batch-Reaction, One-Dimensional Transport and Inverse Geochemical Calculations. Water-Resources Investigations Report 99-4259. U.S. Department of the Interior, U.S. Geological Survey, Denver, Colorado.

Pearson, F.J.P. 1999. What is the porosity of a mudrock? In: Aplin, A.C., A.J. Fleet and J.H.S. Macquaker (eds.) Muds and Mudstones: Physical and Fluid Flow Properties. Geological Society of London Special Publication: 158, 9-21.

Pitzer, K.S. 1973. Thermodynamics of electrolytes. I. Theoretical basis and general equations. Journal of Physical Chemistry: 77, 268-277.

Pitzer, K.S. and G. Mayorga. 1973. Thermodynamics of electrolytes. 2. Activity and osmotic coefficients for strong electrolytes with one or both ions univalent. Journal of Physical Chemistry: 77, 2300-2308.

Pitzer,K.S. and J.J. Kim. 1974. Thermodynamics of electrolytes. 4. Activity and osmotic coefficients for mixed electrolytes. Journal of the American Chemical Society: 96, 5701-5707.

Tidwell, V.C., L.C. Meigs, T. Christian-Frear and C.M. Boney. 2000. Effects of spatially heterogeneous porosity on matrix diffusion as investigated by X-ray absorption imaging. Journal of Contaminant Hydrology: 42, 285-302.

van Loon, L., B. Baeyens and M.H. Bradbury. 2009. The sorption behaviour of caesium on Opalinus clay: A comparison between intact and crushed material. Applied Geochemistry: 24, 999-1004.

van Loon, L.R., B. Baeyens and M.H. Bradbury. 2005. Diffusion and retention of sodium and strontium in Opalinus clay: Comparison of sorption data from diffusion and batch sorption measurements, and geochemical calculations. Applied Geochemistry: 20, 2351-2363.

van Loon, L.R, J.M. Soler and M.H Bradbury. 2003a. Diffusion of HTO, $^{36}Cl^-$ and $^{125}I^-$ in Opalinus Clay samples from Mont Terri. Effect of confining pressure. Journal of Contaminant Hydrology: 61, 73-83.

van Loon, L.R., J.M. Soler, A. Jakob and M.H. Bradbury. 2003b. Effect of confining pressure on the diffusion of HTO, $^{36}Cl^-$ and $^{125}I^-$ in a layered argillaceous rock (Opalinus Clay): diffusion perpendicular to the fabric. Applied Geochemistry: 18, 1653-1662.

Vanýsek, P. 2006. Ionic conductivity and diffusion at infinite dilution. In Lide, D.R. (ed). CRC Handbook of Chemistry and Physics. 87th edition, CRC Press: 5-76 – 5-78.

Vilks, P. and N.H. Miller. 2007. Evaluation of Experimental Protocols for Characterizing Diffusion in Sedimentary Rocks. Prepared by Atomic Energy of Canada Ltd. for Nuclear Waste Management Organization. Nuclear Waste Management Organization Technical Report TR-2007-11, Toronto, Ontario.

APPENDIX A: SUPPORTING DATA FOR DIFFUSION MEASURMENTS ACROSS THE GEORGIAN BAY FORMATION

CONTENTS

Page

LIST OF FIGURES

Page

A.1 PHOTOGRAPHS OF ROCK CORE SAMPLES

The following symbols are used in photograph annotation:

Rad = radiography samples
TD = through diffusion sample
NB = diffusion direction normal to bedding (assuming horizontal bedding planes)
PB = diffusion direction parallel to bedding (assuming horizontal bedding planes)
ϕ = porosity sample (used for water loss porosity measurements)

Top and bottom labels indicate the orientation of the core as retrieved from the drill hole. Diffusion tests normal to bedding were run with the high concentration reservoir in contact with the lower end of the sample, i.e. the direction of diffusion was upwards from bottom to top.

DGR2_535.08 Georgian Bay

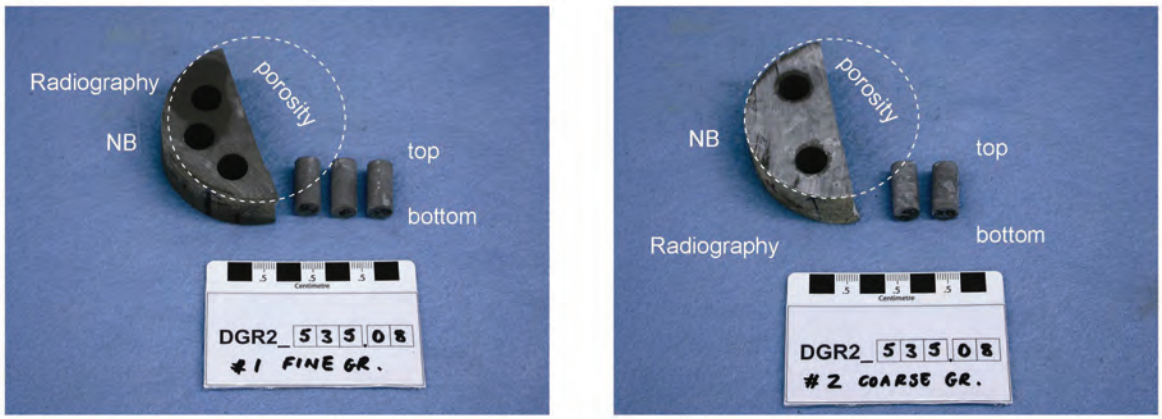

DGR2_535.08 Georgian Bay

Figure A 1: Core Segment and Samples Prepared from DGR2_535.08.

DGR2_537.32 Georgian Bay

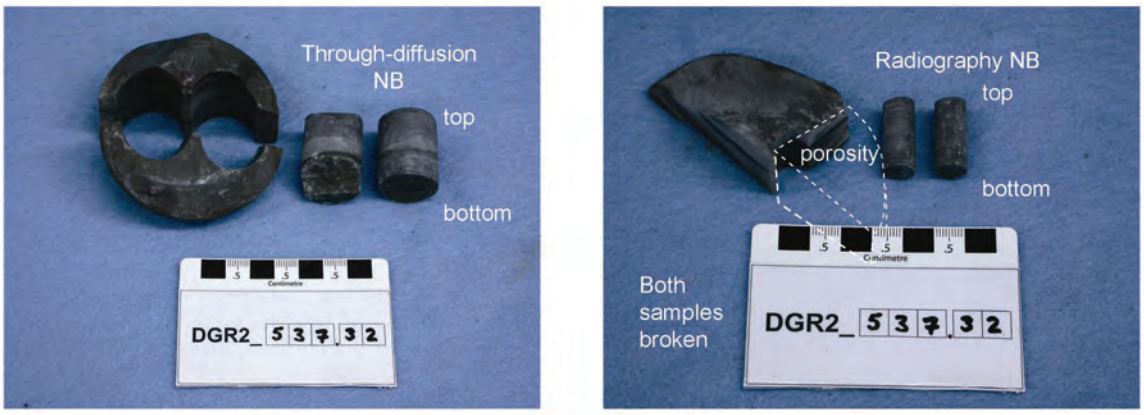

DGR2_537.32 Georgian Bay

Figure A 2: Core Segment and Samples Prepared from DGR2_537.32.

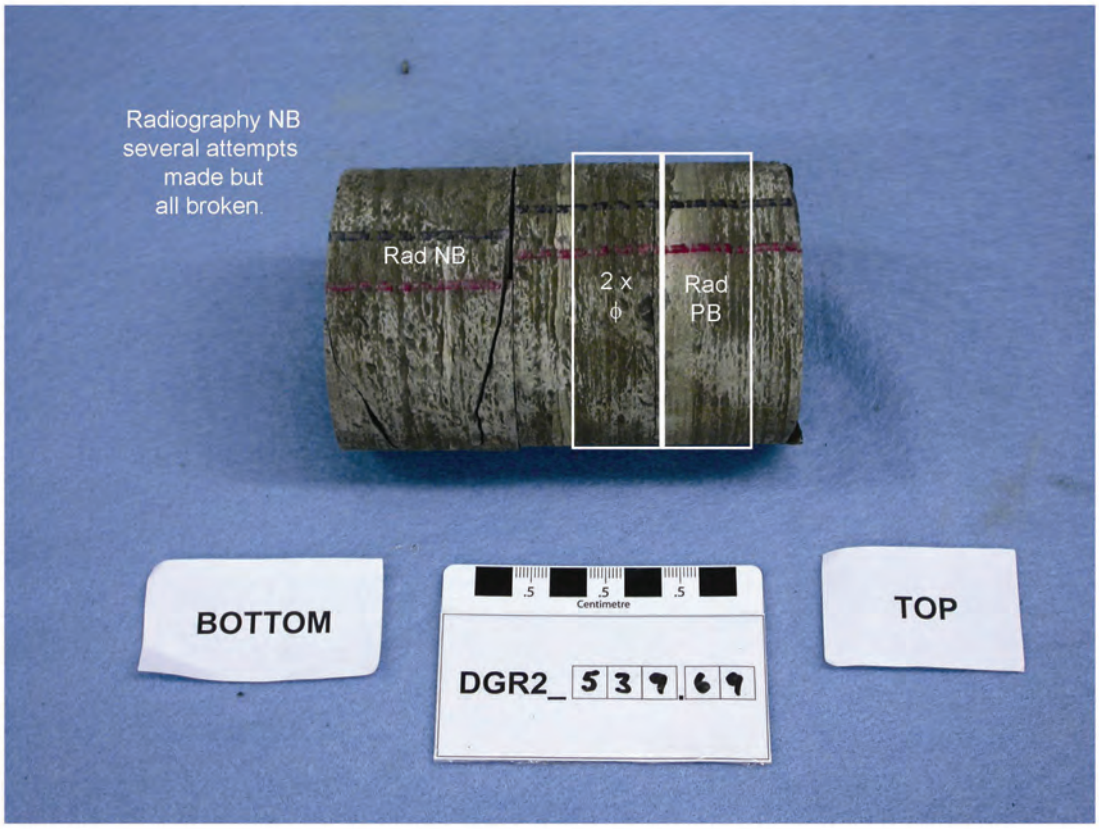

DGR2_539.69 Georgian Bay

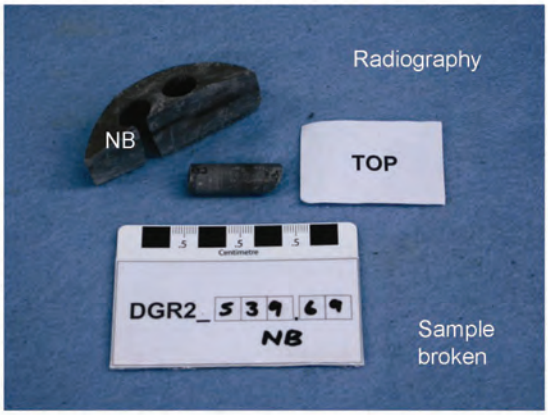

DGR2_539.69 Georgian Bay

Figure A 3: Core Segment and Samples Prepared from DGR2_539.69.

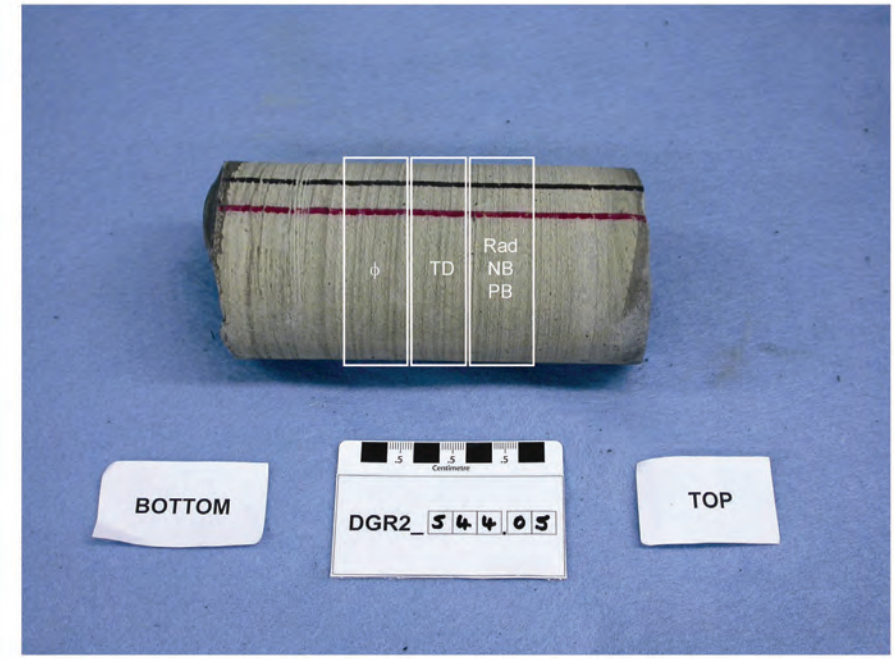

DGR2_544.05 Georgian Bay

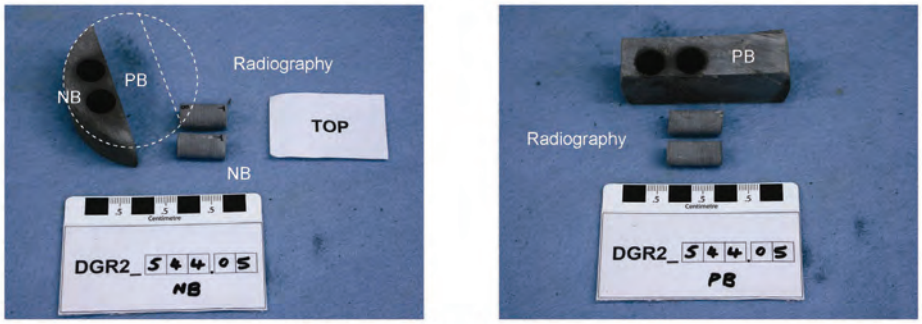

DGR2_544.05 Georgian Bay

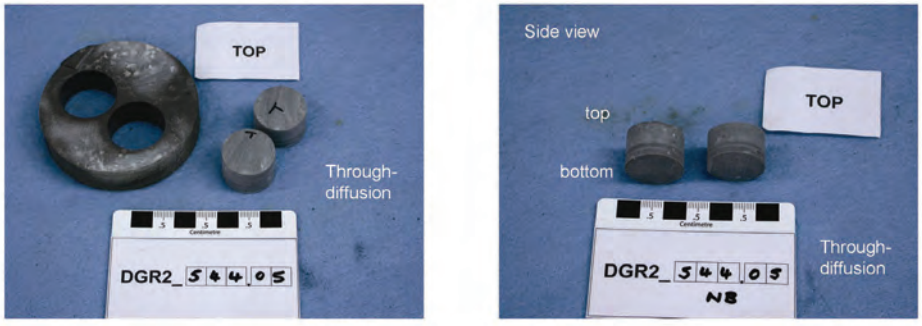

Figure A 4: Core Segment and Samples Prepared from DGR2_544.05.

DGR2_549.63 Georgian Bay

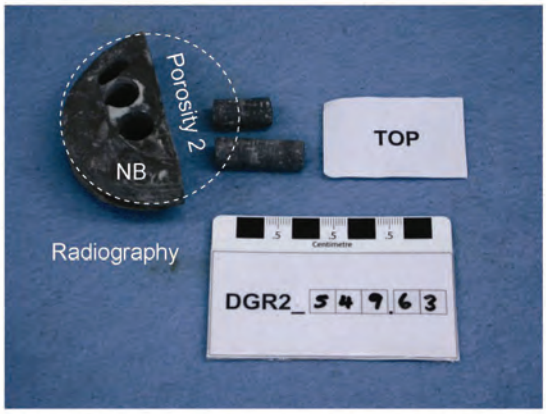

DGR2_549.63 Georgian Bay

Figure A 5: Core Segment and Samples Prepared from DGR2_549.63.

DGR2_553.04 Georgian Bay

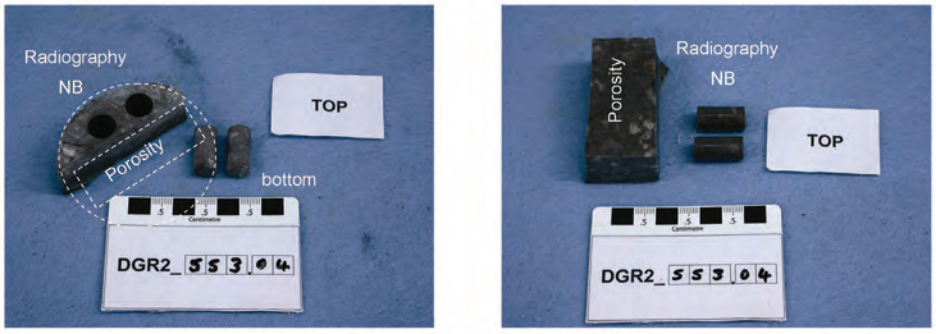

DGR2_553.04 Georgian Bay

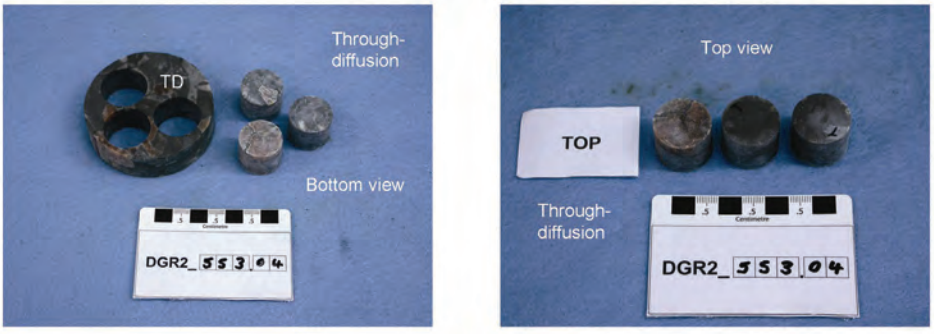

Figure A 6: Core Segment and Samples Prepared from DGR2_553.04.

DGR2_561.90 Georgian Bay

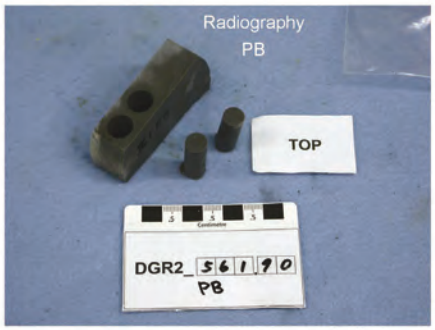

DGR2_561.90 Georgian Bay

Figure A 7: Core Segment and Samples Prepared from DGR2_561.90.

DGR2_568.47 Georgian Bay

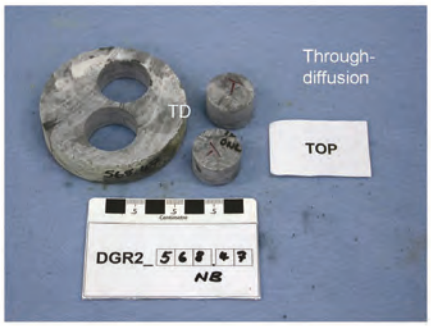

DGR2_568.47 Georgian Bay

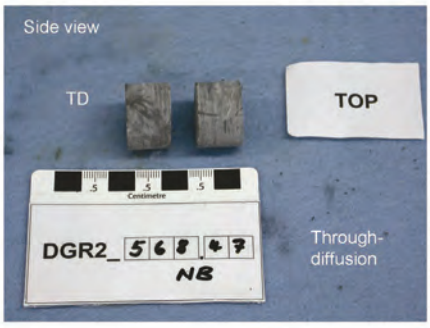

Figure A 8: Core Segment and Samples Prepared from DGR2_568.47.

DGR2_575.36 Georgian Bay

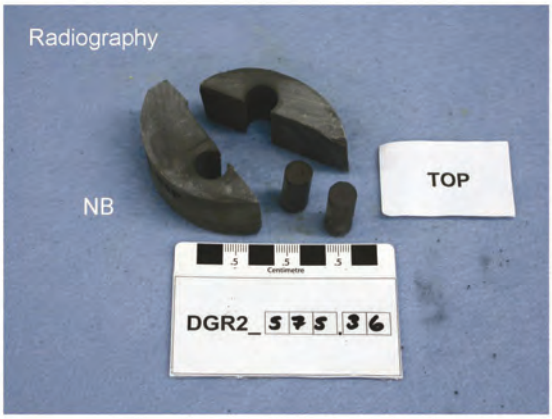

DGR2_575.36 Georgian Bay

Figure A 9: Core Segment and Samples Prepared from DGR2_575.36.

DGR2_583.18 Georgian Bay

DGR2_583.18 Georgian Bay

Figure A 10: Core Segment and Samples Prepared from DGR2_583.18.

DGR2_593.53 Georgian Bay

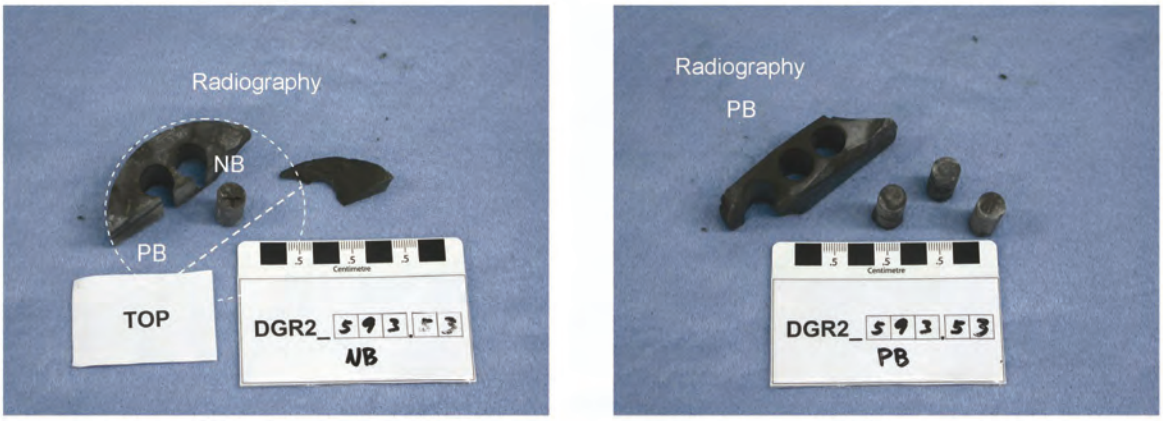

DGR2_593.53 Georgian Bay

Figure A 11: Core Segment and Samples Prepared from DGR2_593.53.

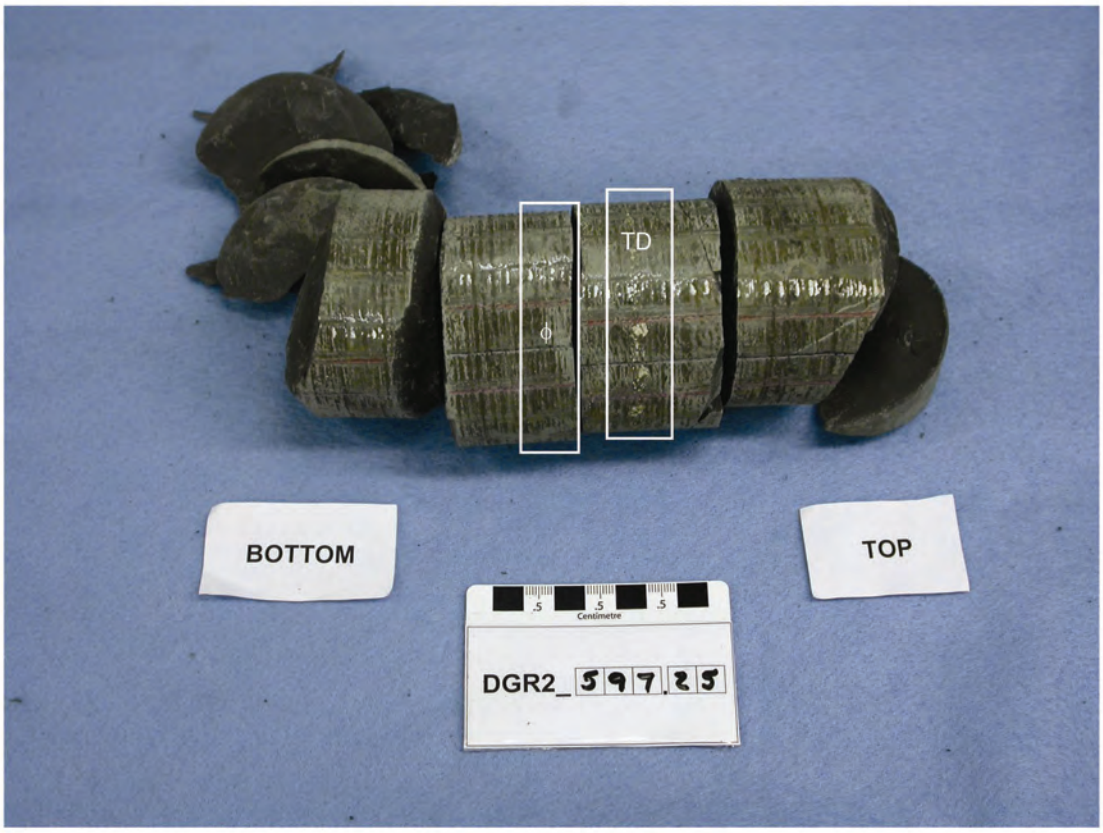

DGR2_597.25 Georgian Bay

DGR2_597.25 Georgian Bay

Figure A 12: Core Segment and Samples Prepared from DGR2_597.25.

DGR2_604.29 Georgian Bay

DGR2_604.29 Georgian Bay

Figure A 13: Core Segment and Samples Prepared from DGR2_604.29.

DGR2_620.95 Blue Mountain

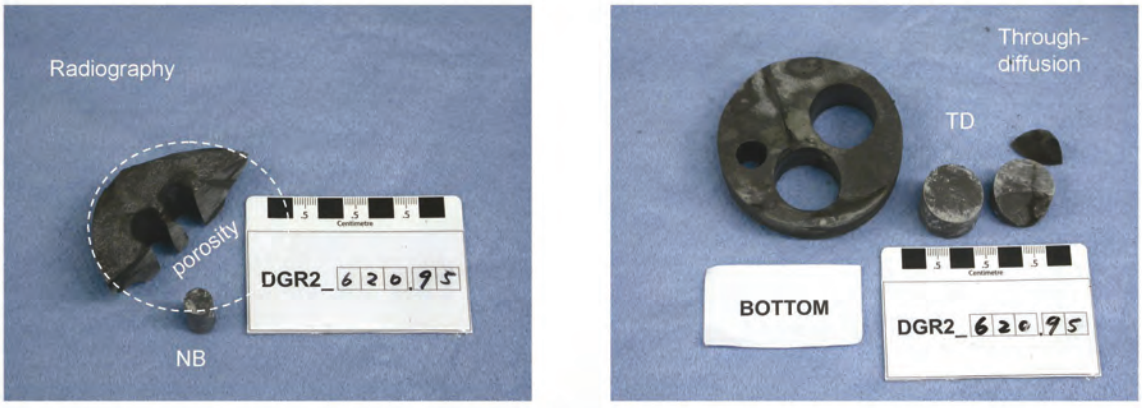

DGR2_620.95 Blue Mountain

Figure A 14: Core Segment and Samples Prepared from DGR2_620.95.

A.2 RADIOGRAPHY DIFFUSION PROFILES

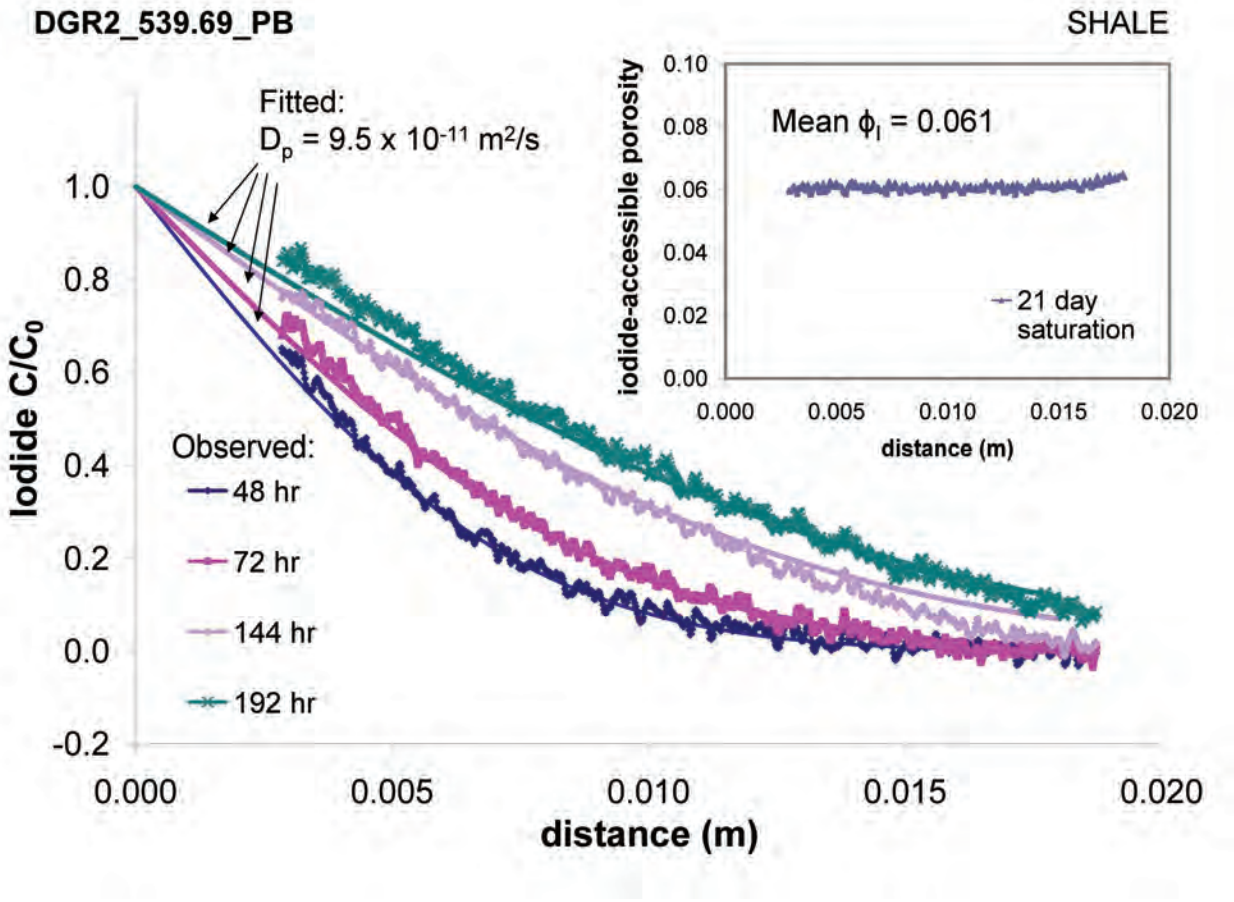

Figure A 15: Diffusion Profiles and Iodide-Accessible Porosity Profile Measured by Radiography for Sample DGR2_539.69_PB.

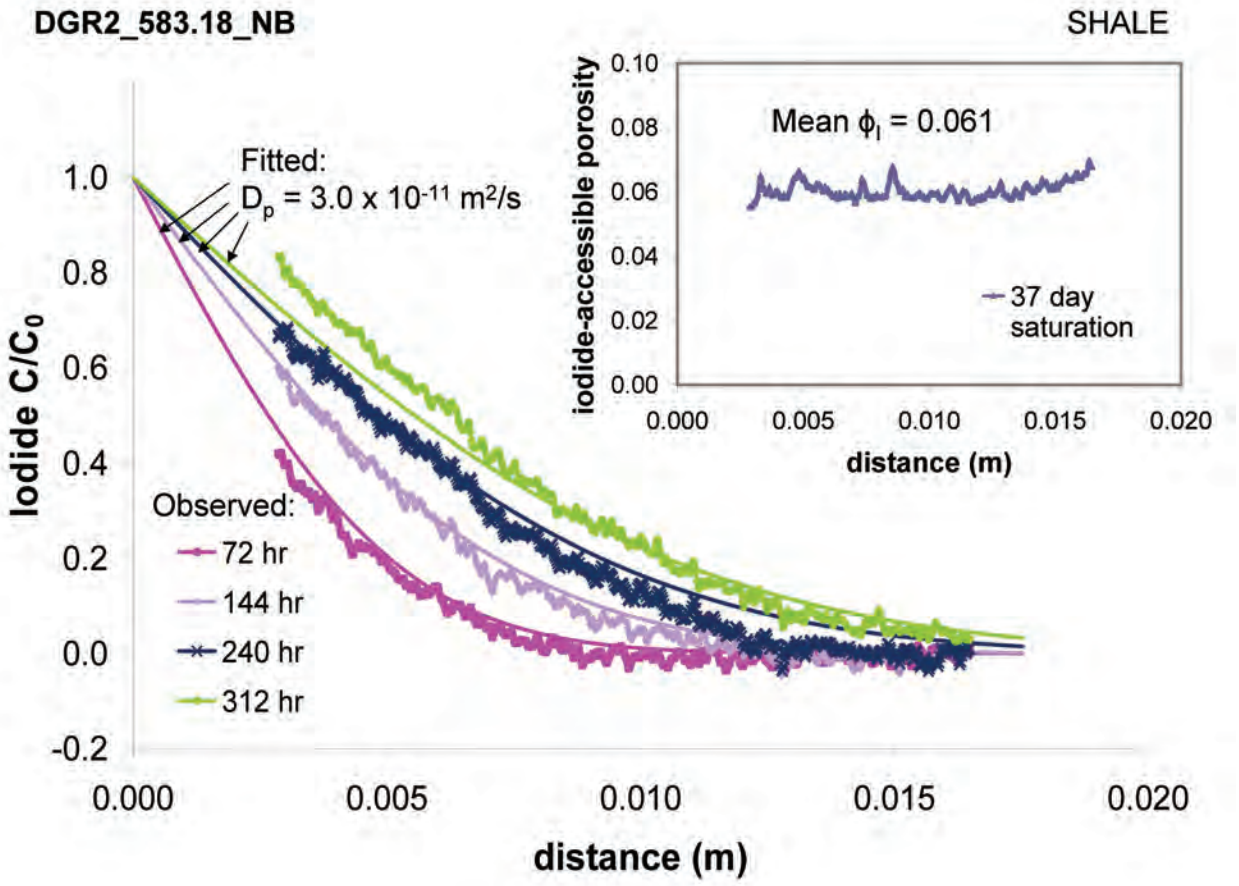

Figure A 16: Diffusion Profiles and Iodide-Accessible Porosity Profile Measured by Radiography for Sample DGR2_583.18_NB.

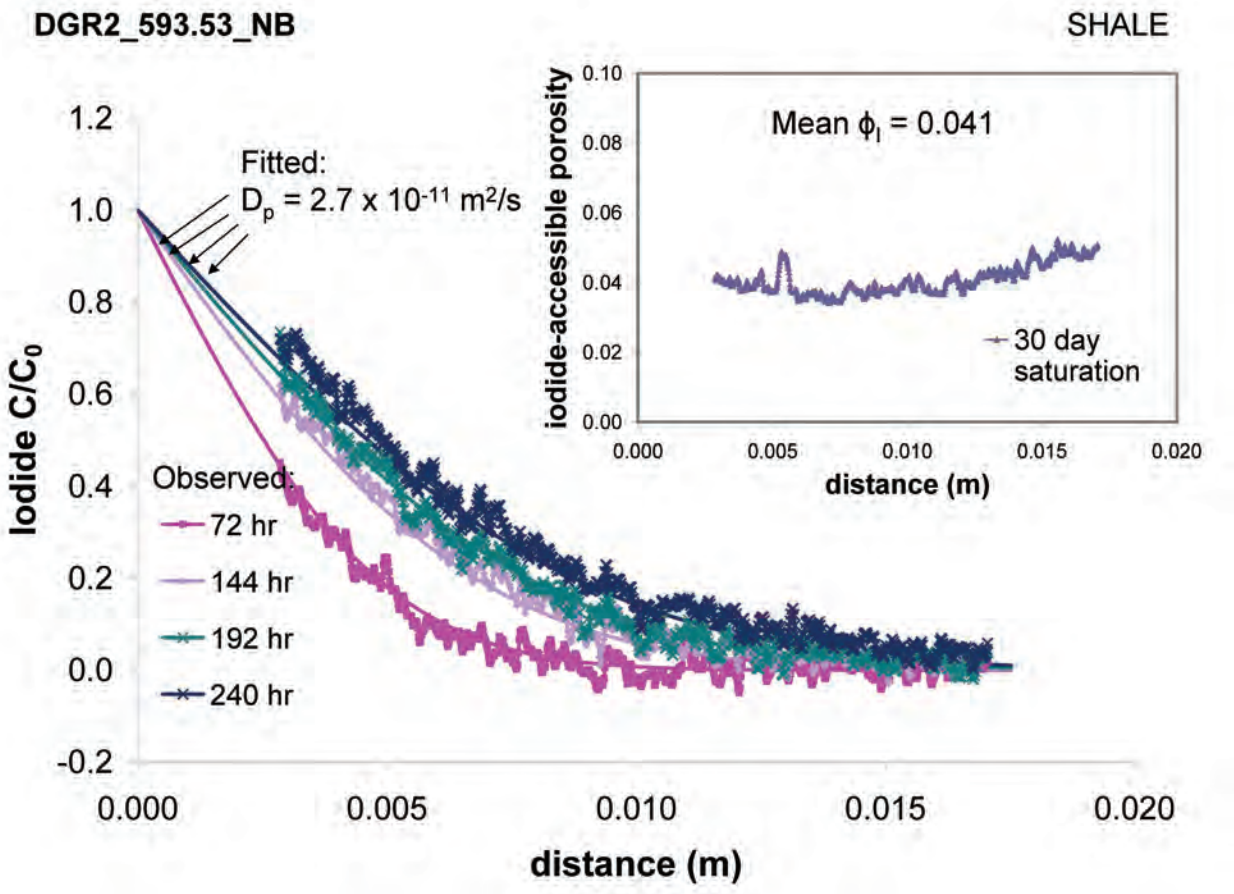

Figure A 17: Diffusion Profiles and Iodide-Accessible Porosity Profile Measured by Radiography for Sample DGR2_593.53_NB.

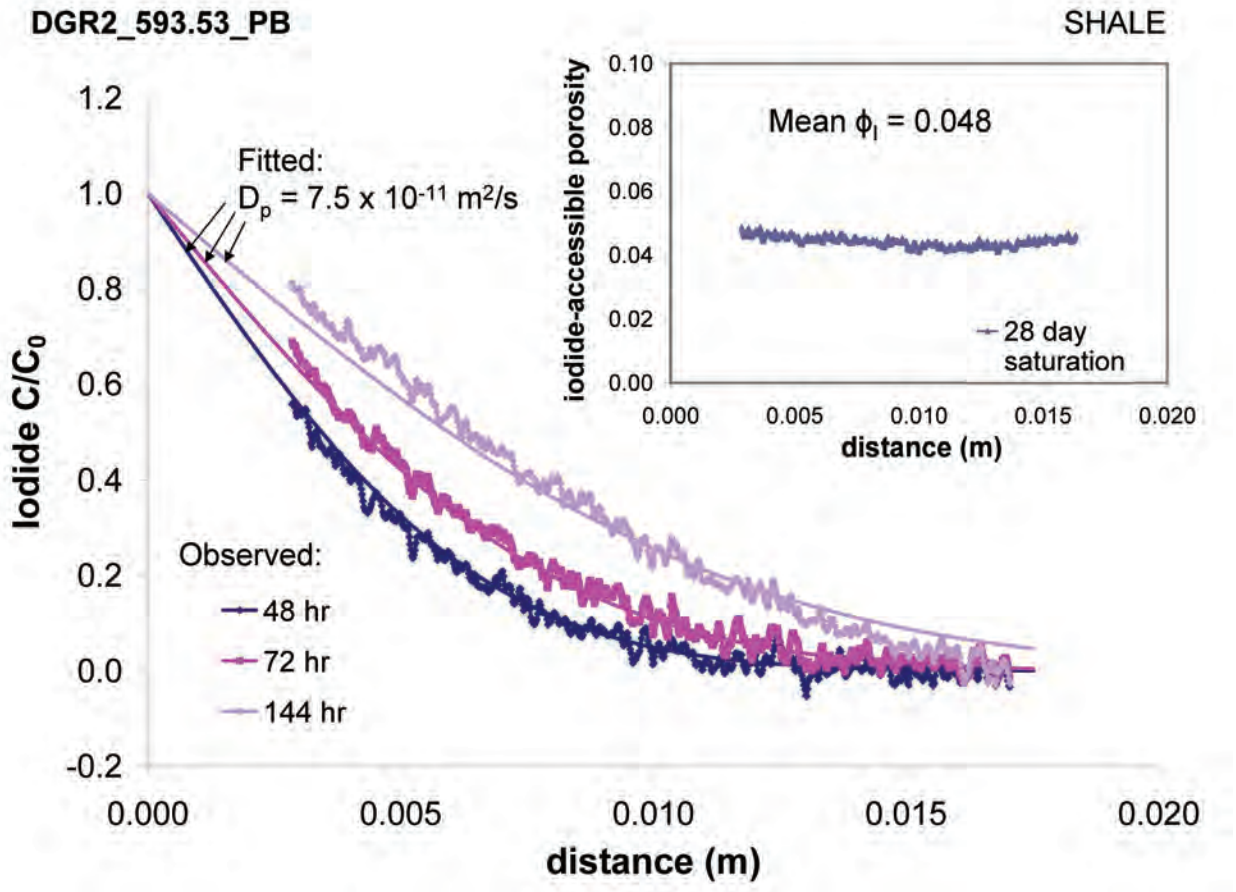

Figure A 18: Diffusion Profiles and Iodide-Accessible Porosity Profile Measured by Radiography for Sample DGR2_593.53_PB.

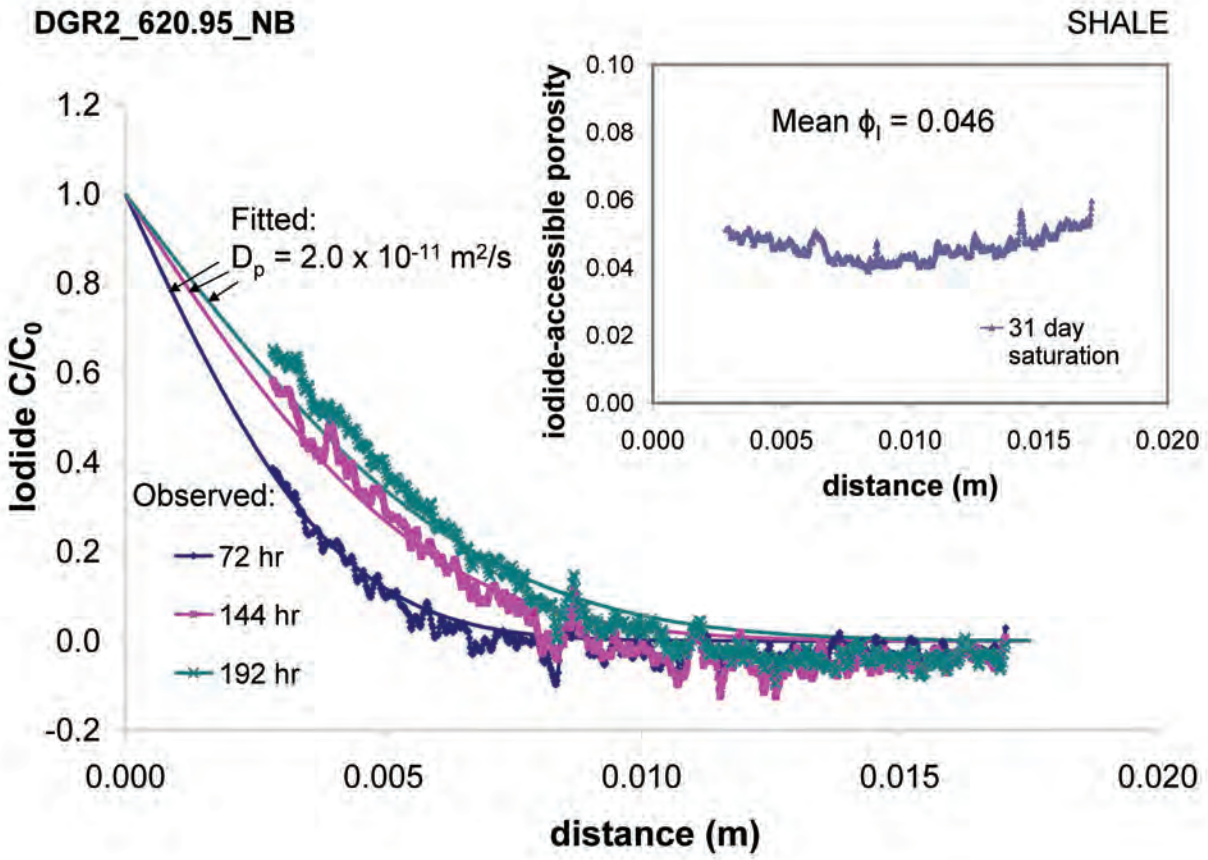

Figure A 19: Diffusion Profiles and Iodide-Accessible Porosity Profile Measured by Radiography for Sample DGR2_620.95_NB.

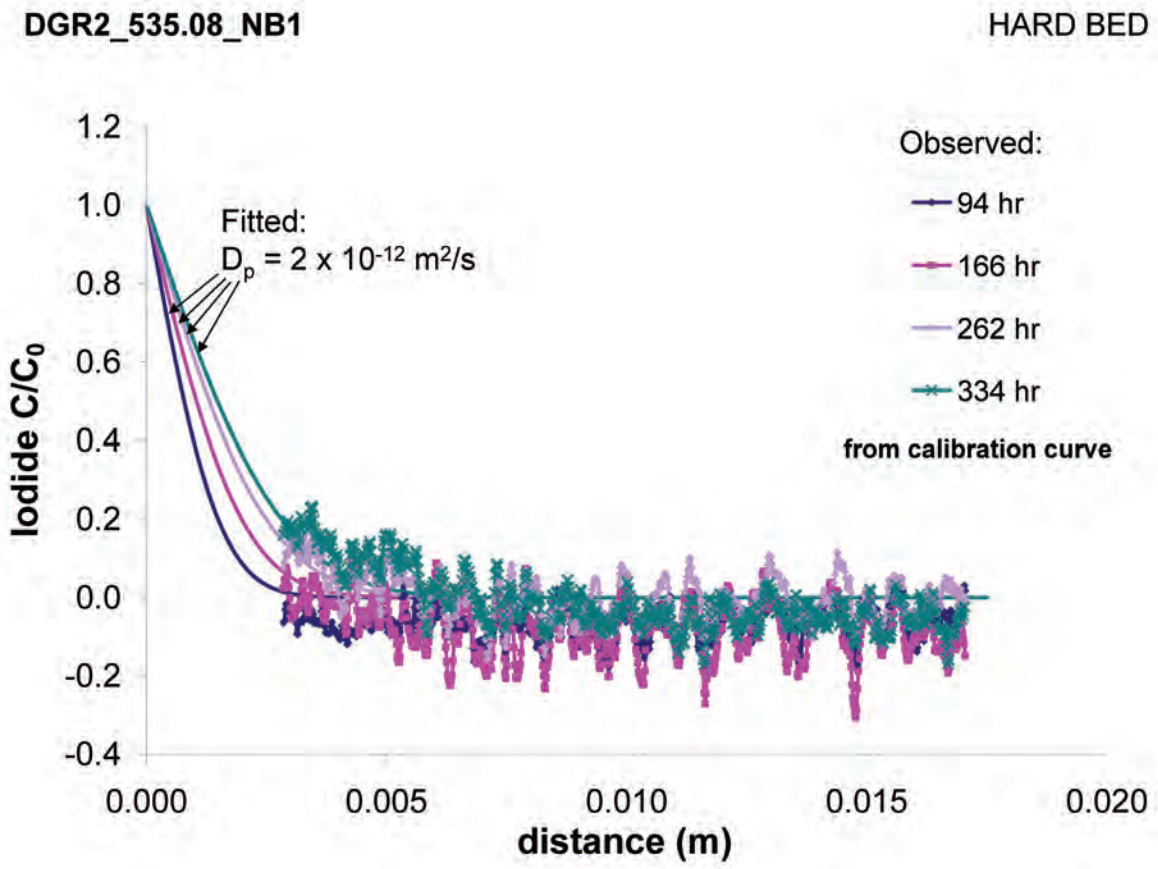

Figure A 20: Diffusion Profiles and Iodide-Accessible Porosity Profile Measured by Radiography for Sample DGR2_535.08_NB1.

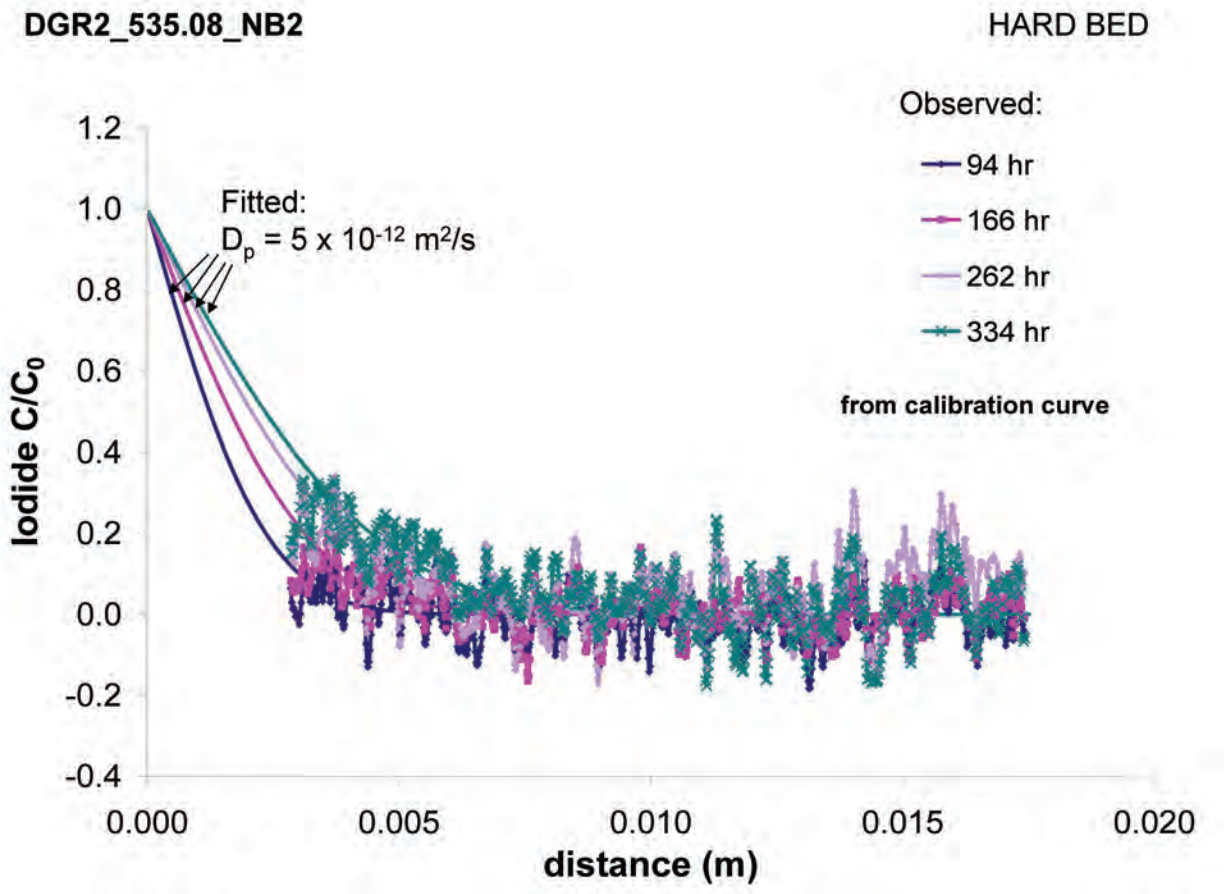

Figure A 21: Diffusion Profiles and Iodide-Accessible Porosity Profile Measured by Radiography for Sample DGR2_535.08_NB2.

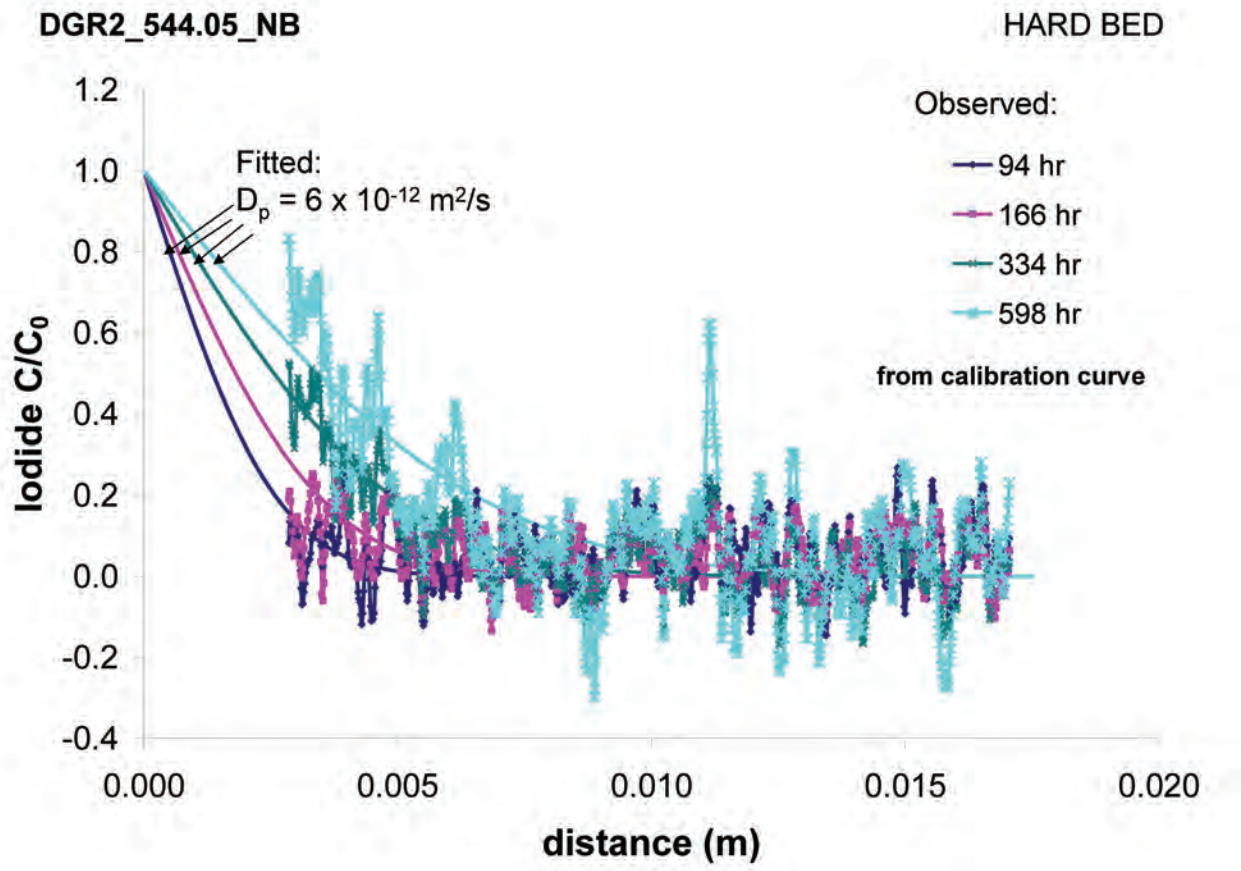

Figure A 22: Diffusion Profiles and Iodide-Accessible Porosity Profile Measured by Radiography for Sample DGR2_544.05_NB.

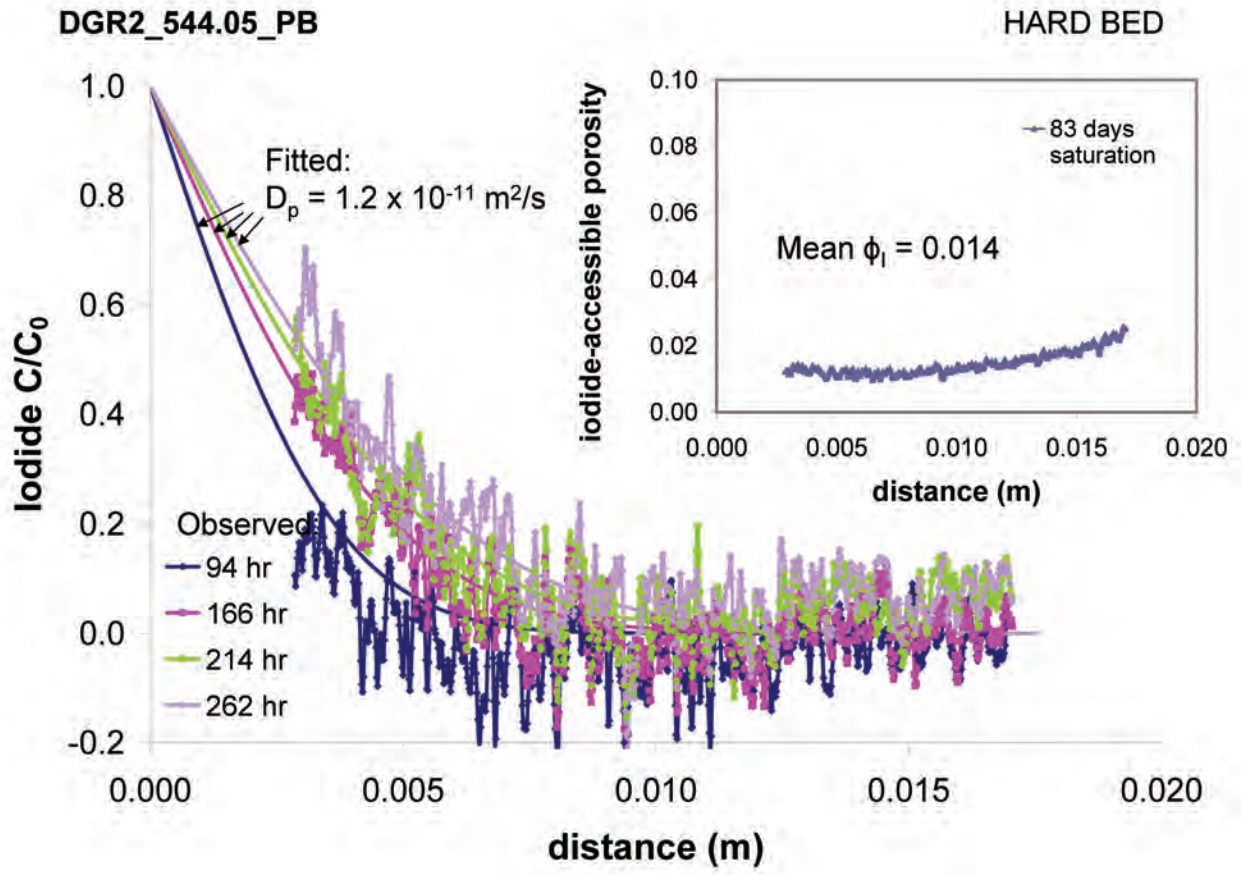

Figure A 23: Diffusion Profiles and Iodide-Accessible Porosity Profile Measured by Radiography for Sample DGR2_544.05_PB.

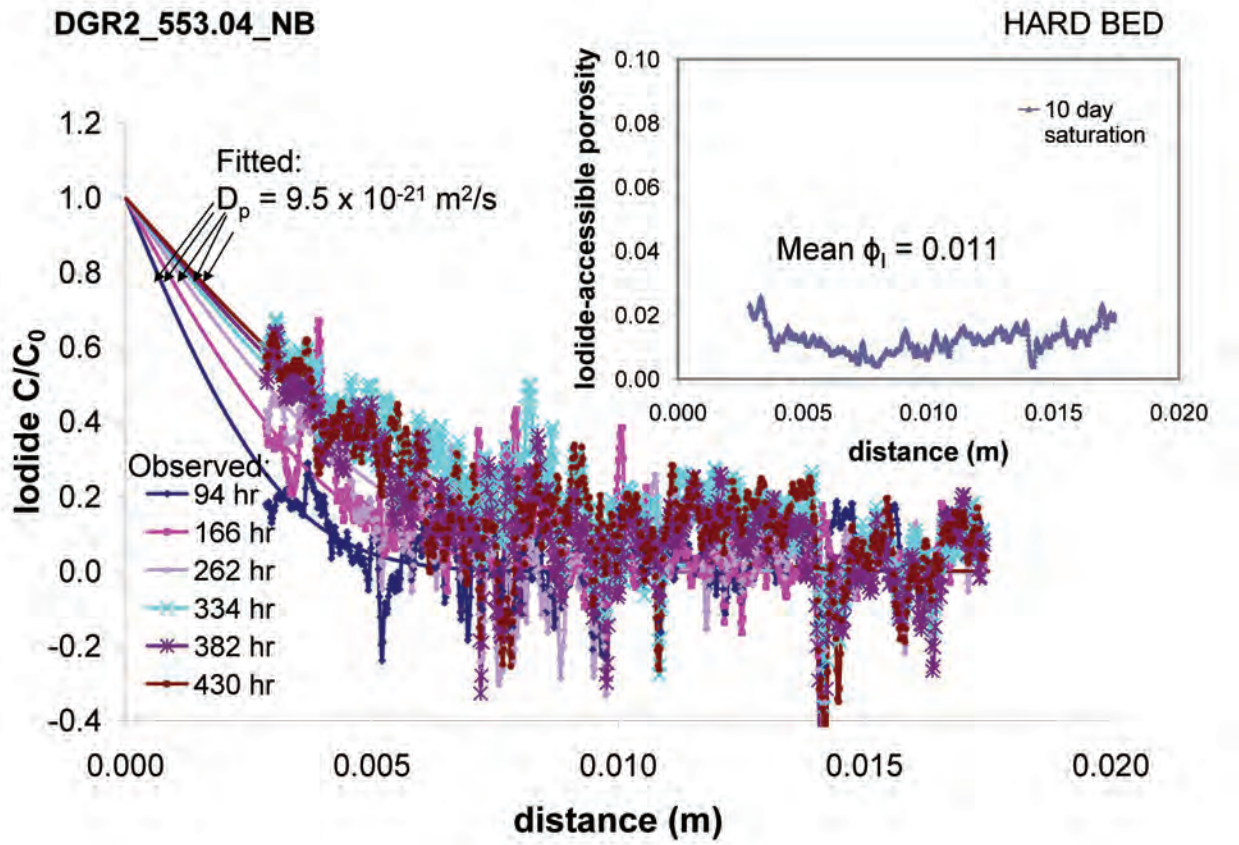

Figure A 24: Diffusion Profiles and Iodide-Accessible Porosity Profile Measured by Radiography for Sample DGR2_553.04_NB.

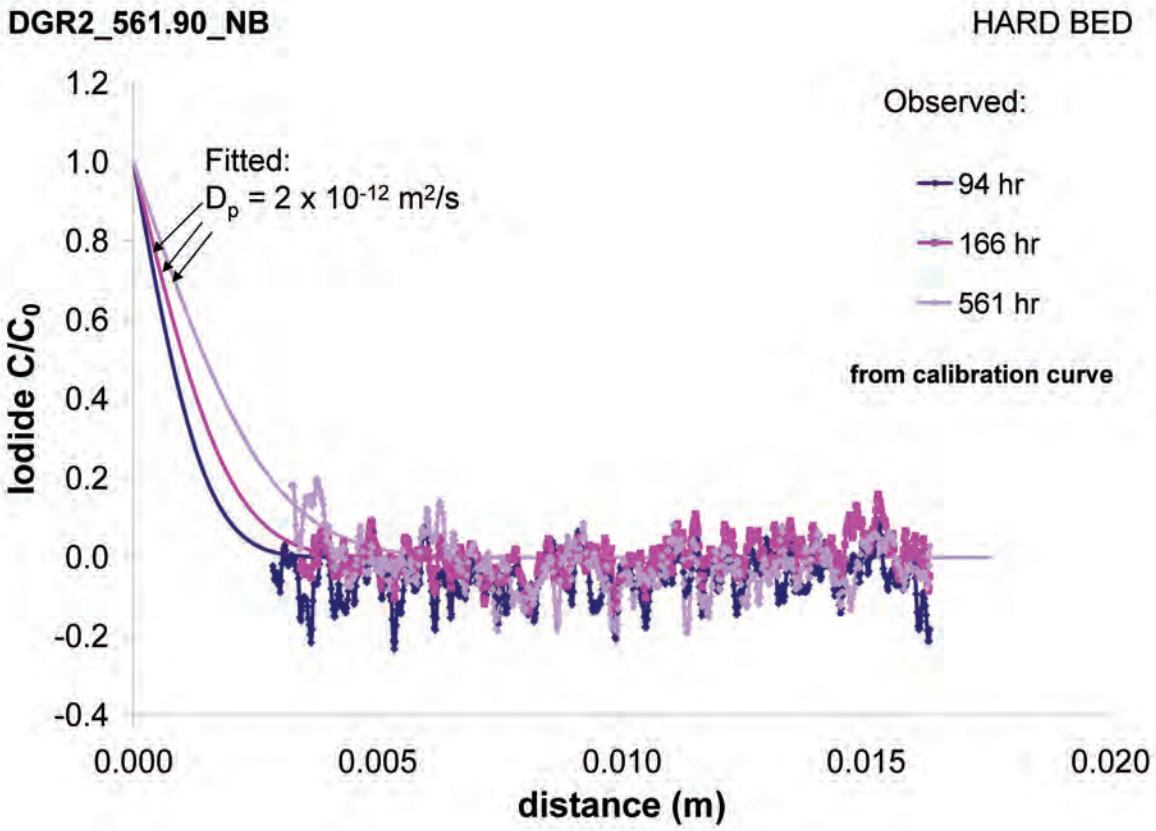

Figure A 25: Diffusion Profiles and Iodide-Accessible Porosity Profile Measured by Radiography for Sample DGR2_561.90_NB.

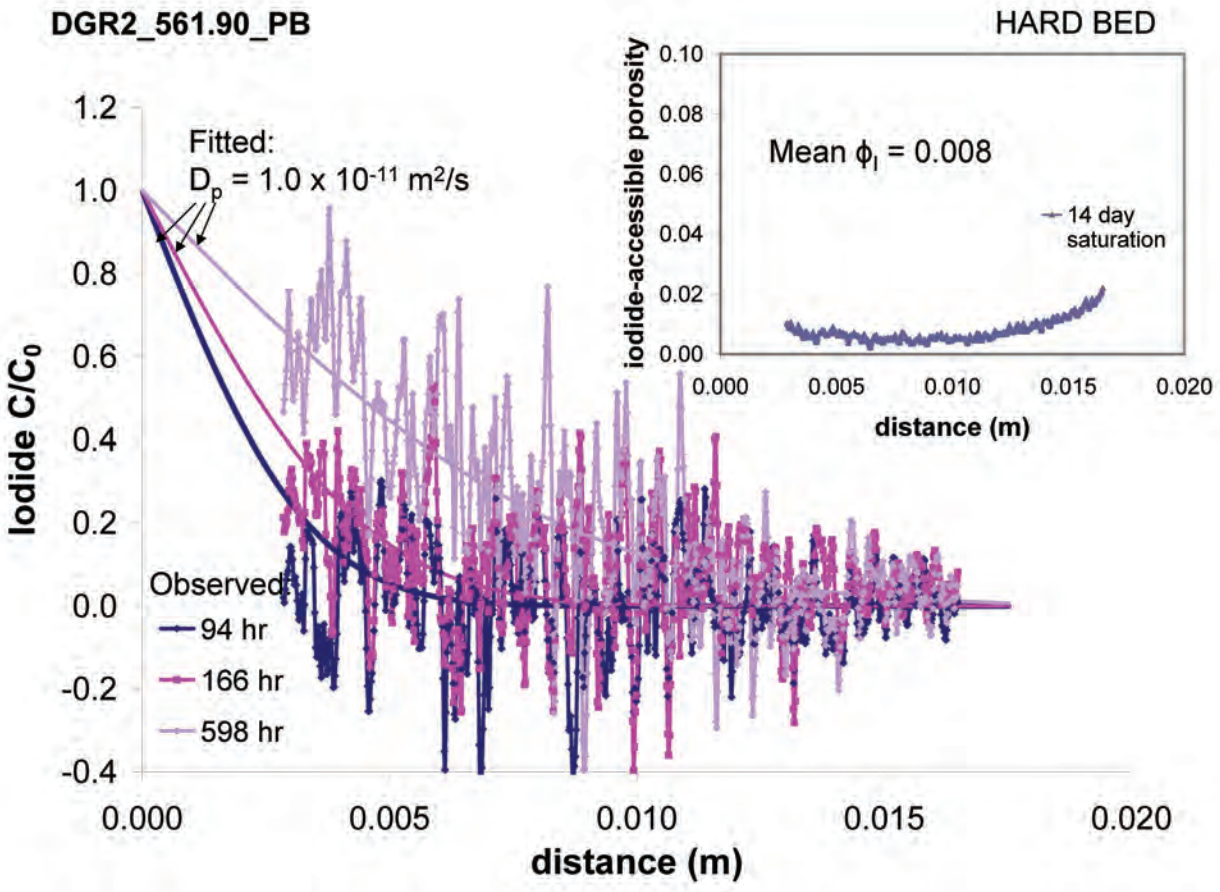

Figure A 26: Diffusion Profiles and Iodide-Accessible Porosity Profile Measured by Radiography for Sample DGR2_561.90_PB.

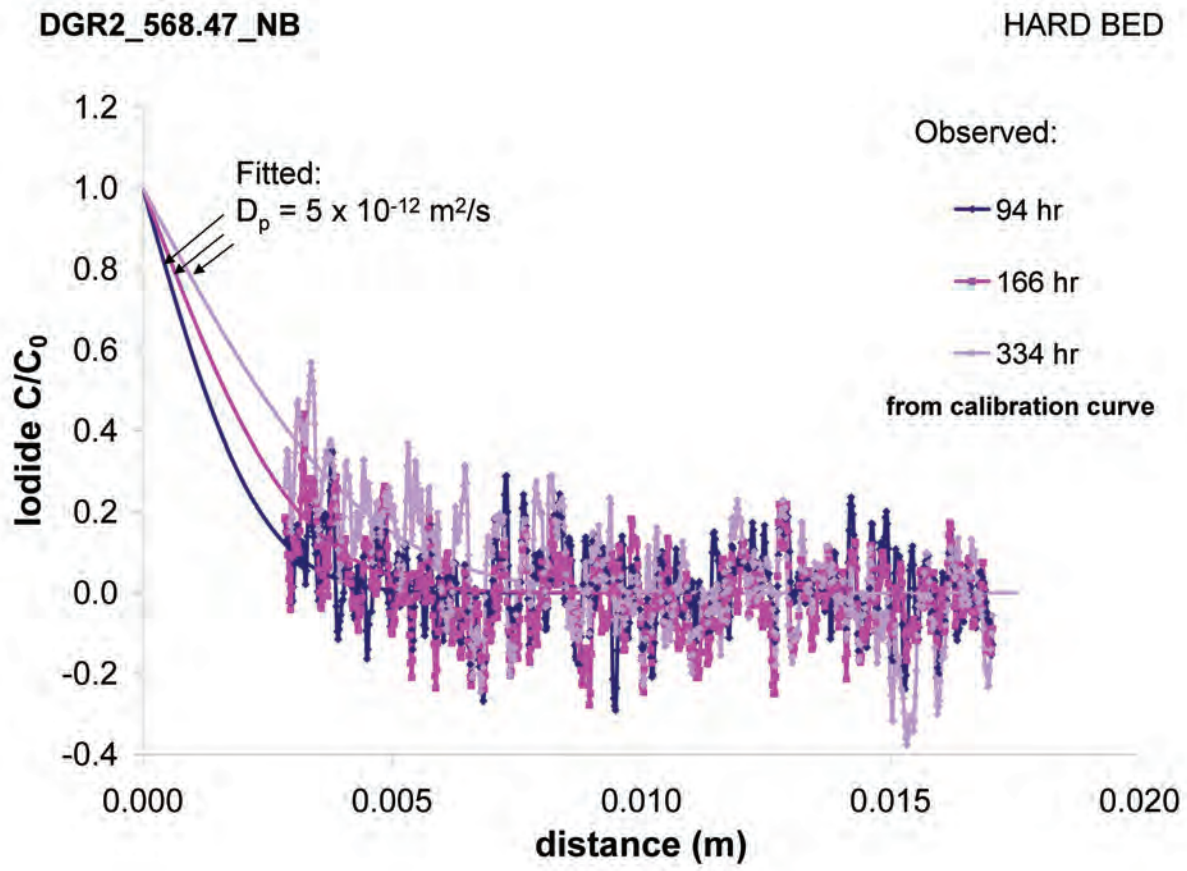

Figure A 27: Diffusion Profiles and Iodide-Accessible Porosity Profile Measured by Radiography for Sample DGR2_568.47_NB.

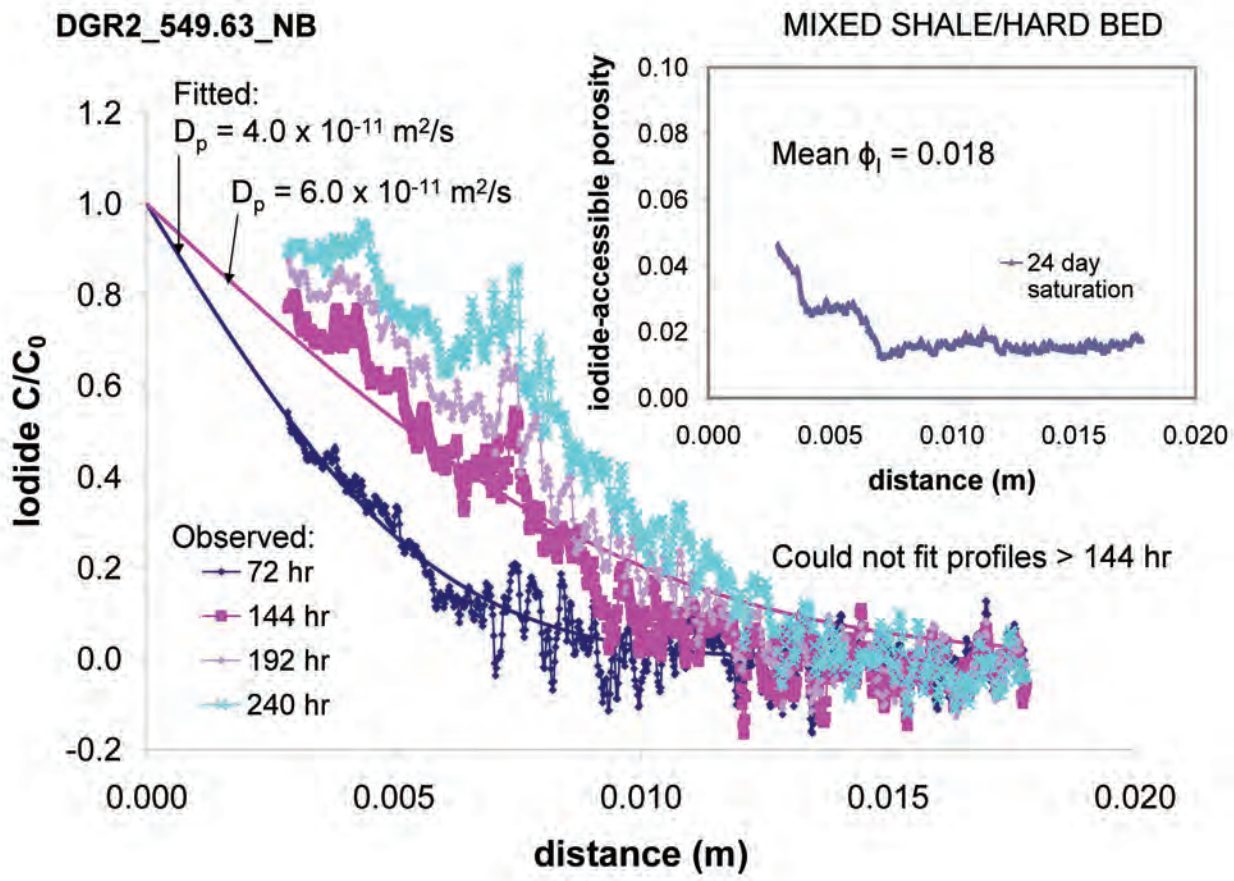

Figure A 28: Diffusion Profiles and Iodide-Accessible Porosity Profile Measured by Radiography for Sample DGR2_549.63_NB.

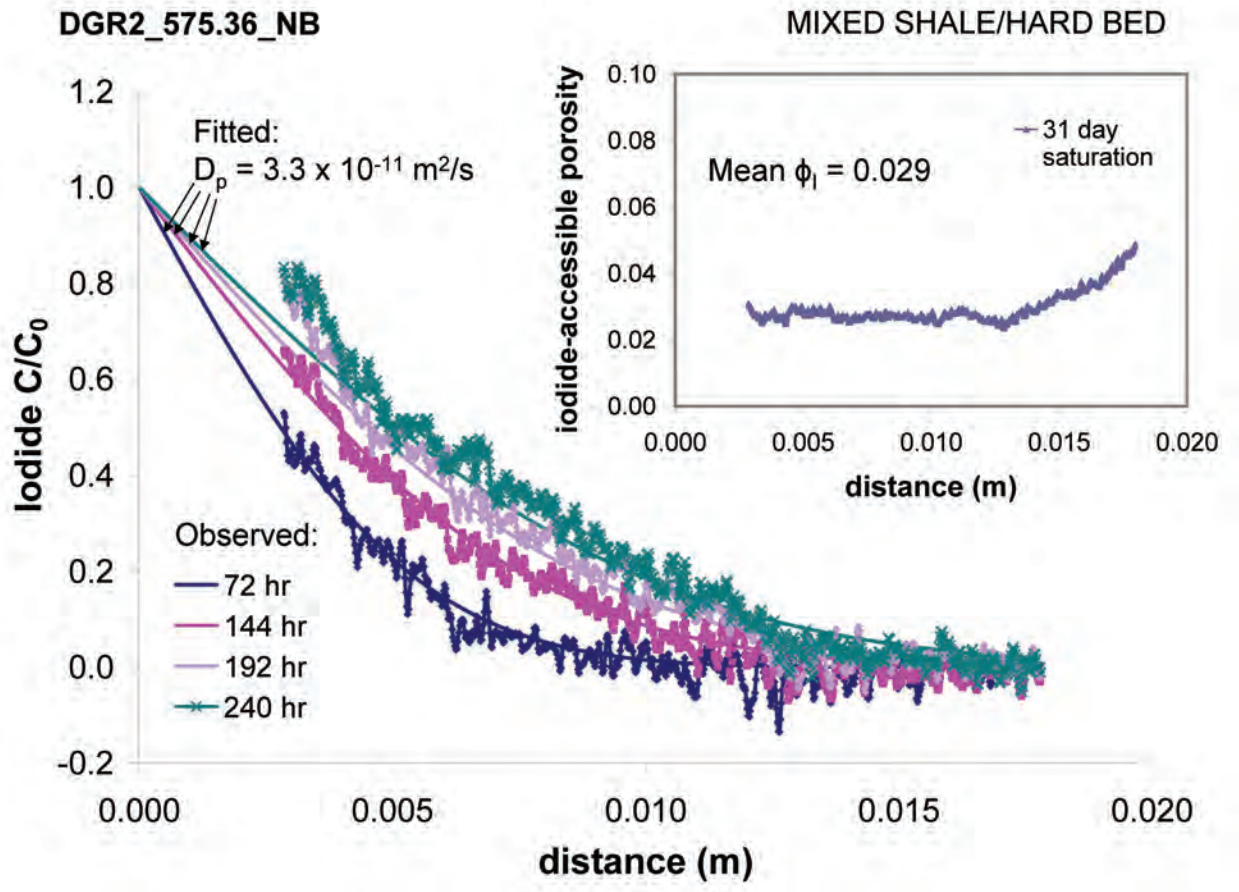

Figure A 29: Diffusion Profiles and Iodide-Accessible Porosity Profile Measured by Radiography for Sample DGR2_575.36_NB.

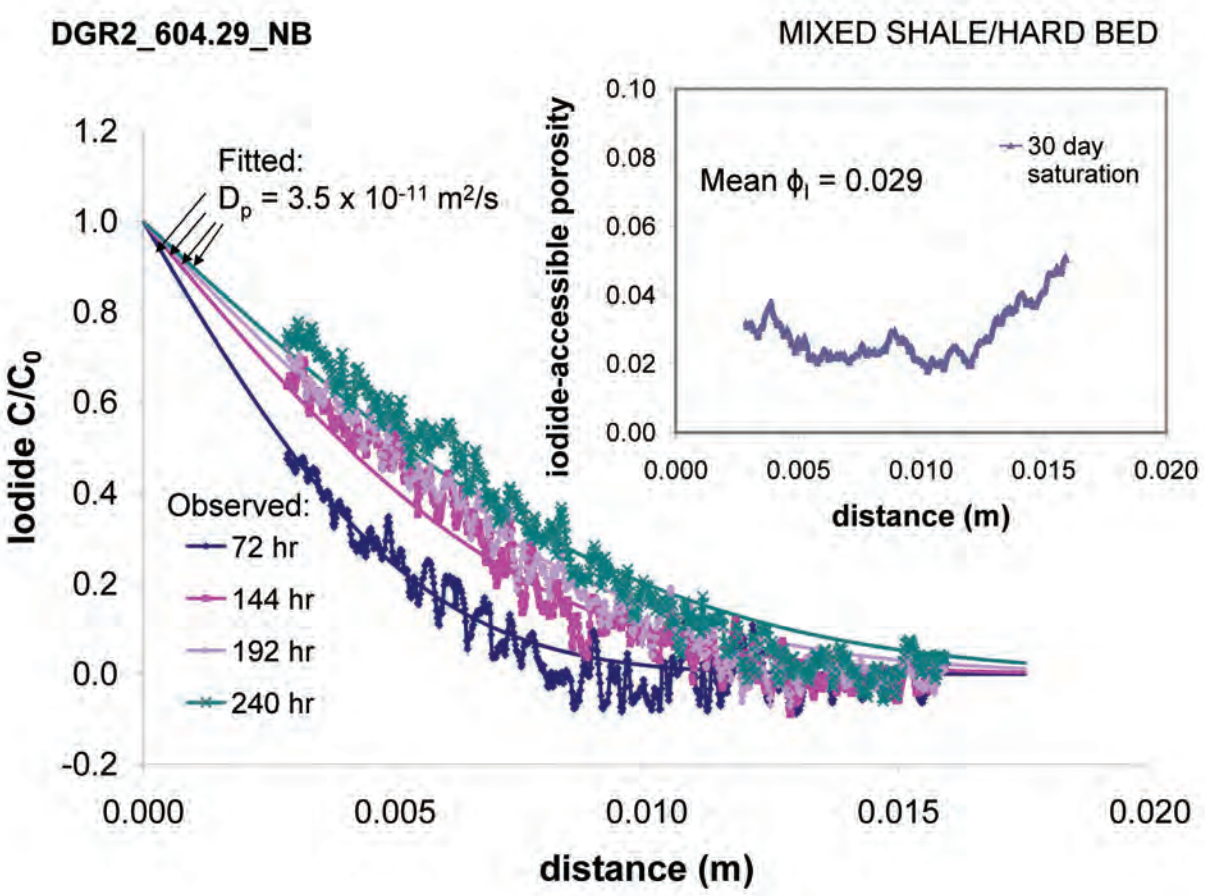

Figure A 30: Diffusion Profiles and Iodide-Accessible Porosity Profile Measured by Radiography for Sample DGR2_604.29_NB.

A.3 THROUGH-DIFFUSION DATA

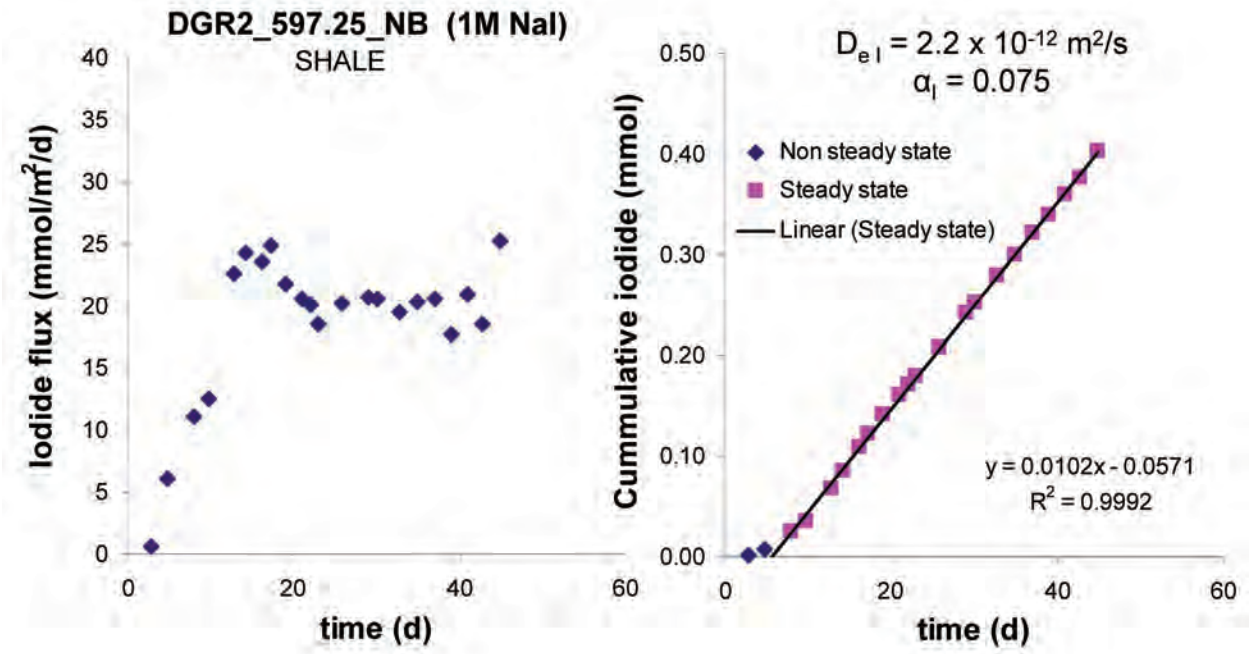

Figure A 31: Flux and Cumulative Mass of Iodide as a Function of Time in Through-Diffusion Experiments Using 1 mol/L NaI Tracer (Sample DGR2_597.25_NB).

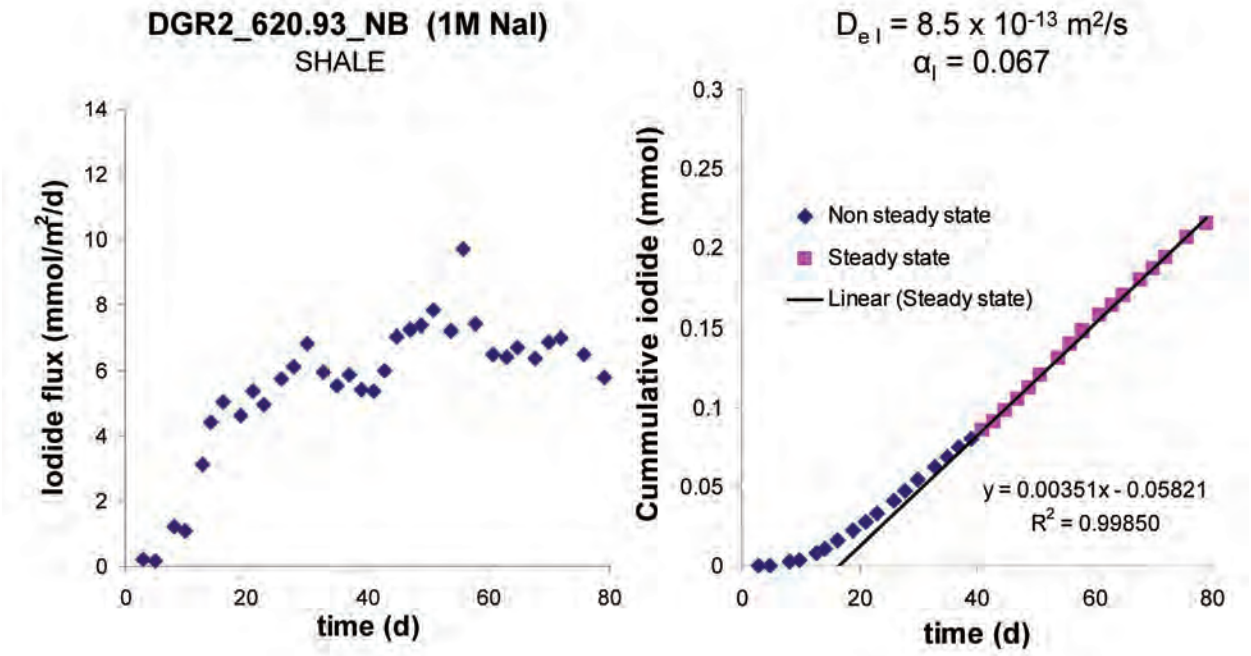

Figure A 32: Flux and Cumulative Mass of Iodide as a Function of Time in Through-Diffusion Experiments Using 1 mol/L NaI Tracer (Sample DGR2_620.93_NB).

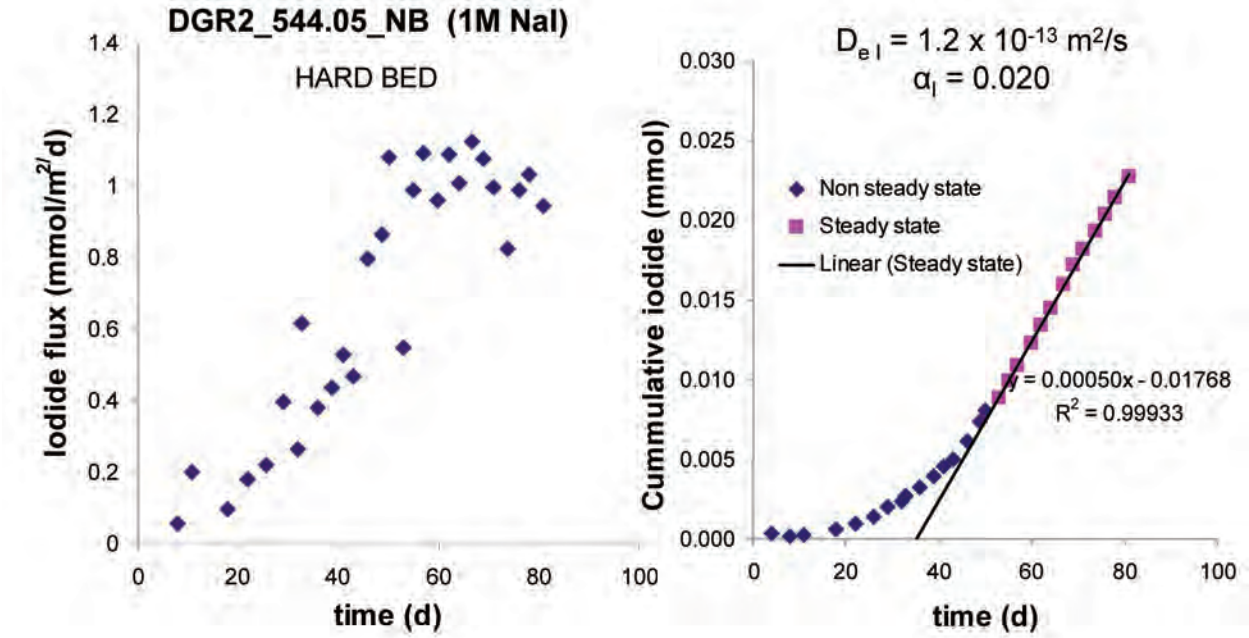

Figure A 33: Flux and Cumulative Mass of Iodide as a Function of Time in Through-Diffusion Experiments Using 1 mol/L NaI Tracer (Sample DGR2_544.05_NB).

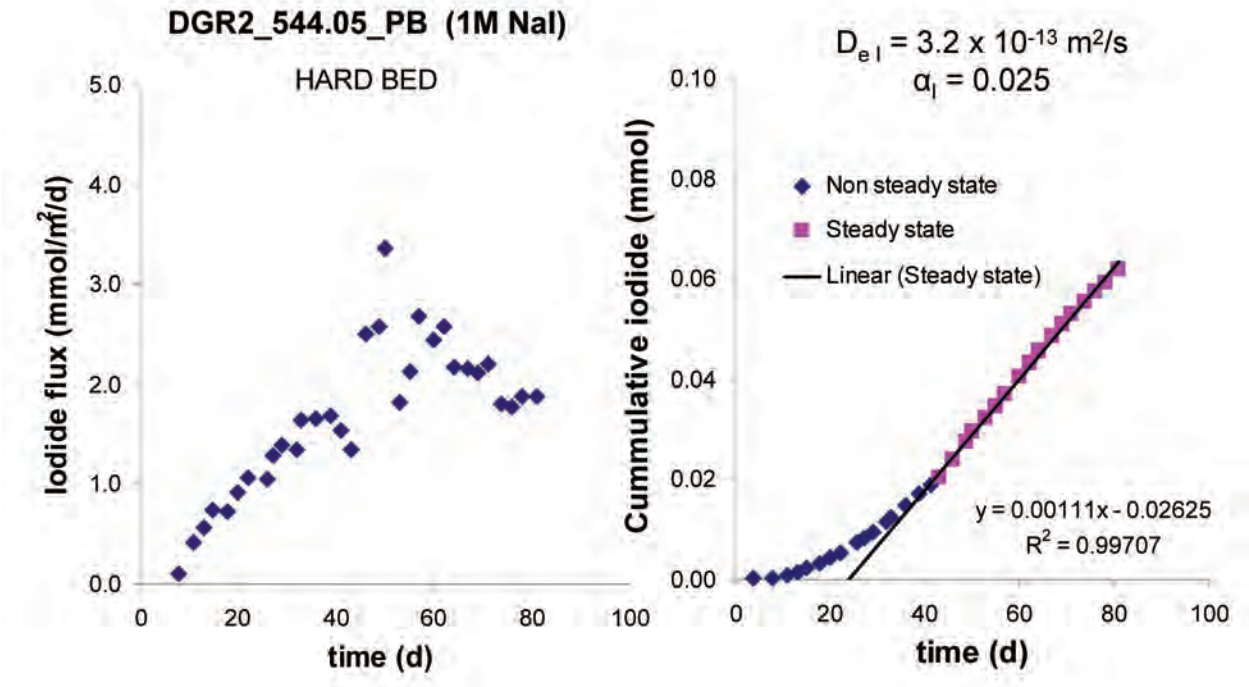

Figure A 34: Flux and Cumulative Mass of Iodide as a Function of Time in Through-Diffusion Experiments Using 1 mol/L NaI Tracer (Sample DGR2_544.05_PB).

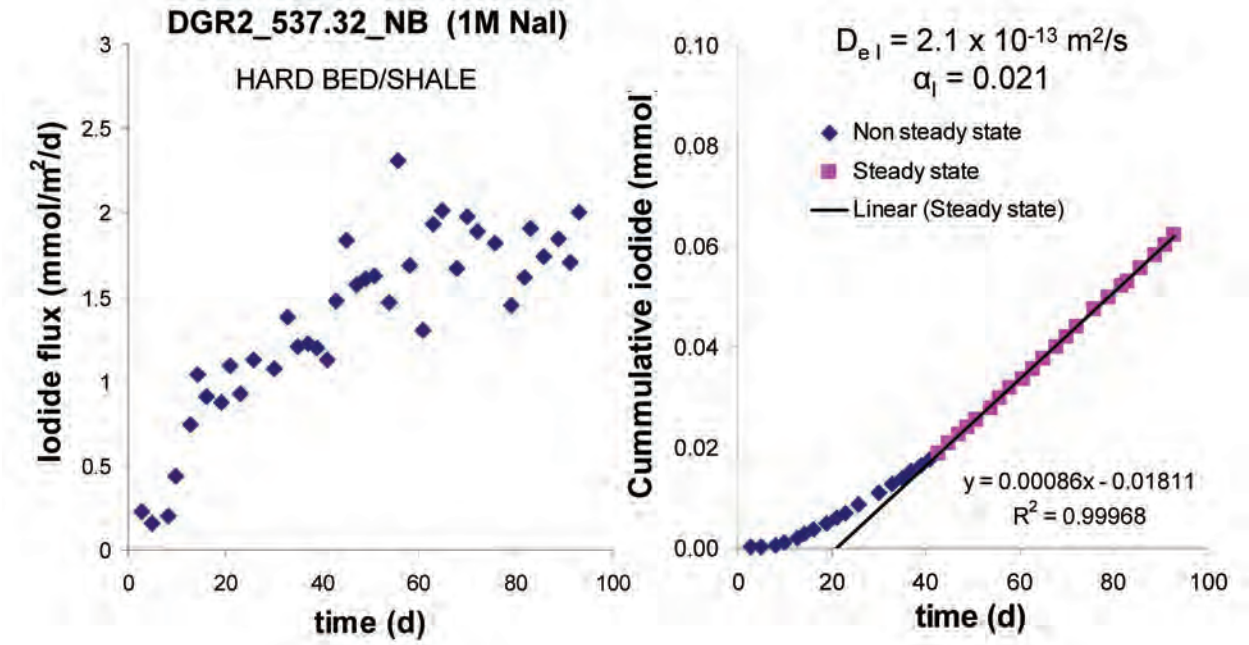

Figure A 35: Flux and Cumulative Mass of Iodide as a Function of Time in Through-Diffusion Experiments Using 1 mol/L NaI Tracer (Sample DGR2_537.32_NB).

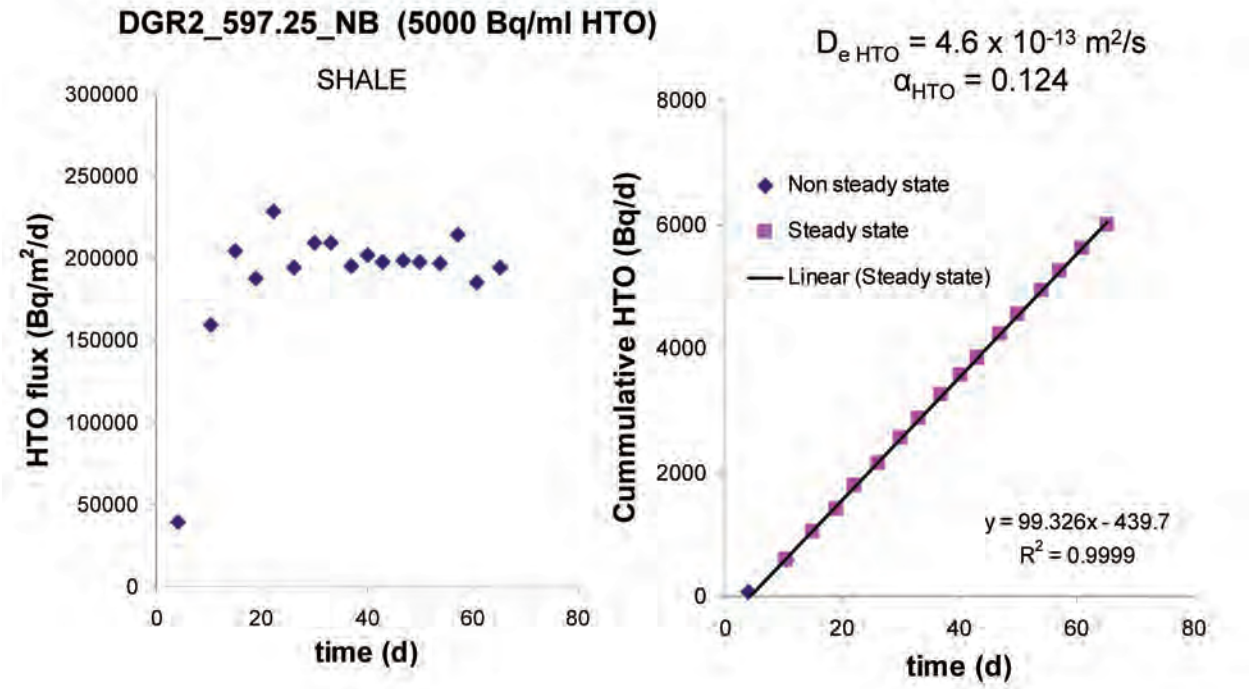

Figure A 36: Flux and Cumulative Mass of Iodide as a Function of Time in Through-Diffusion Experiments Using 1 mol/L NaI Tracer (Sample DGR2_597.25_NB).

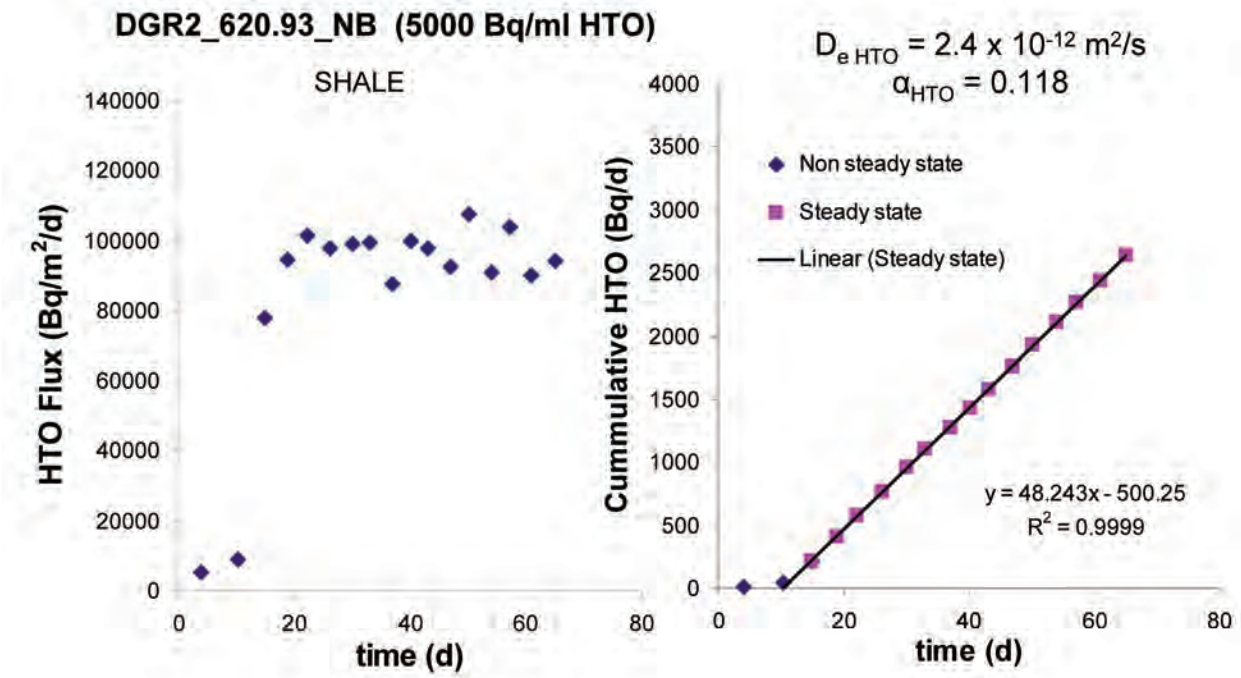

Figure A 37: Flux and Cumulative Activity of HTO as a Function of Time in Through-Diffusion Experiments Using 5000 Bq/ml HTO Tracer (Sample DGR2_620.93_NB).

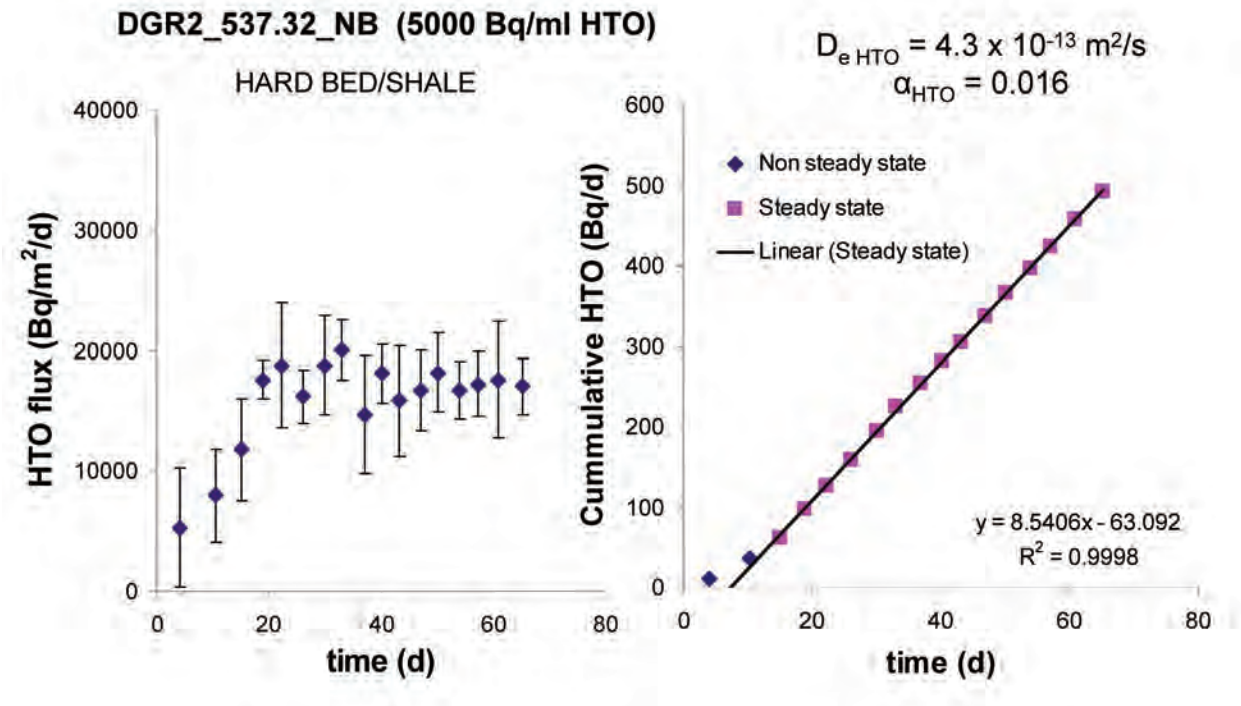

Figure A 38: Flux and Cumulative Activity of HTO as a Function of Time in Through-Diffusion Experiments Using 5000 Bq/ml HTO Tracer (Sample DGR2_537.32_NB).

APPENDIX B: SYNTHETIC PORE WATER AND TRACER SOLUTIONS FOR DIFFUSION EXPERIMENTS

CONTENTS

Page

LIST OF TABLES

Page

B.1 COMPOSITION OF SOLUTIONS USED IN DIFFUSION EXPERIMENTS

A synthetic pore water (SPW) was used in porosity measurements and diffusion experiments for all shale samples in this project. The composition of the SPW (Table B 1) was derived from a crush-and-leach test to determine the pore water composition for another sample of grey shale from the Georgian Bay Formation (DGR2_596.64, Al et al. 2008). Tracer solutions were all prepared in a matrix of SPW, either by molar substitution of sodium iodide or cesium chloride for sodium chloride in the preparation, or by addition of tritiated water to the SPW.

Table B 1: Composition of Solutions Used in Porosity Measurements and Diffusion Experiments

	SPW Solution (mol/L)	Iodide (NaI) Tracer Solution (mol/L)	Cesium (CsCl) Tracer Solution (mol/L)	HTO Tracer Solution (mol/L)
Sodium	2.4	2.4	1.4	2.4
Potassium	0.5	0.5	0.5	0.5
Calcium	1.2	1.2	1.2	1.2
Magnesium	0.25	0.25	0.25	0.25
Chloride	5.8	4.8	5.8	5.8
Sulfate	0.001	0.001	0.001	0.001
Iodide	-	1.0	-	-
Cesium	-	-	1.0	-
Tritium (Bq/mL)	-	-	-	5 000

- = not added to solution.

REFERENCE

Al, T., Y. Xiang, and L. Cavé. 2008. Measurement of Diffusion Properties by X-Ray Radiography and by Through-Diffusion Techniques Using Iodide and Tritium Tracers: Core Samples from OS1 and DGR2. Prepared by University of New Brunswick for Intera Engineering Ltd. Intera Engineering Technical Report TR-08-04. Ottawa, Ontario.

APPENDIX C: EXAMPLE OF REACTIVE TRANSPORT MODEL INPUT FILE

CONTENTS

Page

C.1 PHREEQC INPUT FILE FOR SAMPLE DGR3_468.02D

The following is an example of a PHREEQC input file used for reactive transport calculations with cesium tracer. The three parameters given in bold type were adjusted to optimize the fit of the simulated to observed Cs C/C_0 profiles

```
DATABASE pitzer.dat

TITLE Cesium tracer in Queenston shale sample DGR3_468.02D
# Solute activities calculated with Pitzer ion association model

SOLUTION_MASTER_SPECIES
Cs       Cs+            0.0     Cs              132.91

SOLUTION_SPECIES
# Cs+ primary master species
  Cs+ = Cs+
  log_k    0.000
  -gamma   1.81       0.01
# Truesdell-Jones a,b parameters for Cs from Parkhurst 1990
# cited in Langmuir 1997 p 133

PHASES
CsCl
     CsCl = Cs+ + Cl-
     log_k           3.488       # Hu et al 2007 CCPDTC 31:541-544
CsBr
     CsBr = Cs+ + Br-
     log_k           1.881       # Hu et al 2007 CCPDTC 31:541-544

PITZER

-B0             # Pitzer and Mayorga 1973 J Phys Chem 77 2300-2307
     Cs+   Cl-        0.030
     Cs+   Br-        0.0279
     Cs+   SO4-2      0.0888
     Cs+   OH-        0.150

-B1             # Pitzer and Mayorga 1973 J Phys Chem 77 2300-2307
     Cs+   Cl-        0.0558
     Cs+   Br-        0.0139
     Cs+   SO4-2      1.11075
     Cs+   OH-        0.30

-C0             # Pitzer and Mayorga 1973 J Phys Chem 77 2300-2307
     Cs+   Cl-        0.00038
     Cs+   Br-        0.00004
     Cs+   SO4-2      -0.00599803
```

```
-THETA           # Pitzer and Kim 1974 J Am Chem Soc 96 5701-5707
     Na+   Cs+        -0.033
     K+    Cs+        0.0
     H+    Cs+        -0.044

-PSI             # Pitzer and Kim 1974 J Am Chem Soc 96 5701-5707
     Na+   Cs+   Cl-        -0.003
     K+    Cs+   Cl-        -0.0013
     H+    Cs+   Cl-        -0.019

# Data is also available for Mg+2 and ternary coefficients with SO42-,
# but not consistent with the binary coefficients above.
# For this problem we chose data within the CsCl-NaCl system.

EXCHANGE_SPECIES
     Cs+ + X- = CsX
     log_k       1.1    #  Appelo and Postma 1996 p 160 table

SOLUTION 0  CESIUM TRACER IN SPW #incoming solution
     units       mol/l
     density     1.311
     temp        25
     pH          7
     pe          4
     redox       pe
     Na          1.4
     K           0.5
     Ca          1.201
     Mg          0.250
     Cs          1.0
     Cl          5.8
     S(6)        0.001
     water       1     # kg

SOLUTION 1-40  SHALE SPW
     units      mol/l
     density    1.210
     temp       25
     pH         7
     pe         4
     redox      pe
     Na         2.4
     K          0.5
     Ca         1.201
     Mg         0.250
     Cl         5.8
     S(6)       0.001
     water     1 # kg

SELECTED_OUTPUT
```

```
      -file            DGR3_468Cs_diff_exch_pitz.txt
      -molalities      Cs+ CsX

EXCHANGE 1-40
      equilibrate 1
      X     2.5    # CEC  = 2500 meq/L
                   # = ~8 meq/100g at 0.08 por and 2.54 bulk density

TRANSPORT
      -cells     40
      -length    0.0005     # 40 cells x 0.0005 m = 2 cm
      -shifts    42         # 42 x 8hr intervals = 336 hrs total
      -time_step 28800      # 8 hours
      -flow_direction  diffusion_only
      -boundary_cond   constant closed
      -diffc       7.2 e-11     # higher than Dp values for iodide

END
```

REFERENCES

Appelo, C.A.J. and D. Postma. 1996. Geochemistry, groundwater and pollution. A.A. Balkema, Rotterdam, 536 pp.

Hu, B., P. Song, Y. Li, and W. Li. 2007. Solubility prediction in the ternary systems NaCl-RbCl-H_2O, KCl-CsCl-H_2O and KBr-CsBr-H2O at 25°C using the ion-interaction model. Computer Coupling of Phase Diagrams and Thermochemistry: 31, 541-544.

Langmuir, D. 1997. Aqueous Environmental Geochemistry. Prentice Hall, Upper Saddle River, 602 pp.

Pitzer, K.S. and G. Mayorga. 1973. Thermodynamics of electrolytes. 2. Activity and osmotic coefficients for strong electrolytes with one or both ions univalent. Journal of Physical Chemistry: 77, 2300-2308.

Pitzer,K.S. and J.J. Kim. 1974. Thermodynamics of electrolytes. 4. Activity and osmotic coefficients for mixed electrolytes. Journal of the American Chemical Society: 96, 5701-5707.